

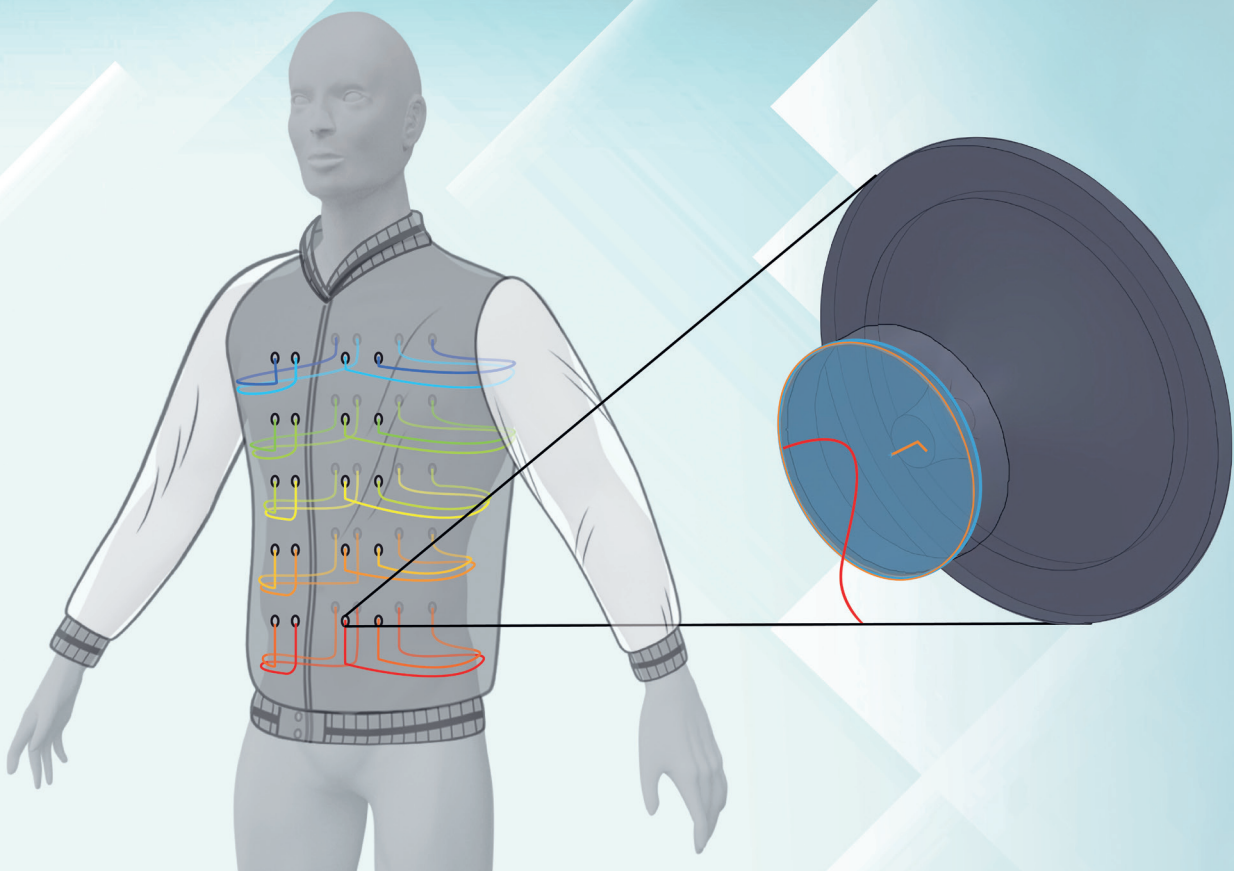


RIGA TECHNICAL  
UNIVERSITY

**Sanjay Rajni Vejanand**

# OPTIMIZATION OF PROPERTIES OF VENTILATED PROTECTIVE CLOTHING

Doctoral Thesis



**RIGA TECHNICAL UNIVERSITY**

Faculty of Civil and Mechanical Engineering  
Institute of Mechanical and Biomedical Engineering

**Sanjay Rajni Vejanand**

Doctoral Student of the Study Programme “Mechanical Engineering and Mechanics (Machine dynamics and design)”

**OPTIMIZATION OF PROPERTIES OF  
VENTILATED PROTECTIVE CLOTHING**

**Doctoral Thesis**

Scientific supervisor:  
Professor Dr. sc. ing.  
ALEKSANDRS JANUŠEVSKIS

RTU Press  
Riga 2024

Vejanand, S. R. Optimization of Properties of  
Ventilated Protective Clothing. Doctoral Thesis.  
Riga: RTU Press, 2024. 144 p.

Published in accordance with the decision of the  
Promotion Council "RTU P-04" of 29 April 2024,  
Minutes No. 61.

# **DOCTORAL THESIS PROPOSED TO RIGA TECHNICAL UNIVERSITY FOR THE PROMOTION TO THE SCIENTIFIC DEGREE OF DOCTOR OF SCIENCE**

To be granted the scientific degree of Doctor of Science (Ph. D.), the present Doctoral Thesis has been submitted for the defence at the open meeting of RTU Promotion Council on x Month 2024 14.30 at the Faculty of Civil and Mechanical Engineering of Riga Technical University, Ķīpsalas 6B, Room 420.

## **OFFICIAL REVIEWERS**

Asoc. Prof. Dr. sc. ing. Marina Čerpinska  
Riga Technical University, Latvia

Asst. Prof. Ph. D. Shравan Koundinya Vutukuru  
MVJ College of Engineering, India

Ph. D. Chawki Abdessemed  
Rolls-Royce Technology Centre, Cranfield University, United Kingdom

## **DECLARATION OF ACADEMIC INTEGRITY**

I hereby declare that the Doctoral Thesis submitted for the review to Riga Technical University for the promotion to the scientific degree of Doctor of Science (Ph. D.) is my own. I confirm that this Doctoral Thesis had not been submitted to any other university for the promotion to a scientific degree.

Sanjay Rajni Vejanand



Date: 15.04.2024

The Doctoral Thesis has been written in English. It consists of an Introduction; 5 Chapters; Conclusion; 77 figures; 12 tables; the total number of pages is 144. The Bibliography contains 159 titles.



## ABSTRACT

To protect the human body from external environmental factors like rain, dust, direct sun radiation, insect access, and bites, the outer layer of clothing may lack air permeability, leading to the accumulation of wet and warm air around the body, which can cause discomfort or even overheating. Clothing with closable vents and openings have been designed to enhance air circulation in areas where significant sweating occurs. Yet, this method only enhances air exchange to a limited extent and does not completely fix the issue. The primary advantage of the future design is to provide efficient protection of the human body from different external environmental conditions, while also maintaining necessary air circulation and ventilation under clothing to minimize the risk of body overheating. The material's technical and functional features provide a strong competitive edge compared to other air-permeable materials on the market for use in the outer layer of ventilating protective clothing.

The objective of the work is to analyse and optimize the aerodynamic characteristics of the material and ventilation elements that will be developed, based on the type of clothing, in order to achieve a proper balance of air permeability, mechanical, and functional characteristics for protection against external environmental factors. The work is focused on creating ventilation elements that can be fixed at the ventilation holes on the inner side of protective clothing. The attached ventilation elements can improve the structural integrity of the clothing by covering the ventilation holes and restricting dust, direct sunlight, insects, and other contaminants from reaching into direct contact with the body, at the same time it permits proper air circulation between the body and clothing. To achieve the objective, various shapes of ventilation elements are created and evaluated to determine the most effective shape. Furthermore, the shape optimization of a suitable ventilation element is achieved through the use of approximation and optimization techniques. SolidWorks Flow Simulation is used to calculate the pressure, temperature, and heat flow for the simplified elliptical model of human body with a protective jacket. The aim is to determine the geometric shape of the element that results in the least flow energy losses in the flow channel of the cell, which is demonstrated by the pressure difference ( $\Delta P$ ). Energy losses in the flow rise with higher  $\Delta P$ , and body cooling reduces when the flow weakens or loses energy. Elements with a higher temperature difference can offer more effective cooling since the heat transfer rate increases with temperature difference. Various criteria such as heat transfer rate, heat flux, and total enthalpy rate were analysed in the following studies to evaluate the efficiency of ventilation elements and the overall efficiency of ventilated clothing.

**Keywords:** CFD, ventilation element, protective clothing, shape optimization, flow simulation.

## ANOTĀCIJA

Lai aizsargātu cilvēka ķermeni no ārējiem vides faktoriem, piemēram, lietus, putekļiem, tieša saules starojuma, kukaiņu piekļuves un kodumiem, apgērba ārējam slānim var nebūt gaisa caurlaidības, kā rezultātā ap ķermeni uzkrājas mitrs un silts gaiss, kas var izraisīt diskomfortu vai pat pārkaršanu. Apgērbs ar aizveramām ventilācijas atverēm un atverēm ir izstrādāts, lai uzlabotu gaisa cirkulāciju vietās, kur notiek ievērojama svīšana. Tomēr šī metode tikai ierobežotā mērā uzlabo gaisa apmaiņu un pilnībā neatrisina problēmu. Topošā dizaina galvenā priekšrocība ir nodrošināt efektīvu cilvēka ķermeņa aizsardzību no dažādiem ārējās vides apstākļiem, vienlaikus saglabājot nepieciešamo gaisa cirkulāciju un ventilāciju zem apgērba, lai samazinātu ķermeņa pārkaršanas risku. Materiāla tehniskās un funkcionālās īpašības nodrošina spēcīgu konkurētspēju salīdzinājumā ar citiem tirgū esošajiem gaisu caurlaidīgajiem materiāliem izmantošanai ventilācijas aizsargapgērba ārējā slānī.

Darba mērķis ir analizēt un optimizēt izstrādājamo materiālu un ventilācijas elementu aerodinamiskās īpašības, pamatojoties uz apgērba veidu, lai panāktu pareizu gaisa caurlaidības, mehānisko un funkcionālo īpašību līdzsvaru aizsardzībai pret ārējie vides faktoriem. Darbs ir vērsts uz ventilācijas elementu izveidi, kurus var nostiprināt pie ventilācijas atverēm aizsargtērpā iekšpusē. Piestiprinātie ventilācijas elementi var uzlabot apgērba strukturālo integritāti, aizsedzot ventilācijas atveres un ierobežojot putekļu, tiešas saules gaismas, kukaiņu un piesārņojumu nokļūšanu tiešā saskarē ar ķermeni, vienlaikus nodrošinot pareizu gaisa cirkulāciju starp ķermeni un apgērbu. Mērķa sasniegšanai tiek izveidotas un izvērtētas dažādas ventilācijas elementu formas, lai noteiktu visefektīvāko formu. Turklāt piemērota ventilācijas elementa formas optimizācija tiek panākta, izmantojot aproksimācijas un optimizācijas metodes. SolidWorks Flow Simulation tiek izmantots, lai aprēķinātu spiedienu, temperatūru un siltuma plūsmu cilvēka ķermeņa vienkāršotajam eliptiskajam modelim ar aizsargjaku. Mērķis ir noteikt elementa ģeometrisku formu, kas rada vismazākos plūsmas enerģijas zudumus šūnas plūsmas kanālā, ko parāda spiediena starpība ( $\Delta P$ ). Enerģijas zudumi plūsmā palielinās ar lielāku  $\Delta P$ , un ķermeņa dzesēšana samazinās, kad plūsma pavājinās vai zaudē enerģiju. Elementi ar lielāku temperatūras starpību var nodrošināt efektīvāku dzesēšanu, jo siltuma pārnese ātrums palielinās līdz ar temperatūras starpību. Lai novērtētu ventilācijas elementu efektivitāti un ventilējamā apgērba

kopējo efektivitāti, tālākajos pētījumos tika analizēti dažādi kritēriji, piemēram, siltuma pārnese ātrums, siltuma plūsma un kopējās entalpijas izmaiņas.

**Atslēgas vārdi:** CFD, ventilācijas elements, aizsargapģērbs, formas optimizācija, plūsmas simulācija.

## PREFACE

This Thesis work represents the result of my study conducted at Riga Technical University, specifically in the institute of Mechanics and Mechanical Engineering, from October 2020 to March 2024. During my PhD journey, I became fascinated by scientific discovery and the difficulties that come with conducting research. This prompted me to focus on the study of air flow analysis of ventilated clothing, this is mainly because of my prior background in CAD, FEM, and Solid Mechanics.

I would like convey my sincere gratitude to Riga Technical University for offering me the opportunity and necessary resources to pursue my doctoral studies. I would like to express my gratitude to the Doctoral Department for their necessary financial fund and support in my research work. I would also like to extend my gratitude to all individuals who provided assistance, both directly and indirectly, in the development of my thesis. In particular, I would like to convey my sincere gratitude to my scientific supervisor, professor, Dr.sc.ing. Alexander Janushevskis and Dr. Ivo Vaicis who helped me with valuable guidance and encouragement. Furthermore, I would like to convey my thanks to Agris Gulevskis for his assistance in providing me with his insightful views and suggestions.

My friends and fellow doctoral candidates provided me with companionship that enhanced and eased my journey. Their strong bond and mutual support greatly helped to smooth my challenging journey of pursuing doctoral study. In particular, I am grateful to Jaymin Sanchaniya and Umesh Vavaliya for all the help and support they gave me throughout this time.

In closing, my deepest and heartfelt gratitude goes to my parents and family for their continuous support and love. Thanks to their unwavering support, I have successfully navigated through all the various levels of my education, and they have consistently stood by my side through all the challenges and achievements of my life. Without their support, I would not be able to attain the level of success and accomplishments that I have attained today.

Sanjay Vejanand

Riga, March 2024

## TABLE OF CONTENTS

ABSTRACT .....	5
ANOTĂCIJA .....	6
PREFACE.....	8
LIST OF FIGURES .....	11
LIST OF TABLES .....	14
LIST OF PUBLICATIONS.....	15
<b>1. INTRODUCTION .....</b>	<b>16</b>
1.1. Main Goal and Tasks of the Work.....	16
1.2. Theory of Object Motion Control, Object Parameter and Shape Optimization .....	17
1.3. The Scientific Novelty of the Given Promotion Work on the Optimization of Object (Clothing) Properties .....	18
1.4. Example of Ventilation Setup on a Model .....	19
<b>2. LITERATURE REVIEW .....</b>	<b>21</b>
2.1. History of Clothing Ventilation .....	21
2.2. Modern Technical Advancements .....	22
2.3. Review of Protective Clothing .....	29
2.4. Review of Clothing Insulation and Human Comfort .....	33
2.5. Review of Thermoregulation of Human Body .....	34
2.6. Theory of Fluid Environment Analysis, Numerical Methods of Modeling and Optimization .....	37
2.6.1. Navier-Stokes Equations in CFD .....	37
2.6.2. Partial Differential Equations and Discretization .....	41
2.6.3. Numerical Methods for Discretization .....	42

2.6.4. Global Optimizatio .....	45
2.6.5. Polynomial Approximation and Interpolation .....	49
2.7. Conclusions of Literature Review .....	54
<b>3. ANALYSIS OF THE STUDIED OBJECT (CLOTHING) AND FLUID FLOW MODEL: SOLIDWORKS FLOW SIMULATION .....</b>	<b>55</b>
3.1. Boundary Conditions of Ventilation Model .....	56
3.2. Analysis of Different Simple Shapes of Ventilation Elements .....	60
3.3. Comparative Analysis of Complex Shape Ventilation Elements .....	76
3.4. Conclusions of the Analysis of Different Shape Ventilation Elements .....	85
<b>4. FORMATION OF THE INPUT DATA FOR THE MODELING OF THE RESEARCH OBJECT (CLOTHING) MODEL .....</b>	<b>87</b>
4.1. Formulation of Task of Shape Optimization of Ventilation Element .....	87
4.2. Analysis of Ventilation Element with and without Constant Cross-Section Area Opening .....	97
4.3. Selection of Appropriate Criteria for Optimization of Ventilation Element .....	108
4.4. Conclusions of Shape Optimization of Ventilation Element.....	115
<b>5. ANALYSING THE EFFICIENCY OF THE STUDIED OBJECT (CLOTHING) AND VENTILATION ELEMENT BY SOLIDWORKS FLOW SIMULATION .....</b>	<b>116</b>
5.1. Analyzing Efficiency of Ventilation Element with Simplified Model.....	116
5.2. Simplified Model Design and Boundary Conditions .....	117
5.3. Selection of Appropriate Criteria for Analysing the Efficiency of Ventilated Clothing.. .....	124
5.4. Conclusions of Appropriate Criteria for Analysing the Efficiency of Ventilated Clothing .....	132
<b>CONCLUSIONS.....</b>	<b>134</b>
<b>REFERENCES .....</b>	<b>136</b>

## LIST OF FIGURES

Figure 1.4. Manikin model with the ventilated jacket .....	20
Figure 2.2.1. A three-dimensionally, partly sectioned representation of the spacer mesh fabric used in accordance with the invention .....	22
Figure 2.2.2. A jacket with ventilation system containing spacer mesh fabric .....	23
Figure 2.2.3. Moisture wicking fabric .....	24
Figure 2.2.4. Ventilated jackets with fans and different openings .....	24
Figure 2.2.5. Liquid cooling system.....	25
Figure 2.2.6. Air cooling technique.....	26
Figure 2.2.7. Thermoelectric (TE) cooling.....	27
Figure 2.2.8. Thermoelectric device (TED) .....	29
Figure 2.3.1. Classification of protective clothing .....	30
Figure 2.3.2. Example of protective clothing .....	31
Figure 2.3.3. Graphene-enhanced protective gear with multifunctional characteristics .....	32
Figure 2.5.1. Heat dissipation from human body to surrounding.....	35
Figure 2.5.2. Factor influencing thermal comfort of human .....	36
Figure 2.6.2. Solution process .....	42
Figure 2.6.3. The concepts of mesh.....	44
Figure 2.6.4. The local and global maxima and minima of the function $\cos(3\pi x)/x$ , $0.1 \leq x \leq 1.1$ .....	46
Figure 2.6.5.1. Approximation .....	51
Figure 2.6.5.2. Interpolation .....	53
Figure 2.6.5.3. Combination of approximation and interpolation.....	53
Figure 3. Schematic diagram of cylindrical model.....	55
Figure 3.1.1. Computational domain with initial conditions.....	56
Figure 3.1.2. Flow pressure plot: Pressure distribution in air gap.....	57
Figure 3.1.3. Surface temperature of body .....	57
Figure 3.1.4. Flow pressure plot, ANSYS.....	58
Figure 3.1.5. Surface temperature plot, ANSYS .....	59
Figure 3.2.1. Elliptical model of body and jacket .....	61

Figure 3.2.2. Different simple shapes of ventilation elements .....	62
Figure 3.2.3. Flow pressure trajectories (E1 to E5).....	68
Figure 3.2.4. Surface temperature of body for E1 .....	69
Figure 3.2.5. Flux plot for E1 at 2 m/s .....	70
Figure 3.2.6. Pressure difference v/s velocity .....	73
Figure 3.2.7. Surface temperature difference ( $\Delta T$ ) v/s velocity .....	74
Figure 3.2.8. Heat flux v/s velocity .....	74
Figure 3.3.1. Elliptical model design with single ventilation element comprising four ventilation holes .....	77
Figure 3.3.2. Three different geometric dimensions of ventilation element .....	78
Figure 3.3.3. Pressure plots for E1, E2 and E3.....	79
Figure 3.3.4. Surface temperature plots of body for E1, E2 and E3.....	80
Figure 3.3.5. Heat flux for element E1 at 2 m/s .....	81
Figure 3.3.6. Pressure difference ( $\Delta P$ ) v/s velocity.....	83
Figure 3.3.7. Temperature difference ( $\Delta T$ ) v/s velocity.....	83
Figure 3.3.8. Heat flux v/s velocity .....	84
Figure 4.1.1. Ventilation element CAD model with lower bounds of design variables.....	88
Figure 4.1.2. Ventilation element CAD model with upper bounds of design variables.....	89
Figure 4.1.3. MSDLH DOE with 12 trials for 2 factors generated by KEDRO.....	90
Figure 4.1.4. Elliptical model design (with an air gap of 3.4 mm) .....	91
Figure 4.1.5. Response Surface $\Delta P = f(R60, R90)$ for wind velocity 4 m/s .....	93
Figure 4.1.6. Optimization results for case of wind velocity 4 m/s .....	94
Figure 4.1.7. Approximation of response surface at 8 m/s.....	95
Figure 4.1.8. Optimization results for case of wind velocity 8 m/s.....	96
Figure 4.2.1. Elliptical model design.....	98
Figure 4.2.2. Design of element E0-90 .....	99
Figure 4.2.3. Flow pressure plots .....	103
Figure 4.2.4. Surface temperature plots for element E0-90.....	104
Figure 4.2.5. Pressure difference at different air velocities.....	106
Figure 4.2.6. Temperature difference at different air velocities.....	107
Figure 4.3.1. Twelve geometrical design of element constructed using DOE .....	109



Figure 4.3.2. Response surface $dT = f(R60, R90)$ using 12 DOE for Kriging approximation .....	111
Figure 4.3.3. Optimization result (red point indicates global minimum of $-dT$ ) .....	112
Figure 4.3.4. Pressure plot for optimal element design .....	113
Figure 4.3.5. Surface temperature of body .....	114
Figure 5.2.1. Case 1: Simplified elliptical model of human body and jacket .....	118
Figure 5.2.2. Ventilation element E1 .....	118
Figure 5.2.3. Ventilation element E2 .....	118
Figure 5.2.4. Case 2: Simplified model with two square plates .....	119
Figure 5.2.5. Case 2: Computational domain .....	119
Figure 5.2.6. Flow pressure trajectories in case 1 .....	120
Figure 5.2.7. Surface temperature plots of body in case 1 .....	121
Figure 5.2.8. Flow pressure trajectories in case 2 .....	122
Figure 5.2.9. Surface temperature plots in case 2.....	123
Figure 5.3.1. Case 1: model design with 11 ventilation holes .....	126
Figure 5.3.2. Case 2: model design with 48 ventilation holes.....	127
Figure 5.3.3. Case 3: model design with 105 ventilation holes .....	128
Figure 5.3.4. Ventilation element .....	128
Figure 5.3.5. Computational domain and boundary conditions in case 1 .....	129
Figure 5.3.6. Flow pressure and surface temperature plots in each case.....	130
Figure 5.3.7. Flow pressure and surface temperature variation near ventilation hole.....	132

## LIST OF TABLES

Table 3.1. Numerical results comparison; SolidWorks v/s ANSYS .....	59
Table 3.2.1. Material properties .....	62
Table 3.2.2. Numerical values of results .....	70
Table 3.3. Numerical values of the results (E1 – E3) .....	82
Table 4.1. Simulation results of 12 elements generated using DOE .....	92
Table 4.2.1. Coordinate Design Values of Elements .....	100
Table 4.2.2. Numerical Values of Simulation Results .....	105
Table 4.3.1. Numerical values of simulation results .....	110
Table 4.3.2. Results comparison .....	114
Table 5.2.1. Numerical values of results for case 1 .....	121
Table 5.2.2. Numerical values of results for case 2 .....	123
Table 5.3. Numerical values of analysed criteria .....	131

## LIST OF PUBLICATIONS

1. A. Janushevskis, J. V. Sanchaniya, S. R. Vejanand. Designing of Catamaran Hull Spine Beam. 20th International Scientific Conference “Engineering for Rural Development”. ISSN 1691-5976, Volume 20, pp. 1685-1691, Jelgava, 2021. <https://www.tf.llu.lv/conference/proceedings2021/Papers/TF365.pdf>
2. A. Janushevskis, S. R. Vejanand, A. Gulevskis. Comparative Analysis of Different Shape Ventilation Elements for Protective Clothing. 21th International Scientific Conference Engineering for Rural Development. ISSN 1691-5976. Volume 21, pp. 179– 186. Jelgava, 2022. <https://www.tf.llu.lv/conference/proceedings2022/Papers/TF052.pdf>
3. A. Janushevskis, S. R. Vejanand, A. Gulevskis. Analysis of Different Shape Ventilation Elements for Protective Clothing. WSEAS Transactions on Fluid Mechanics, Volume 17, ISSN: 1790-5087, E-ISSN: 2225-347X, DOI: [10.37394/232013.2022.17.14](https://doi.org/10.37394/232013.2022.17.14), 2022. pp. 140-146. <https://wseas.com/journals/fluids/2022/a285113-338.pdf>
4. A. Janushevskis, S. R. Vejanand, A. Gulevskis. Air Flow Analysis for Protective Clothing Ventilation Elements with and without Constant Cross-section Area Opening. Latvian Journal of Physics and Technical Sciences. 60 (2), DOI: [10.2478/lpts-2023-0012](https://doi.org/10.2478/lpts-2023-0012), pp. 63-73, 2023. Published Online: 15 Apr 2023 Volume & Issue: Volume 60 (2023) - Issue 2 (April 2023). <https://sciendo.com/article/10.2478/lpts-2023-0012>
5. A. Janushevskis, S. R. Vejanand, A. Gulevskis. Shape Optimization of Ventilation Elements for Protective Clothing by Using Metamodeling Approach. 22th International Scientific Conference Engineering for Rural Development. ISSN 1691-5976, Vol.22, pp. 164-172, Jelgava, 2023. <https://www.tf.llu.lv/conference/proceedings2023/Papers/TF032.pdf>
6. Sanchaniya, J. V., Rana, V., & Vejanand, S. R. (2024). Optimization of Electrospinning Parameters for High-Strength Oriented Pan Nanofiber Mats. Latvian Journal of physics and technical sciences. (Accepted).
7. S. R. Vejanand, A. Janushevskis, I. Vaicis. Selection of Appropriate Criteria for Optimization of Ventilation Element for Protective Clothing Using a Numerical Approach. MDPI Journal of Computation. (Accepted).

# 1. INTRODUCTION

## 1.1. Main Goal and Tasks of the Work

The main objectives and tasks of the work are listed below.

1. The initial task of the study is to examine the flow simulation and analyse air flow interaction of a simplified model of the human body with a protective jacket using the SolidWorks flow simulation tool. The circular model of the body and jacket is considered initially to study air flow interaction and to analyse flow pressure and surface temperature of the body. A simulation study is made with jacket having three inlets and ten outlets. The same analysis is done in ANSYS fluent to compare results of SolidWorks and ANSYS to check reliability of results. Further the model is modified into an elliptical shape representing body and the jacket.
2. Different simple shapes of ventilation elements are studied and analysed by attaching each at the inlet ventilation hole, respectively. The flow pressure and surface temperatures are recorded for each shape of ventilation elements to predict the efficiency of ventilation element. The analysis is done at different air velocities of 2, 5 and 8 m/s to understand effect of air velocity on the results.
3. Further the more complex shape of ventilation element is analysed by varying geometrical dimension of the model to study the flow variations in element flow channel with respect to change in dimensions.
4. Once the efficient shape of the ventilation element is found, the next task is to optimize the design of the element. Shape optimization of element is achieved by building metamodel in software KEDRO, where 12 design of experiment (DOE) were created based on two coordinate values of the geometrical shape of ventilation elements. Twelve geometrical model of ventilation element are created using these DOE and each were simulated in SolidWorks flow simulation to obtain values of pressure and temperature differences. The recorded values from SolidWorks are used in KEDRO for further approximation and optimization using Kriging method.

## **1.2. Theory of Object Motion Control, Object Parameter and Shape Optimization**

Exposure to extreme temperatures can hinder people's thermoregulation. Therefore, it is essential to take into account the impact of fabric cooling and ventilation on human comfort during the clothing design and development procedure [1]. Fabric ventilation and cooling play a crucial role in ensuring human comfort in clothing design. Exposure to extremely high temperatures may hinder individuals' capacity to regulate their body temperature, resulting in symptoms such as heat exhaustion and heat stroke [2, 3]. Many professions sometimes need workers to execute activities in hot surroundings, exposing them to considerable heat stress that can reduce job performance and productivity [3]. Heat stress is a significant contributor to industrial accidents and injuries, impairing individuals' cognitive function, concentration, and motor skills [3, 4]. Personal cooling (PC) systems are a practical and cost-effective method to decrease the micro-climate experienced by individuals in any of these situations. Personal cooling clothing can be beneficial in situations when protective clothing is required to regulate the micro-climate of individuals for heat-stress management [5].

There is a market demand for improved technical solutions and materials for the exterior part of protective clothing. These solutions should provide good ventilation, especially in warm weather conditions and during heavy physical activities. This is due to the growing interest in the market for efficient protection of the human body against exposure to extreme weather conditions. Many different kinds of protective clothing are readily available to shield the human body from diverse external weather conditions like rain, dust, direct solar radiation, insect access, and their bites. The danger of body overheating might occur when individuals are needed to wear protective clothes in warm environments or during times of heavy load conditions [6]. This is due to the insufficient air permeability of the outer layer of cloth, resulting in the collection of warm and wet air on the body, leading to discomfort. To optimize air circulation, a range of adjustable vents and breathable areas have been created in clothes. Nevertheless, this approach only leads to a limited enhancement in air circulation while simultaneously compromising the structural integrity of the garments. Attaching suitable ventilation elements on the inner side of ventilation holes can enhance the mechanical durability of the clothes. This allows for proper air circulation while also preventing dust, rain drops, sun radiation, insects from directly reaching the body.

This research is associated with the analyzing and optimizing the aerodynamic properties of the material and ventilation elements that will be created, to achieve a balance between air permeability, mechanical strength, and functional features, with the goal of offering protection against external environmental conditions. The work refers to the creation of new techniques for the development of experimental designs, approximations, and optimizations. The thesis will facilitate the implementation of newly created algorithms and approaches by integrating them into a specific methodology. This will allow the execution of complex tasks, such as optimizing the design of ventilation elements. Gaining understanding of the interaction of fluid flow with the model is a crucial and complex task. In order to reduce the complexity of the problem, a simplified elliptical model of the human body and jacket is designed and utilized in the study. SolidWorks flow simulation tool is used to compute air flow interaction with the model and analyse the results. The analysis of different shapes of ventilation elements are mentioned in this work. Furthermore, it discusses metamodeling approach using different order polynomial local and global approximations, as well as Kriging approximations, for the purpose of shape optimization of ventilation element. The software KEDRO is used to created design of experiments and further approximation and optimization task. Various criteria are used to evaluate the efficiency of ventilation elements. These criteria are also utilized to assess the efficiency of the ventilated model with different numbers of ventilation. Ultimately, numerical simulation and physical experiments are conducted using a realistic model of the human body with a jacket in order to draw conclusions through a comparison of the results.

### **1.3. The Scientific Novelty of the Given Promotion Work on the Optimization of Object (Clothing) Properties**

The scientific novelty of this work lies in its concept of creating appropriate ventilation elements for the protective clothing which can be attached at the ventilation holes to provide proper air circulation between the body and clothing to avoid over heating of the body in extreme environmental conditions and during heavy work load conditions. One major drawback of most of the personal protective clothing with the external cooling system is that they make structure

bulky which makes garments heavy and uncomfortable to wear. In addition, their cooling efficiency is not steady and reliable for personal clothing cooling devices. These small ventilation elements can be used to overcome these issues as they are very light weight and do not require any external power to operate.

### **1.4. Example of Ventilation Setup on a Model**

The execution of physical experiment with a thermal manikin model wearing a jacket is taking place at the Personal Protective Equipment (PPE) laboratory at Riga Technical University (RTU). This experiment is carried out using two separate jackets: 1) A normal jacket without ventilation features, and 2) Jacket with the attached ventilation elements.

Figure 1.4 shows a manikin model wearing a ventilated jacket. The detail view 'A' in Figure 1.4 provides an enlarged view of four ventilation holes in the jacket that make up a single ventilation unit, while the detail 'B' is the backside view of detail 'A', displaying the ventilation element attached to the holes.

This experiment shows the significant advantages of a ventilated jacket. These results are currently not attached and will be published as soon as possible after the data declassification procedure, i.e. after the acceptance of the patent application of the industrial partner (European Patent Application No. 21816861.5 by Agris Gulevskis).

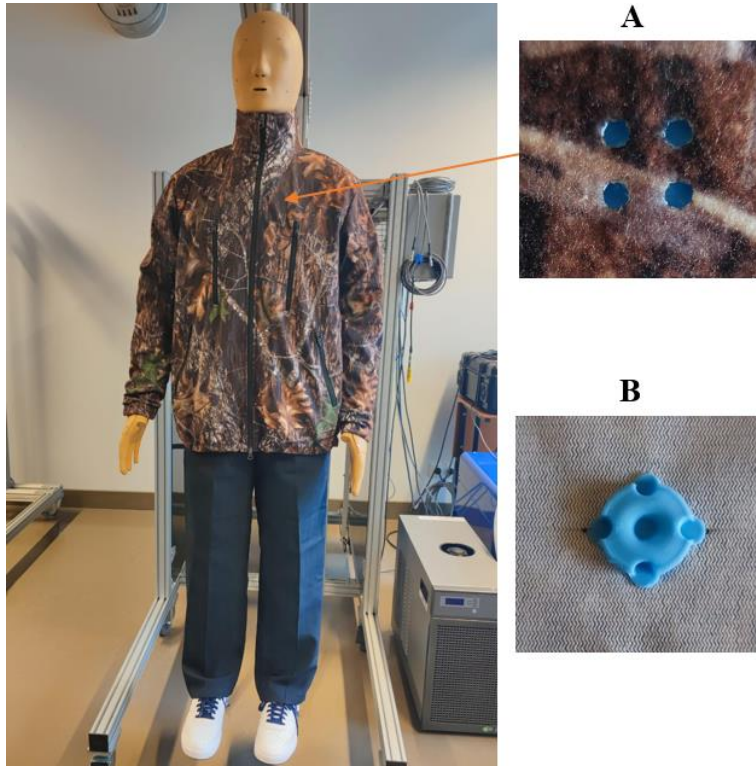


Figure 1.4. Manikin model with the ventilated jacket: (A) Enlarged view of ventilation holes.  
(B) Attached ventilation element at ventilation holes.



## 2. LITERATURE REVIEW

### 2.1. History of Clothing Ventilation

The history of ventilation in clothing in the form of light weight and colored linen, cotton fabrics, or different air circulation elements used in Jackets or protective clothing to lower body temperature in hot and humid environment when performing heavy work can be traced back to ancient times. Various materials and techniques have been used to build the mythology of ventilation in clothing over the years. Few of them are described in following text.

- **Ancient Egypt:** A lightweight, generally white or light-colored, and loose-fitting linen clothing were regularly used by both working situations and interior other activities in ancient Egypt around 3,000 BCE. Linen fabric naturally permits air to circulate, providing air circulation between the body and the material [7].
- **Ancient Rome and Greece:** The ancient Romans created the "subucula" or "subligaculum," a lightweight, sleeveless tunic worn beneath clothing as undergarments and bedclothes. The breathable clothing materials, such as linen or cotton, were used to allow air to circulate around the body and offer ventilation [8].
- **Industrial Revolution:** When the industrial revolution began in the 18th century, it brought about major changes in working conditions. Workers faced lengthy hours in hot conditions as factories became more popular. Lightweight cotton clothes with looser fits were designed to solve this problem, allowing better air circulation and sweat dissipation.
- **Modern Innovations:** Specific ventilation components were added into clothing designs in the 20th century as textile technology and manufacturing techniques advanced. Mesh panels, vents, perforations, or breathable fabrics in critical regions such as the back, underarms, or sides of jackets were included. These components enhanced ventilation and contributed in better regulation of body temperature [9]. Nowadays, to improve cooling and comfort in work wear and athletics, several ventilation technologies and materials are used. Fabrics having moisture-wicking characteristics, for example, are frequently used to move sweat away from the skin, allowing it to evaporate more effectively and keeping

the body dry. Advanced techniques, such as laser holes or 3D mesh structures, are also used to generate targeted ventilation zones in clothes [9, 10].

## 2.2. Modern Technical Advancements

Advancement in technology and material science have led to the creation of new ventilation features in clothing with the goal to improve comfort and regulate body temperature in a variety of conditions in the modern era. Here are a few noteworthy examples:

- **Mesh panels and venting systems:** Mesh panels are often used in clothing such as jackets, shorts, and shirts, as well as sportswear such as football, cycling, and tennis. Panels are constructed of breathable, lightweight mesh fabric that is specifically positioned in locations where heat tends to build, such as the back, underarms, or sides. This increases air flow between the body and the jacket, providing thermal comfort to the users [11].

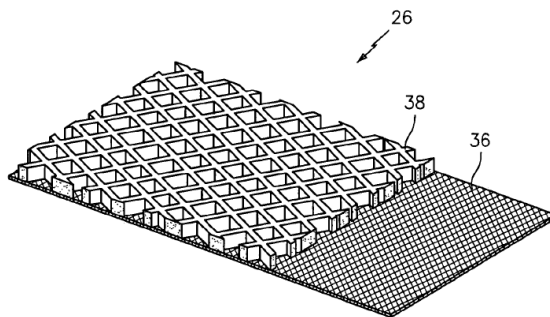


Figure 2.2.1. A three-dimensionally, partly sectioned representation of the spacer mesh fabric used in accordance with the invention: 26 - spacer material design, 36 – thin fabric layer, 38 – thick mesh structure layer [12].

The spacer material's design 26 as shown in figure 2.2.1, this is used in the embodiment. A spacer fabric with two layers is depicted in this image. On one hand, a fairly thin fabric layer 36 composed of water repellent plastic material forms one side. To form a unit, a thicker mesh structure layer 38 is joined to this fabric layer 36 [12].

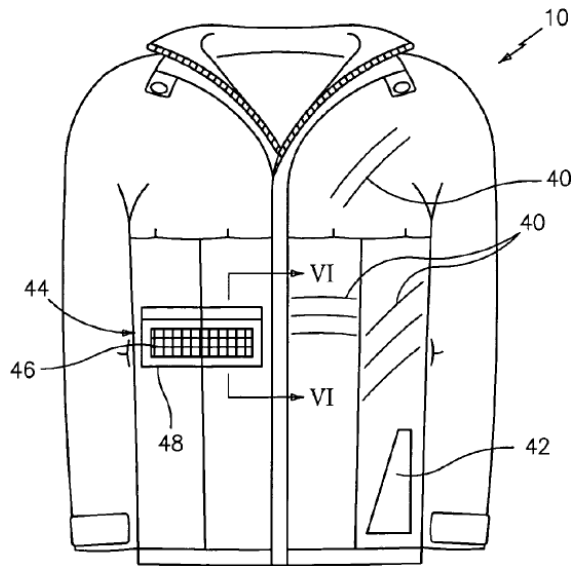


Figure 2.2.2. A jacket with ventilation system containing spacer mesh fabric [12].

Figure 2.2.2 depicts additional potential versions of the ventilation system in accordance with the invention. For example, a variation in the width of ventilation systems US 7,043,767 B2 5 is shown here in a sports jacket 10 with multi slit-like ventilation systems 40, arranged next to one another, and these able to be arranged as multiple ventilations, for example, under arms, in the upper body region, or in the shoulder region. A perpendicular variant is illustrated by 42, with the spacer material created in an approximate wedge-shape. An alternative ventilation system 44 is depicted on the left side of the sports jacket 10 in figure 2.2.2. The flexible, three-dimensionally cross-linked spacer material is incorporated as an areal, for example, a strip-like, element 46 into the garment surface. This indicates that the element 46 is sewed to the remaining clothing material at the edges in each case. A flap 48 is positioned above this areal part 46 and can cover it [12].

- **Moisture-wicking fabrics:** The garment engineering has come a long way, and one of the most exciting discoveries was the development of moisture-wicking materials, which are now widely used in sportswear and outdoor clothes where sweating is a big discomfort. These garments, which are usually made of synthetic materials such as polyester or specialised blends, are intended to quickly draw moisture away from the skin and towards

the fabric's outer surface, where it may evaporate more easily. It prevents the body from sweating during tough physical activities or exercise, and keeping it dry and cool [13].

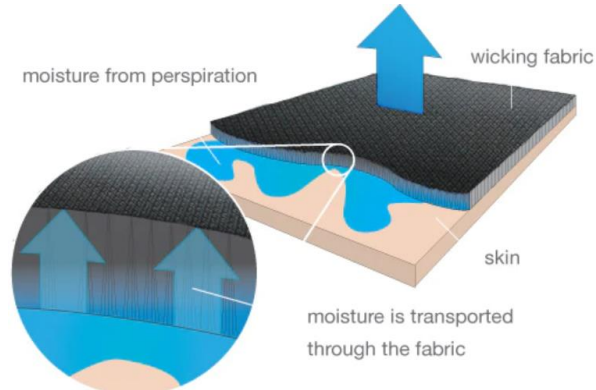


Figure 2.2.3. Moisture wicking fabric [14].

- **Active Cooling techniques:** Some innovations go beyond natural ventilation to include active cooling solutions. Certain specialised clothes, for example, include built-in fans (air cooling), cooling packs, or liquid cooling systems that actively circulate cool air or fluids around the body to cool the skin [15].

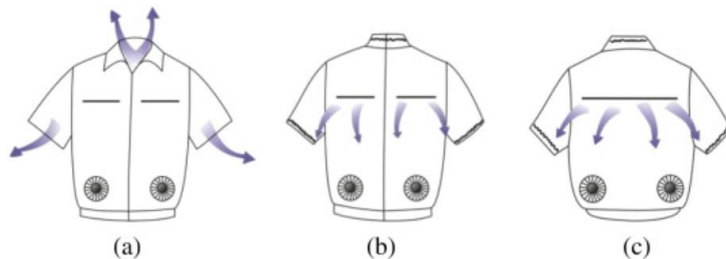


Figure 2.2.4. Ventilated jackets with fans and different openings. (a) Normal opening; (b) Front opening; (c) Back opening [15].

In the figure 2.2.4 (a) normal opening, the collar and cuff openings were opened, while the chest and back openings were closed. In (b) front opening; only the chest openings were left open and strings were used to close the collar and cuff openings, and the back opening was closed. Similarly, in (c) back opening; only the back ventilation was opened

and strings were used to close collar and cuff openings, and chest zippers were closed. Such ventilated systems are usually comprised of a short-sleeved jacket as well as two ventilation units, where each ventilation unit consisted of a small fan with a 10 cm diameter. They were powered by four 2300 mAh AA batteries. The portable fans were implanted in the jackets and secured with a plastic ring which on activation could circulate ambient air around the chest or torso at a rate of around  $0.012 \text{ m}^3/\text{s}$  [15].

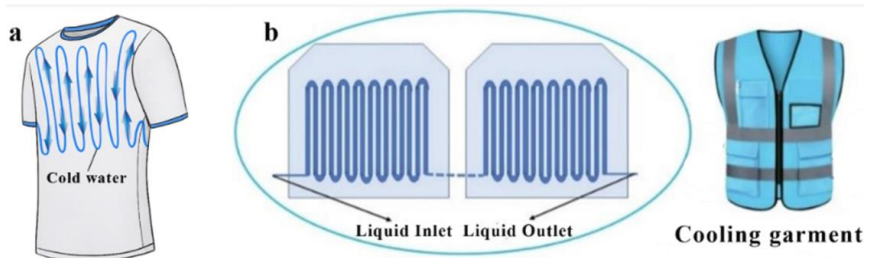


Figure 2.2.5. Liquid cooling system; (a) Schematic diagrams of a liquid cooling garment. (b) Liquid cooling garment with a Thermoelectric (TE) device [16, 10].

As illustrated in figure 2.2.5, liquid cooling garments usually come with circulating water tubes filled with a cold liquid resource and a micro water pump device at the inner layer to drive the liquid flowing in the tube to reduce the temperature [17, 18]. The Liquid Cooling Garments (LCG) has been demonstrated to be one of the most promising technologies in the clothing cooling arena after multiple investigations and is employed in a variety of fields, including military [19], mining [20], and sports [21]. Guo et al. developed a LCG with heat transfer model to analyse the effects of various parameters on LCG performance and optimize its design [18]. Their optimization resulted in a maximum cooling rate of  $243.2 \text{ W}/\text{m}^2$  and a maximum work duration time of 3.36 h [18, 10]. However, because of the built-in heavy device and the possibility of skin burn from steam generation [22], the LCG requires additional efforts to modify the cooling systems for both security and comfort. Grazyna et al. created a unique LCG with a sensor to control the microclimate temperature and modular knitted fabric that can be worn directly on the human body [23], resulting in increased user safety and comfort.

Combining different cooling technologies with LCGs has great practical application potential for significantly improving the LCG [24]. Zhang et al. reported a unique LCG

with Thermoelectric (TE) materials that significantly reduces the thermal stress danger [16, 10], this arrangement is shown in figure 2.2.5 (b).

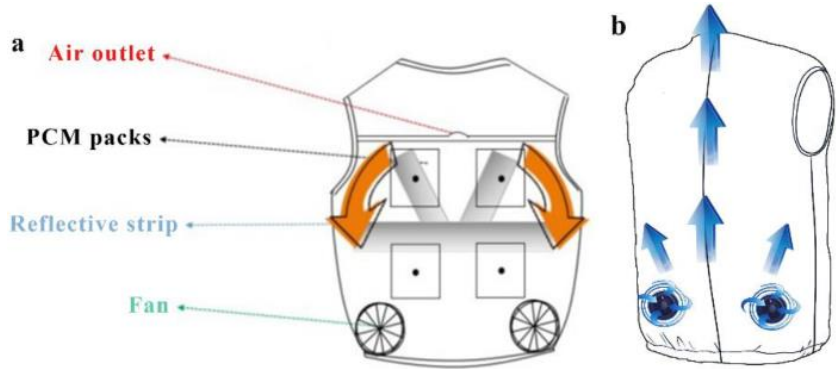


Figure 2.2.6. Air cooling technique. (a) Air cooling with a PCM cooling vest (PCV) [25]; (b) An air cooling garment's schematic illustrations [10].

An Air Cooling Garment (ACG) provides thermal comfort as a typical cooling approach by forcing air to flow through the microenvironment between the clothes and the human body [26]. The primary benefits of ACGs are their affordable cost, light weight, and portability [27]. According to Hadid et al., an ACG resulted in a lower body temperature and a 20% reduction in perspiration with the same level of activity [28]. However, more complicated living and working environments necessitate higher cooling performance with improved ACG comfort and security. Furthermore, ACG designs are typically heavy and bulky, restricting their general use in our daily lives [10]. Hence, enhancing cloth wearing and thermal comfort is in high demand [29, 30]. Yang et al. examined the impacts of clothing size and air ventilation rate on the cooling performance of ACGs, demonstrating that air ventilation highly reduced the predicted core temperatures in two garment sizes; however, the clothing size had almost no influence on the predicted thermos-physiological responses in high ventilation [31]. To meet the ever-increasing cooling needs, the cooling effect offered by a single air-cooling approach can be improved further. As a result, considerable effort has been done on researching the prospect of combining an air-cooling technique with other cooling methods in order to investigate novel cooling methods [10]. Figure 2.2.6 (a) shows a novel hybrid personal

cooling vest (PCV) designed by Ni et al. [25]. Their unique PCV was combined with PCMs and ventilation fans, demonstrating the adaptability and reliability of this hybrid cooling garment. Phase change materials (PCMs) cooling can use latent heat from the body or the environment directly to reduce the temperature of the microclimate between the clothing and the body, without additional energy usage [32]. Based on an air tubing network and TE cooling plates, Lou et al. examined the relationship between the cooling effect and different body positions, which is useful for improving the combination of the cooling system and the clothing in an efficient and easy way in daily life [33].

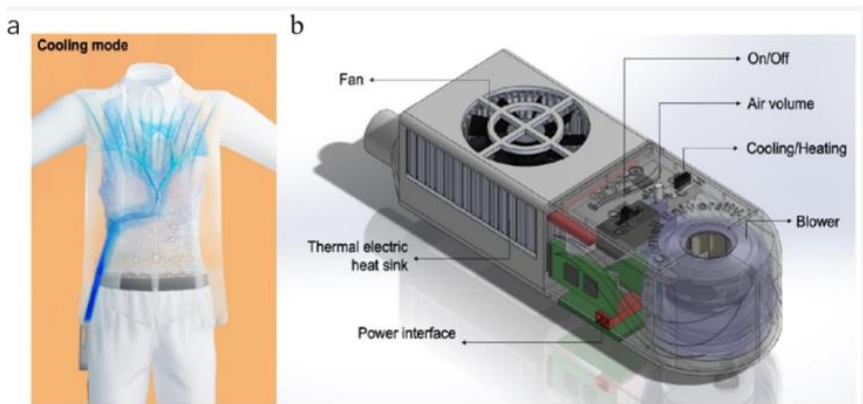


Figure 2.2.7. Thermolectric (TE) cooling; (a) TE cooling undergarment and (b) Illustration of a TE cooling module [34, 10].

Air cooling and liquid cooling garments are uncomfortable and heavy, with bulky air or fluidic pathways, and their cooling efficiency is not steady and reliable for personal clothing cooling devices [35]. Considering these inherent drawbacks, homeostatic solid-state cooling techniques such as electrocaloric [36, 37], multicaloric [38], and TE cooling [39] have received considerable attention. Because of its consistent cooling ability and small device size, TE cooling has a high potential for practical industrial cooling applications [40]. Wearable TE cooling thus offers a desirable alternate option for personal thermal comfort [41]. The TE materials composed of distinct types of conductors or semiconductors (N- and P-type) can be utilised to convert heat energy to electricity and vice versa [42]. TE gadgets are compact and have no moving components or noise,

making them the most promising cooling solution for the future [43]. As per the Peltier effect [44, 45], when a direct current runs across different TE materials, heat is absorbed or dissipated at the junctions, resulting in a hot side and a cool side [46]. The TE cooling plate (TECP) is an ideal choice for small solid-state cooling in industrial TE applications due to its substantial commercial production, cheap cost, and light weight [47]. Luo et al. efficiently mounted a TECP cooling system in a lightweight and portable undergarment [48]. As illustrated in figure 2.2.7, the TE cooling module comprises of heatsink as a cooling source and is linked to a tubing network to offer uniform and appropriate cooling performance, resulting in a 15% energy savings of indoor heating, ventilation, and air conditioning [34, 10]. Yet, the rigid and heavy heatsink, significantly lowers the wearability of TE and hinders the development of flexible TE cooling technology. A novel mask coupled with thermoelectric devices and a 3D printed framework was recently reported [49]. With a low voltage application, the temperature was reduced about 3.5 °C during the test.

However, further efforts have to be made to develop efficient and wearable thermoelectric devices with potential flexibility. As shown in figure 2.2.8, Hong et al. created a flexible and portable thermoelectric cooler with a scalable applications [50]. To boost thermal conductivity, inorganic semiconductor thermoelectric pillars were mounted on two elastic flexible Ecoflex films that were filled with thermally conductive filler aluminum nitride. This device can run continuously for 8 hours without a heatsink and provides more than 7.6 °C cooling effects [10]. Zhang et al. presented a wearable TEC based on a two-layer flexible heatsink [51] made of hydrogel and nickel foam as phase change material to absorb heat and thermally conductive material to conduct heat, respectively. Furthermore, the separate heatsink they investigated provided the needed flexibility while achieving a significant temperature drop of 10 °C under 0.3A input current [10].



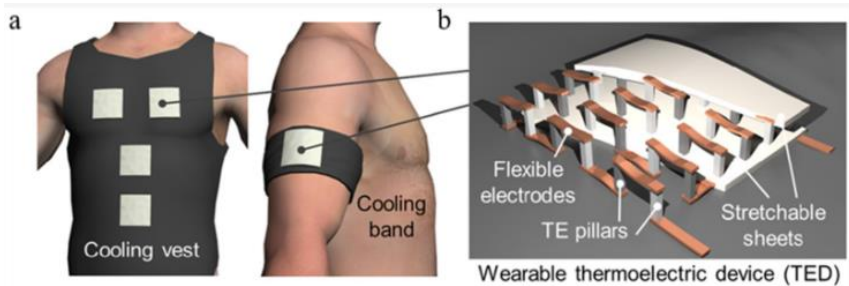


Figure 2.2.8. Thermoelectric device (TED); (a) cooling garments with wearable TE devices (TEDs) (b) the structure of a TED [52, 10].

To further improve flexibility and support the advancement of flexible TEC, TE fibre has been extensively researched to provide improved wearing comfort. Hot drawing technology was used by Zhang et al. to create very long flexible TE micro/nanowires [53]. They moulded N and P-type semiconducting materials into fibers and coated them with borosilicate glass to preserve and prevent them from oxidation. The fibre was flexible and had a high TE properties, allowing it to be easily woven into the textile and provide 6.2 °C cooling capability [10]. Zheng et al. proposed a unique design for fiber-based thermoelectric textiles (TETs) [53, 54]. Inorganic TE materials and liquid metal were used to fabricate their TE fibre, which was then encapsulated in polydimethylsiloxane. The TET generated a consistent cooling capability of 3.1 °C while being stretchable and flexible [10].

### 2.3. Review of Protective Clothing

The main purpose of every clothing is to shield the human body from harmful weather conditions. However, the phrase "protective clothing" is employed when clothing is specifically designed to provide proper protection against hazards such as fire, wind, microorganisms, chemicals, gas, radiation, electricity, and so on [55]. Protective clothing items provide a practical purpose, such as personal protective clothing, which primarily aims to shield the human body from unfavorable environmental factors, including physical, chemical,

biological, and thermal hazards [56]. Common types of Protective Clothing (PC) include ballistic PC for protection against weapons hazards, firefighter's PC for protection against the heat and flame, NBC suits for protection against nuclear, biological, and chemical warfare agents, cold-weather clothing, and sports clothing for swimming and scuba diving. Researchers created electro spun polyurethane (PU) nanofibrous membranes (ENMs) for PC and conducted a comparative analysis with Gore-Tex™, a windproof and breathable membrane [57]. ENMs have been utilized to develop advanced and efficient protective clothing for several purposes [58], including safety against chemical and biological substances, sports, sensors, ballistic applications, wearable energy generation etc. A detail classification of protective clothing is described in figure 2.3.1 and some examples of PC are mentioned in figure 2.3.2.

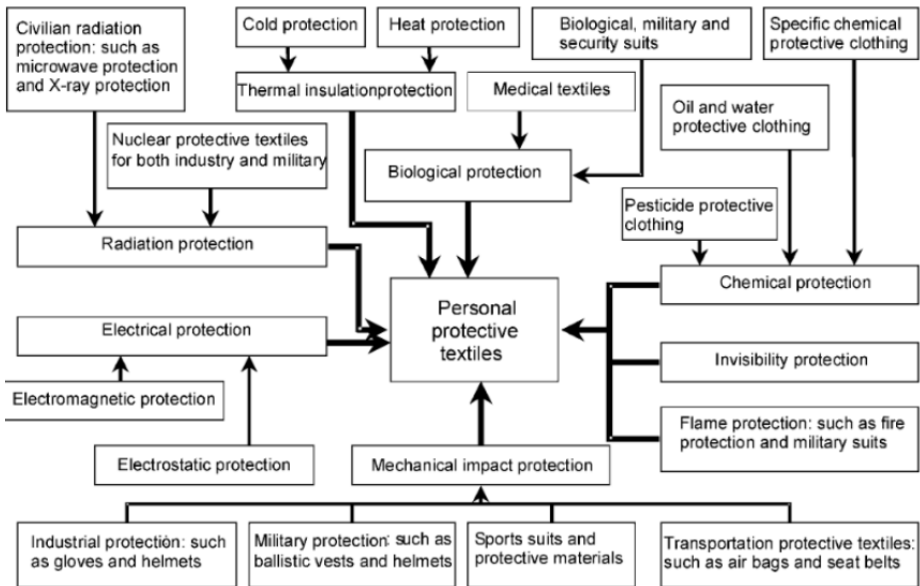


Figure 2.3.1. Classification of protective clothing [58].



Figure 2.3.2. Example of protective clothing [59].

Choosing the suitable protective clothing based on the type of danger is essential to safeguard oneself from potential hazards [60]. Nevertheless, the issue with the majority of personal protective equipment (PPE) lies in the fact that enhanced safety can only be guaranteed at the expense of increased expenditures and physical discomfort, which includes reduced flexibility, accuracy, comfort, and vision [61]. Additional inherent risks associated with traditional PPE include heat-induced strain, restricted movement, risk of accidents, seizures, physiological problems, and anxiety [61]. Graphene is a two-dimensional sheet made up of carbon atoms connected in a planar arrangement. It has been widely recognized as a revolutionary material in various technological fields due to its outstanding mechanical, thermal, chemical, electrical, and antibacterial characteristics [62]. Its outstanding characteristics make it an appealing material with potential for various technical applications, giving it an edge over other similar materials [63]. The integration

of graphene or its derivatives to polymers/textiles can enhance the characteristics of fabrics for particular usage [64]. Integrating graphene into fabrics or modifying a textile surface with graphene can enhance mechanical strength, fire resistance, conductivity, antibacterial properties, resistance to abrasion, and UV protection [64]. Additionally, Graphene-based woven fabrics demonstrate exceptional flexibility. The addition of all these features to PPE clothes can potentially be achieved by a single lightweight application if graphene or its derivatives could be used to modify textile materials [65]. Thus, a new performance fabric enhanced with graphene might be the solution to the issues associated with PPE. Such example of multi-functional protective clothing is represented in figure 2.3.3.

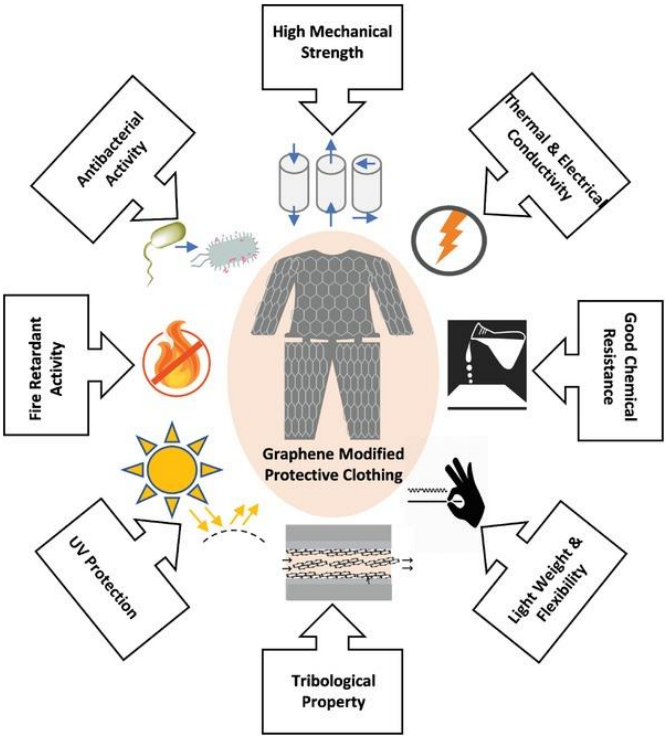


Figure 2.3.3. Graphene-enhanced protective clothing with multifunctional characteristics [62].

## 2.4. Review of Clothing Insulation and Human Comfort

The level of thermal insulation that a person wears significantly affects their thermal comfort [66]. Clothing adaptation is a behavior that has a direct impact on the heat balance [67]. The thermal insulation of textiles and ensembles of clothing can be measured using the unit "clo", where 1 clo being equal to  $0.155 \text{ m}^2 \text{ }^\circ\text{C}/\text{W}$ . For tasks that involve minimal movement that having a metabolic rate of around 1.2 met, the change in clothing insulation has an impact of approximately  $6^\circ\text{C}$  per clo on the ideal operating temperature. For instance, incorporating a thin, full-sleeved sweater into an outfit enhances the insulation of the garment by around 0.25 clo. The inclusion of this insulation would result in a decrease of the ideal operating temperature by roughly  $1.5^\circ\text{C}$ , calculated as  $6^\circ\text{C}/\text{clo}$  multiplied by 0.25 clo [68]. The impact becomes greater for individuals with higher metabolic rates [69]. Among all of the thermal comfort adjustments accessible to users at workplaces, clothing adjustment is possibly the most crucial [70]. Clothing is a factor that influences the calculation of the predicted mean vote (PMV) and predicted percentage of dissatisfied (PPD) [71]. Hence it is considered as an input for thermal comfort calculation as per American (ANSI/ASHRAE, 2010), European (CEN, 2007), and International (ISO, 2005) thermal comfort standards. The base thermal comfort ranges are typically derived for clothing insulation equal to 0.5 clo and 1 clo. In the absence of additional data, thermal comfort assessments during the cooling season are conducted using a garment insulation value of 0.5 clo, whereas during the heating season, a clothing insulation value of 1 clo is employed. The choice of clothing insulation for thermal comfort calculations has an impact on the design, sizing, and analysis of HVAC systems, as well as the energy assessment and operation of buildings [72].

Along with environmental parameters such as air temperature, mean radiant temperature, air velocity, humidity, and metabolic level of heat generation, various standards for assessing human exposure to thermal environments (e.g., ISO 79331 for heat [73], ISO 77302 for indoor climate [74], ISO 110793 for cold [75]) utilize basic clothing insulation ( $I_{cl}$ ) as one of the input variables. The insulation of a clothing ensemble can be determined by measuring it on a thermal manikin [76, 77] or by estimating it based on existing literature or databases that contain measurements of similar clothing goods and ensembles [78-80]. The total insulation ( $I_T$ ) or resultant total insulation ( $I_{T,r}$ ) can be directly obtained from manikin measurements. An air insulation ( $I_a$ ) and clothing area factor ( $f_{cl}$ ) are required to calculate  $I_{cl}$ .

$$I_{cl} = I_T - (I_a \div f_{cl}) \quad (2.4)$$

Here,  $I_{cl}$  is clothing insulation;  $I_T$  is the total insulation;  $I_a$  is air insulation and  $f_{cl}$  is clothing area factor.

Where,  $f_{cl}$  represents the ratio of the outer surface area of a clothed body to the surface area of the body when it is nude. It accounts for the increase in surface area that is in contact with the surrounding air, where heat exchange takes place.  $I_a$ , on the other hand, can be measured on a nude manikin and is commonly used as a solid reference value in manikin testing. The value of  $f_{cl}$  can be estimated using methods such as photography, 3D scanning [81-83], or by calculating it based on various equations derived from literature and standards [84, 85].

## **2.5. Review of Thermoregulation of Human Body**

Thermoregulation refers to the process of maintaining the body's core temperature by effectively managing the production and dissipation of heat. An individual in good health typically possess a core body temperature of  $37 \pm 0.5^\circ\text{C}$  ( $98.6 \pm 0.9^\circ\text{F}$ ), which is the optimal temperature range required for the body's metabolic systems to work properly [86]. There is a thermostat in our bodies called the hypothalamic thermoregulatory center. It is situated in the preoptic zone of the hypothalamus. This area manages the body's set point and keeps the temperature stable. The human body possesses both peripheral and central thermoreceptors. Peripheral thermoreceptors are situated in the skin and detect surface temperatures, whereas central thermoreceptors are present in the viscera, spinal cord, and hypothalamus and detect the core temperature [87]. These thermoreceptors are activated by changes in body temperature and relay this information to the preoptic portion of the hypothalamus. Subsequently, this region stimulates thermoregulatory processes to either rise or lower the body's temperature in order to restore it to its normal level [88]. It is necessary to understand that temperature fluctuates within the body, having the core body temperature being higher and more consistent, while the skin temperature is lower and more fluctuating to changes caused by external variables. The lowest level of body temperature is often observed about 4 AM, while the highest point is reached at 6

PM [89]. Heat dissipation from the skin to the surrounding environment takes place through radiation, conduction, convection, and evaporation.

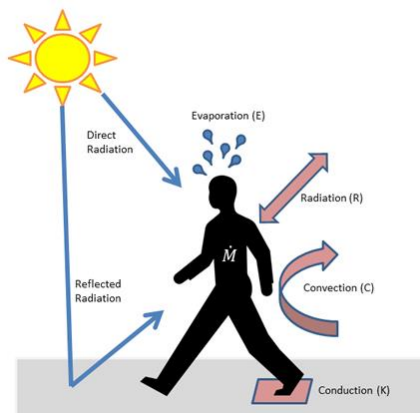


Figure 2.5.1. Heat dissipation from human body to surrounding [88].

**Radiation:** Heat dissipation by radiation takes place in the form of infrared rays and constitutes roughly 60% of the whole body heat loss. When the body temperature surpasses the ambient temperature, the body emits heat in a higher amount than it absorbs [87].

**Conduction and Convection:** Conduction-based heat loss happens either through the air, about 15% or through direct contact with a solid object, roughly 3%. Once heat is transferred to the air, it is subsequently dissipated by the movement of air currents, a process known as convection. A small degree of convection is consistently present, resulting in a 15% heat dissipation through the surrounding air via combined conduction and convection [87].

**Evaporation:** The regulation of heat loss through sweat evaporation is determined by the amount and pace of sweating, and it constitutes around 22% of the overall heat loss in the body. For every gram of water that evaporates, 0.58 kilocalories of heat is lost. Even in the absence of perspiration, water evaporates from the skin and lungs at a consistent pace of 600 to 700 mL per day, resulting in continuous dissipation of heat [87].

In order to maintain thermal equilibrium between the body and the environment, the heat transfer into the body and the heat production within the body must be balanced by heat outputs from the body. The thermal equilibrium is characterized by a dynamic balance rather than a steady

state [90]. There are various ways to express the human body's heat balance equation, but in all of them, terms relating to internal heat development, heat transit, and heat storage are present.

An equation representing the body's thermal equilibrium [90]:

$$M - W = E + R + C + K + S \quad (2.5)$$

**Heat generation within the body:** M = metabolic rate of the body.

The metabolic rate refers to a rate at which chemical energy is transformed into mechanical energy, which is used to generate work (W) and thermal energy, which leaves the body as heat (M-W).

**Heat transfer from body:** W = amount of energy that is released outside of the body in the form of mechanical work. E = Evaporation; R = Radiation; C = Convection, and K = Conduction.

**Heat storage:** S = heat storage rate.

Clothing is essential for maintaining thermal comfort by balancing the body's heat generating and heat loss. Clothing serves as a barrier that shields the heart and facilitates the transfer of body heat to the surrounding environment. It acts as the interface between the skin and the external surroundings.



Figure 2.5.2. Factor influencing thermal comfort of human [90].



The factors that influence human thermal comfort can be primarily categorized into two categories:

**Personal factor:** personal factors that influence thermal comfort include metabolism, which can be influenced by age, sex, health, and other conditions. Slight modifications in clothing layers can lead to significant variations in thermal comfort. Wearing a sweater and socks during the winter provides more comfort, whereas wearing lightweight clothing during the summer offers enhanced comfort [91].

**Environmental factors:** The environmental factors influencing thermal comfort are, air velocity, temperature of air, radiant temperature, and relative humidity. However, the extent to which this radiation heat flux may penetrate and pass through the fabric depends on factors such as the fabric structure and the wavelength of the radiation. The convective component of a heat source, however, is limited to merely reaching the surface of the cloth. The garment facilitates the passage of heat to the body by conduction and radiation, resulting in an increase in temperature and subsequent transfer into the air gap. Consequently, wearing suitable clothing, together with considering other factors in the surroundings, enhances comfort both at home and in professional settings such as corporate offices and study rooms [92].

## **2.6. Theory of Fluid Environment Analysis, Numerical Methods of Modeling and Optimization**

### **2.6.1. Navier-Stokes Equations in CFD**

Computational Fluid Dynamics (CFD) is an application of computer power to solve the governing equations and mathematically predict the flow of physical fluids [93]. In other words, CFD is a branch of science that uses computer programs to make numerical predictions about fluid flow based on the three conservation principles that govern fluid motion: momentum, mass, and energy [94]. Mathematical equations, generally in the form of partial differential equations, represent the fluid behavior in the flow domain. CFD techniques are used to illustrate the solutions and interactive behavior of solid boundaries with fluid or interaction between fluid layers during flow. CFD converts the governing differential equations of fluid flow into numerical values,

allowing for a quantitative representation of the entire fluid flow in either time or space dimensions[95]. CFD is an efficient tool for analyzing the behavior of a system. It offers numerous benefits and is particularly effective in the design process and promoting innovation [96]. Moreover, it is effective in analyzing the system's performance indicators, whether it is to increase profitability or improve operational safety, and offers several beneficial features [97].

In the context of a CFD software analysis, the computation of fluid flow and its corresponding physical attributes, including velocity, pressure, viscosity, density, and temperature, is conducted by taking into account predetermined operating conditions. To provide a precise, tangible result, these quantities are computed simultaneously [98]. Each computational fluid dynamics tool, whether it is a commercial or open source software, employs a mathematical model and numerical method to accurately forecast the intended flow phenomena. CFD tools commonly utilize the Navier-Stokes (N-S) equations [99]. Although the majority of the components in the Navier-Stokes equations stay unchanged, additional terms can be included or excluded depending on the underlying physics. If there is a requirement to take into account heat transmission, phase change, or chemical reactions, additional terms will be incorporated into the governing equations.

The Navier-Stokes equations are a set of partial differential equations that describe the motion of fluids that are incompressible. These equations are the fundamental equations of fluid mechanics [99]. When analyzing fluid flow, it is crucial to simultaneously evaluate the primary parameters of velocity, pressure, temperature, density, and viscosity. Physical phenomena, such as combustion, multiphase flow, turbulence, and mass transport, exhibit a wide range of characteristics. These characteristics can be classified into categories such as kinematic, transport, thermodynamic, and miscellaneous properties [100]. Thermo-fluid events, which are guided by governing equations, rely on the principles of conservation laws. The Navier-Stokes (N-S) equations are a widely used mathematical model for studying changes in characteristics during dynamic and/or thermal interactions. The equations can be modified according to the problem's substance and are formulated based on the concepts of mass, momentum, and energy conservation [98, 100]:

- **Conservation of Mass:** Continuity Equation
- **Conservation of Momentum:** Newton's Second Law

- **Conservation of Energy:** First Law of Thermodynamics or Energy Equation

These concepts assert that mass, momentum, and energy remain constant within a closed system. Basically, all things must be preserved. The study of fluid flow with thermal variations is dependent upon specific physical characteristics. Simultaneously, the three fundamental conservation equations must be solved to determine the three unknowns: velocity  $\vec{v}$ , pressure  $p$ , and temperature  $T$ . However,  $p$  and  $T$  are regarded as the two essential independent thermodynamic variables. The ultimate expression of the conservation equations includes four additional thermodynamic variables: density ( $\rho$ ), enthalpy ( $h$ ), viscosity ( $\mu$ ), and thermal conductivity ( $k$ ), with the last two being classified as transport characteristics. The value of  $p$  and  $T$  uniquely determine these four features. Analysis of fluid flow is necessary to determine the velocity ( $\vec{v}$ ), pressure ( $p$ ), and temperature ( $T$ ) at any point within the flow regime. Moreover, the technique of observing fluid flow by analyzing its kinematic features is a crucial concern. Fluid dynamics can be examined using either Lagrangian or Eulerian approaches [98, 100].

**Lagrangian method:** We consider each point at the start of the domain and track its trajectory until it reaches its end.

**Eulerian method:** We focus on a certain region called Control Volume inside the fluid and examine the movement of particles within it.

**Continuity Equation:**

The equation governing the principle of Conservation of Mass is defined as:

$$\frac{D\rho}{Dt} + \rho(\nabla \cdot \vec{v}) = 0 \quad (2.6.1.1)$$

Where, the variables  $\rho$  is density,  $\vec{v}$  is velocity, and  $\nabla$  is the gradient operator.

$$\vec{\nabla} = \vec{i}\frac{\partial}{\partial x} + \vec{j}\frac{\partial}{\partial y} + \vec{k}\frac{\partial}{\partial z} \quad (2.6.1.2)$$

Under constant density, the flow is considered incompressible, leading in the reduction of the continuity equation:

$$\frac{D\rho}{Dt} = 0 \xrightarrow{\text{yields}} \nabla \cdot \vec{v} = \frac{\partial u}{\partial x} + \frac{\partial v}{\partial y} + \frac{\partial w}{\partial z} = 0 \quad (2.6.1.3)$$

**Conservation of Momentum:** The equation commonly known as the Navier-Stokes Equation is expressed as follows:

$$\underbrace{\frac{\partial}{\partial t}(\rho \vec{v})}_a + \underbrace{\nabla * (\rho \vec{v} \vec{v})}_b = \underbrace{-\nabla p}_c + \underbrace{\nabla * (\tau)}_d + \underbrace{\rho \vec{g}}_e \quad (2.6.1.4)$$

Where, variables p is static pressure,  $\tau$  is viscous stress tensor, and  $\rho \vec{g}$  is the gravitational force per unit volume. In equation, term a is local change with time; b is momentum convection; c is surface force; d is diffusion term; and e is mass force.

The viscous stress tensor  $\tau$  can be defined according to Stoke's Hypothesis as follows:

$$\tau_{ij} = \mu \frac{\partial v_i}{\partial x_j} + \frac{\partial v_j}{\partial x_i} - \frac{2}{3} (\nabla * \vec{v}) \delta_{ij} \quad (2.6.1.5)$$

Assuming the fluid is incompressible and has a constant viscosity coefficient  $\mu$ , the Navier-Stokes equation can be simplified to:

$$\rho \frac{D\vec{v}}{Dt} = -\nabla p + \mu \nabla^2 \vec{v} + \rho \vec{g} \quad (2.6.1.6)$$

**Conservation of Energy:** which is the first law of thermodynamics, asserts that sum of the work and added heat to a system will correspondingly increase the system's energy.

$$dE_t = dQ + dW \quad (2.6.1.7)$$

Where, dQ represents the heat introduced into the system, dW is the work done on the system, and dE<sub>t</sub> represents the increase in the system's total energy. Following is a common form of energy equation is:

$$\rho \left[ \underbrace{\frac{\partial h}{\partial t}}_1 + \underbrace{\nabla * (h\vec{v})}_2 \right] = \underbrace{-\frac{\partial p}{\partial t}}_3 + \underbrace{\nabla * (k\nabla T)}_4 + \underbrace{\Phi}_5 \quad (2.6.1.8)$$

Where, term 1 represents local change with time; 2 is convective term; 3 is work pressure; 4 is heat flux and 5 is source term.

## 2.6.2. Partial Differential Equations (PDEs) and Discretization

The Mathematical model simply provides a systematic representation of the relationships between the transport parameters that are directly or indirectly involved in the entire process. While each item in these equations contributes to the physical event, it is important to examine changes in parameters together using the numerical solution, which involves differential equations, vector notations, and tensor notations. A partial differential equation (PDE) involves many variables and is represented by the symbol " $\partial$ ". If the equation is derived using the symbol "d", it is referred to as an Ordinary Differential Equation (ODE), which involves a single variable and its derivative. The PDEs are utilized to convert the differential operator ( $\partial$ ) into an algebraic operator in order to obtain a solution. PDEs are extensively employed to develop solutions in the disciplines of heat transfer, fluid dynamics, acoustics, electronics, and quantum mechanics [98, 101].

An example (ODE):

$$\frac{d^2x}{dt^2} = x \rightarrow x(t) \text{ Where, } t \text{ is single variable} \quad (2.6.2.1)$$

An example:

$$\frac{\partial f}{\partial x} + \frac{\partial f}{\partial y} = 5 \rightarrow f(x, y) \quad (2.6.2.2)$$

where, x and y are variables.

The importance of partial differential equations (PDEs) lies in their ability to provide solutions to governing equations. For example:

$$\frac{\partial^2 f}{\partial x^2} + \frac{\partial^2 f}{\partial y^2} = 0 \rightarrow f(x, y) \rightarrow \text{Laplace Equation} \quad (2.6.2.3)$$

Equation (2.6.1.3) and (2.6.2.3) determines the Laplace part of the continuity equation [98]. To begin solving these large equations, the following step is discretization, which initiates the numerical solution process.

**Discretization:** The numerical solution is a method that involves discretization and is employed to generate approximate solutions for complex problems that cannot be addressed using analytic

approaches. Furthermore, the precision of the numerical solution is greatly influenced by the level of the discretization. Commonly employed discretization techniques include finite difference, finite volume, finite element, spectral (element) approaches, and boundary element.

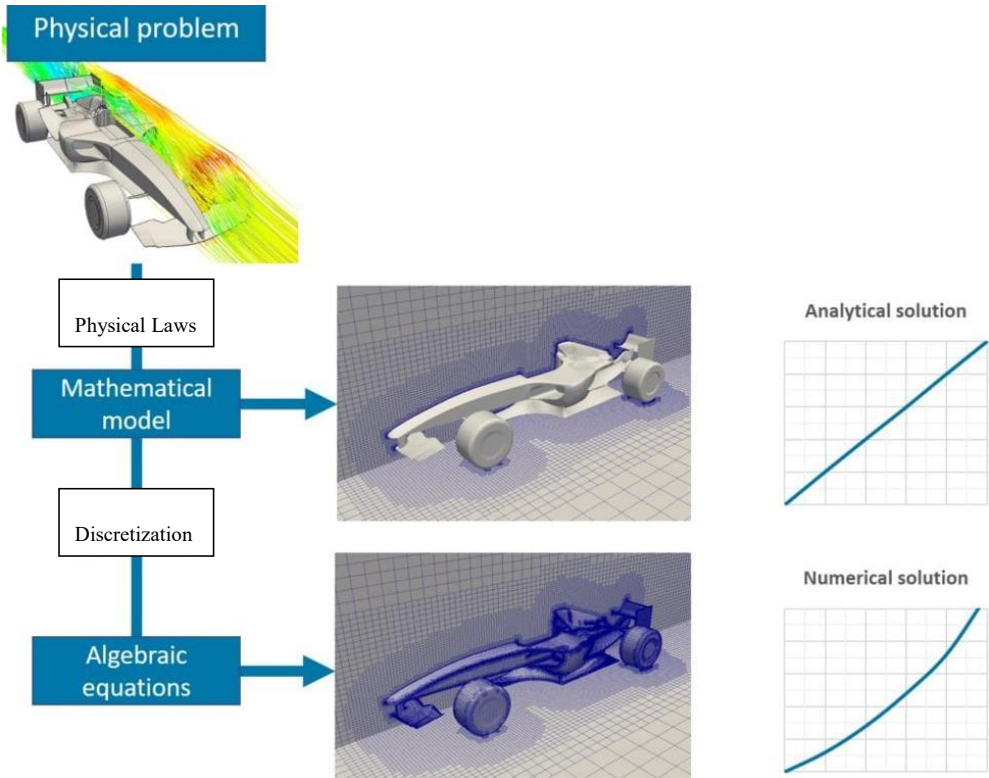


Figure 2.6.2. Solution process [98].

### 2.6.3. Numerical Methods for Discretization

To solve the governing equations of fluid motion, it is necessary to first develop its numerical version. This is achieved using a procedure known as discretization. During the discretization process, each term in the partial differential equation that describes the flow is expressed in a way that allows the computer to perform calculations. The most common methods for numerical

discretization are, finite difference method (FDM), finite element method (FEM), the finite volume method (FVM), and spectral methods [102]. These strategies generally differ in terms of their overall applicability, resilience, and computational expense. Generally speaking, Finite Element Method (FEM) is considered the most robust and widely used method. The mesh generation of this method is highly adaptable and may be customized to accommodate a wide range of geometries. The Finite Volume Method (FVM) have a lower flexibility compared to the Finite Element Method (FEM), but it offers a higher level of accuracy. Furthermore, it enables adaptation to various geometries and typically provides better results accuracy. The FDM technique provides more accurate outcomes, but its applicability is relatively limited. The main reason for this is the utilization of typical components like cubes (three-dimensional) and squares (two-dimensional), which possess limited flexibility in adapting to curved surfaces. Furthermore, the approach is susceptible to numerical instability, particularly when dealing with singularities in the solution. However, for typical geometries observed in microfluidics, the Finite Difference Method (FDM) is appropriate for achieving highly precise results. Spectral approaches are limited in their applicability to a narrow set of situations that involve periodic boundary conditions [102].

**Finite volume method (FVM):** FVM is a computational technique employed to solve elliptic, parabolic, or hyperbolic partial differential equations by converting them into algebraic equations. This method relies on the principles of conservation laws [103]. The finite volume method is a discretization technique that is highly suitable for numerically simulating different types (e.g., elliptic, parabolic, or hyperbolic) of conservation laws. It has been widely employed in various engineering disciplines, including fluid mechanics, heat and mass transfer, and petroleum engineering. The finite volume approach shares several key characteristics with the finite element method, including its applicability to arbitrary geometries, utilization of structured or unstructured meshes, and generation of robust schemes. The finite volume method exhibits local conservation properties as it employs a "balance" approach. This involves formulating a local balance equation for each discretization cell, commonly referred to as a "control volume." By applying the divergence formula, an integral representation of the fluxes across the control volume's boundary is derived. The boundary fluxes are discretized based on the discrete unknowns [103]. Similar to the FEM, the FVM builds finite or control volumes (a dual mesh) by dividing a geometrically arbitrary region into a finite number of elements (a structured or unstructured mesh). Instead of using a cell-centered approach, which involves control volumes converging with elements, as

shown in figure 2.6.3 for the two-dimensional case, a vertex-centered approach can be used to discretize the domain into control volumes. In this method, each node of the mesh is the center of a finite volume, and the boundaries of this volume are obtained by connecting the centroids of each element and the midpoints of their edges [103].

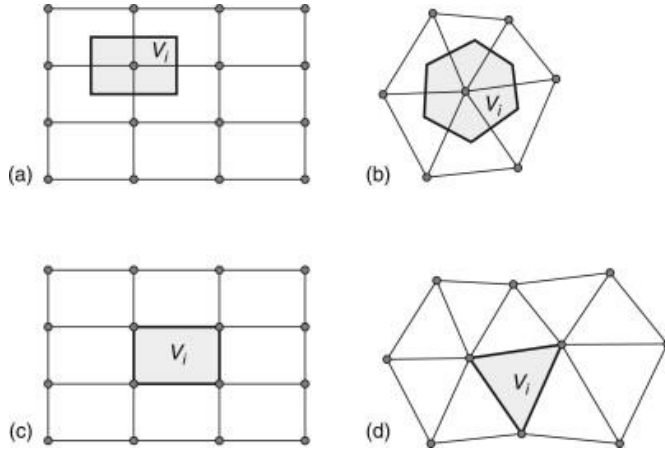


Figure 2.6.3. The concepts of mesh and dual mesh are used in vertex-centered FVM and cell-centered FVM, denoted as (a, b) and (c, d) respectively. The grey-colored areas define the control volumes. [103].

Following the domain decomposition, it is necessary to establish an integral formulation of the balancing equations and then employ sequential approximation techniques to numerically integrate the integrals for each control volume. When examining the mass transport balance for an incompressible fluid, assuming a fixed (non-deformable) mesh and excluding source terms, the conservation rule can be expressed.

$$\frac{\partial \rho}{\partial t} + \rho \nabla \cdot \mathbf{v} = 0 \quad (2.6.3.1)$$

Here,  $\rho$  represents the density and  $\mathbf{v}$  represents the velocity vector. The fundamental concept of the Finite Volume Method (FVM) is to ensure that equation (2.6.3.1) is satisfied within the small control volume defined by the computational mesh. Thus, within the  $i$ th cell, which has a volume  $V_i$  and a boundary surface  $S_i$ , the desired outcome is obtained as under.



$$\int_{V_i} \frac{\partial \rho}{\partial t} dV + \int_{V_i} \rho \nabla \cdot \rho v dV = 0 \quad (2.6.3.2)$$

The integral conservation law stated in Equation (2.6.3.2) can be reformulated by calculating the average value of the first term over the volume and using the Gauss theorem to the second term. Basic operation give,

$$\frac{d\rho_i}{dt} + \frac{1}{V_i} \oint_{S_i} \rho v \cdot n dV = 0 \quad (2.6.3.3)$$

The normal vector to  $S_i$  from  $V_i$  is given by  $n$ . Function values and derivatives can be estimated using a finite difference approach. By utilizing a first-order Euler arrangement, the outcome for the initial component of Equation (2.6.3.3) can be expressed as follows:

$$\frac{d\rho_i}{dt} \approx \left( \frac{\rho - \rho^{(n-1)}}{\Delta t} \right) \quad (2.6.3.4)$$

Here,  $\Delta t$  represents the time interval and the index  $(n - 1)$  corresponds to the prior time step. The second term can be seen as the summation extended to all integration points within the control volume. The equations corresponding to each volume are subsequently combined, yielding in a distinctive algebraic system that can be solved by numerical methods [103].

#### 2.6.4. Global Optimization

Global optimization is a field within applied mathematics and numerical analysis that aims to determine the global minimum or maximum values of a function or a group of functions within a specified set [104]. In other words, global optimization is a systematic approach that aims to identify the points that yield the lowest value for a given function within a defined domain, bounded by certain constraints [105]. The problem is generally referred to as a minimization problem because of the objective of maximizing the real-valued function  $g(x)$  is equivalent to minimizing the function  $f(x) = (-1) * g(x)$  [106]. Given a continuous function,  $f: \Omega \subset \mathbb{R}^n \rightarrow \mathbb{R}$ , which may be nonlinear and non-convex, with the global minima  $f^*$  and the set of all global minimizers  $X^*$  in  $\Omega$ , the standard minimization problem can be defined as [107]:

$$\min_{x \in \Omega} f(x)$$

That is, determining the function  $f^*$  and a global minimizer in  $X^*$ ; where  $\Omega$  is a compact set (which may not be convex) defined by inequality  $g_i(x) \geq 0$ ,  $i = 1, \dots, r$ . Global optimization differs from local optimization as it specifically aims to identify the minimum or maximum value within a given set, rather than focusing on identifying local minima or maxima. Discovering an arbitrary local minimum can be accomplished with reasonable ease by employing traditional local optimization techniques. Determining the global minimum of a function is considerably more challenging: analytical techniques are mostly not feasible, and employing numerical solution approaches frequently presents significant difficulties [107]. In the field of mathematical analysis, the maximum and minimum of a function refer to the highest and lowest values that the function can attain, respectively. Referred to as extremum, these points can be defined either within a specific range (local or relative extrema) or across the entire domain (global or absolute extrema) of a function [108].

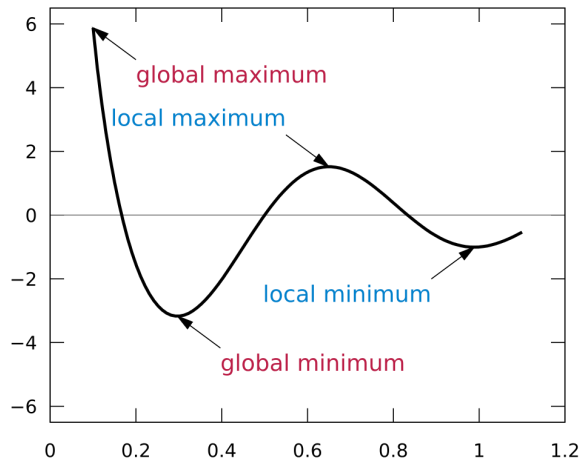


Figure 2.6.4. The local and global maxima and minima of the function  $\cos(3\pi x)/x$ ,  $0.1 \leq x \leq 1.1$  [109].

Global optimization can be achieved using deterministic and stochastic methods, respectively. Certain deterministic strategies depend on assumptions about the cost function that are challenging to verify [110].

### **Deterministic methods:**

Deterministic global optimization techniques are designed to identify the global optimum by systematically investigating the whole search space. These solutions frequently rely on mathematical models that accurately depict the problem and its limitations. Several prevalent deterministic approaches include [106, 110]:

- **Inner and outer approximation:** Both of these solutions involve approximating the set over which a function is to be optimized using polyhedra. In the context of inner approximation, the polyhedra belong to the set, but in outer approximation, the polyhedra consist of the set.
- **Branch and bound methods:** It is an approach for solving discrete and combinatorial optimization problems in algorithm design. A branch-and-bound approach involves systematically exploring potential solutions through a search of the state space. The set of potential solutions is represented as a rooted tree, with the complete set at the root. The algorithm examines the branches of this tree, which correspond to subsets of the solution set. Prior to listing the potential solutions of a branch, the branch is evaluated against upper and lower estimated bounds on the optimal solution. If the branch is unable to generate an effective solution compared to the best one discovered so far by the algorithm, it is discarded.
- **Cutting-plane method:** It refers to a collection of optimization techniques that systematically improve a set of possible solutions or an objective function using linear inequalities known as cuts. These approaches are commonly employed to discover whole number solutions for mixed integer linear programming (MILP) issues, as well as solving generic convex optimization problems that may not necessarily be differentiable.
- **Interval methods:** It is also known as interval arithmetic, interval mathematics, interval analysis, or interval computation, is a mathematical technique that has been developed by mathematicians since the 1950s and 1960s. Its purpose is to establish limits on rounding errors and measurement errors in mathematical calculations. By doing so, it enables the development of numerical methods that produce reliable and accurate outcomes. Interval arithmetic facilitates the discovery of accurate and reliable solutions to equations and optimization problems.

### **Stochastic methods:**

Stochastic optimization (SO) methods are optimization techniques which forms and utilize random variables. In stochastic problems, the optimization problem incorporates random variables, which can be found in the formulation of the problem. These random variables can be in the form of random objective functions or random constraints. Stochastic optimization approaches include techniques that involve the use of random iterates. Certain stochastic optimization techniques employ random iterations to tackle stochastic problems, effectively integrating both aspects of stochastic optimization [111]. Some of common methods are as under [106]:

- **Direct Monte-Carlo sampling:** It involves utilizing random simulations to provide an approximate solution. The traveling salesman problem is referred to as a conventional optimization problem. In other words, all the relevant information (distances between each destination point) required to calculate the most efficient route is known with absolute accuracy. The objective is to evaluate the various travel options and select the one that results in the shortest overall distance. However, let's say that instead of aiming to decrease the overall distance traveled to reach each desired location, our goal is to minimize the total time required to reach each destination. This surpasses traditional optimization methods as trip time is fundamentally unpredictable due to factors such as traffic congestion and time of day. In order to ascertain the most advantageous route, it is advisable to employ simulation-optimization techniques. This approach involves initially understanding the possible time intervals required to travel between two points, which are represented by a probability distribution rather than a precise distance. Subsequently, travel decisions can be optimized by considering this uncertainty, thereby determining the optimal path to follow.
- **Stochastic tunneling (STUN):** It is a global optimization technique that utilizes the Monte Carlo method [112] to sample a nonlinearly transformed function. This enables easier movement between regions that contain the minimum values of the function, with the purpose of minimizing the function. Easier tunneling facilitates faster exploration of the sample space and accelerated convergence towards an optimal solution.
- **Parallel tempering:** It is often referred to as replica exchange Markov chain Monte Carlo (MCMC) sampling, is a simulation technique designed to enhance the dynamic characteristics of Monte Carlo method simulations of physical systems, as well as MCMC

sampling methods in general. Sugita and Okamoto developed a molecular dynamics approach for parallel tempering [112]. This method is commonly referred to as replica-exchange molecular dynamics, or REMD. In essence, the system is repeated N times, each with a random initial state, and operated at various temperatures. Subsequently, in accordance with the Metropolis criterion, one swaps configurations at varying temperatures. The objective of this technology is to enable the utilization of high temperature settings in low temperature simulations and vice versa. This leads to a very resilient ensemble that can effectively sample configurations with both low and high energy levels. By employing this approach, it is possible to accurately calculate thermodynamic parameters, such as specific heat, which is typically challenging to quantify using the simulated annealing.

#### **Metamodeling approach:**

Metamodels, often referred to as approximations, response surfaces, or surrogate models, are utilized to reduce the time needed for optimization due to the computationally intensive procedures involved in solving complete models [113]. CFD simulations, which are time-consuming, are commonly used as the basis for designing systems that involve fluid flows. The Efficient Global Optimization (EGO) technique [114, 115], which uses Kriging, is commonly used to solve deterministic optimization problems that involve complex models [116, 117]. For computationally intensive simulations, Kriging or Gaussian Process (GP) regression has gained popularity as a metamodeling method because it offers surfaces with variable complexity (potentially interpolative) within a probabilistic framework [118]. This approach is used in software KEDRO [119] to find global minimum or maximum of a given problem with approximation and optimization. Global optimization techniques are employed across various domains such as engineering, economics, finance, and machine learning.

### **2.6.5. Polynomial Approximation and Interpolation**

Interpolation refers to the task of determining a curve that intersects a specified set of real values at actual data points, sometimes referred to as abscissae or nodes. The theory of interpolation is crucial as a foundation for numerical integration, sometimes referred to as quadrature. On the

contrary, approximation theory aims at minimizing the error norm by finding a suitable approximation. The degree of an interpolating polynomial can be enhanced by adding additional points and more terms. The accuracy of an interpolation polynomial depends on how far the point of interest is from the middle of the interpolation points utilized [120]. Numerical mathematics focuses on the estimation or approximation solution of mathematical issues. There are several branches of mathematics that focus on numerical calculations, such as numerical mathematics, numerical linear algebra, numerical solution of nonlinear equations, and approximation and interpolation methods. In order to utilize the techniques of numerical mathematics, it is essential to understand and analyze the error estimation [120].

**Approximation:** Approximation implies "bringing something close enough". When we want to replace anything complicated with something simple, we utilize this word [121]. By approximation, we get a functions that pass through a set of data in the best possible way, without the necessity to pass exactly through the provided positions. The approximation is applicable to datasets of significant size, well-organized datasets, and datasets with both low and large degrees of scatter. Approximation comes in two distinct forms. We possess knowledge about the function  $f$ , but, its structure is intricate and challenging to determine. For this scenario, we opt for the utilization of the function information. The error of the resulting approximation can be assessed in relation to the actual value of the function [121]. The polynomial approximation involves constructing a polynomial that is capable of replacing another function or a given set of points. By utilizing a collection of points, we may employ a matrix equation that efficiently performs the necessary calculations [122].

$$\begin{bmatrix} n & \sum_{k=1}^n x_k & \sum_{k=1}^n x_k^2 \\ \sum_{k=1}^n x_k & \sum_{k=1}^n x_k^2 & \sum_{k=1}^n x_k^3 \\ \sum_{k=1}^n x_k^2 & \sum_{k=1}^n x_k^3 & \sum_{k=1}^n x_k^4 \end{bmatrix} \begin{bmatrix} a_0 \\ a_1 \\ a_2 \end{bmatrix} = \begin{bmatrix} \sum_{k=1}^n y_k \\ \sum_{k=1}^n y_k x_k \\ \sum_{k=1}^n y_k x_k^2 \end{bmatrix}$$

$$P(x) = a_2x^2 + a_1x + a_0$$

The matrix originates from the orthogonality concept. Essentially, our objective is to minimize the squared difference between the polynomial and the given points, making it a minimization problem. However, based on the orthogonality principle, the position at which the sum of squared residuals is minimized is also the point where all the residuals, when combined into a single vector, are perpendicular to the vector of polynomial values [122].

Polynomial regression is a statistical technique that models the relationship between the independent variable  $x$  and the dependent variable  $y$  as a polynomial function of degree  $n$ . Polynomial regression is a method used to model a non-linear relationship between the value of  $x$  and  $y$ , which is represented as  $E(y | x)$ . Polynomial regression, despite modeling a nonlinear relationship between variables, is considered a linear statistical estimation issue. This is because the regression function  $E(y | x)$ , which represents the expected value of  $y$  given  $x$ , is linear with respect to the unknown parameters that are estimated using the available data [122].

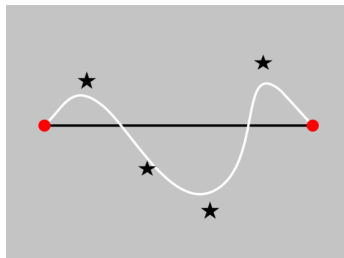


Figure 2.6.5.1. Approximation [123].

**Interpolation:** The term "interpolation" originates from Latin and can be broadly defined as the process of "smoothing things in between". Interpolation is a method used to determine values that lie between a given set of points [121]. In the context of interpolation, the task of finding the function  $f$  is referred to as the interpolation problem, while the specified points and  $x_i$  are referred to as nodes (base points or interpolation points). The selection of function  $f$  is based on the characteristics of the model, while ensuring that its calculation is relatively simple. These functions typically consist of polynomials, trigonometric functions, exponential functions, and, more recently, rational functions [121]. Polynomial interpolation involves determining a polynomial function that precisely passes into the desired points. You can add and remove points, but you can't select a polynomial degree as it depends on the number of points [123].

$$\begin{bmatrix} 1 & x_1 & x_1^2 & x_1^3 & x_1^4 & x_1^5 \\ 1 & x_2 & x_2^2 & x_2^3 & x_2^4 & x_2^5 \\ 1 & x_3 & x_3^2 & x_3^3 & x_3^4 & x_3^5 \\ 1 & x_4 & x_4^2 & x_4^3 & x_4^4 & x_4^5 \\ 1 & x_5 & x_5^2 & x_5^3 & x_5^4 & x_5^5 \\ 1 & x_6 & x_6^2 & x_6^3 & x_6^4 & x_6^5 \end{bmatrix} \begin{bmatrix} a_0 \\ a_1 \\ a_2 \\ a_3 \\ a_4 \\ a_5 \end{bmatrix} = \begin{bmatrix} y_1 \\ y_2 \\ y_3 \\ y_4 \\ y_5 \\ y_6 \end{bmatrix}$$

$$P(x) = a_5x^5 + a_4x^4 + a_3x^3 + a_2x^2 + a_1x + a_0$$

This is known as Vandermonde matrix [124], which is derived from the basic insight that if a polynomial passes through a point  $(x_i, y_i)$ , then evaluating the polynomial at  $x_i$  will yield  $y_i$ . Simply write it for each point and organize them in matrix format [121].



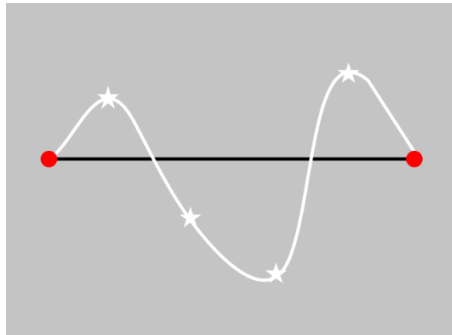


Figure 2.6.5.2. Interpolation [123].

A question may arise, if it is possible to have a polynomial function that passes through specific points and also provides a close approximation for the other data points. The answer can be yes. However, it is worth noting that there is no readily available concise algorithm to accomplish this task. Therefore, the options at hand are either resorting to numerical methods or employing a hack.

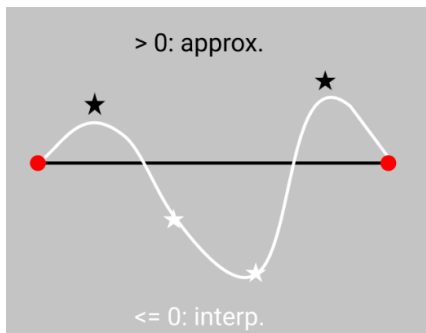


Figure 2.6.5.3. Combination of approximation and interpolation [123].

We know that the degree of the interpolating polynomial can exceed the number of points in a given set. We can capitalize on that. We can construct a Vandermonde matrix using all the given interpolating points, and add it with additional imaginary points to ensure the matrix is square. Following that, we could use the imaginary ones as variables for any numerical optimizer, which will then determine the optimal solution for us. We will have an approximating and interpolating polynomial after the optimizer has finished [121].

## **2.7. Conclusions of Literature Review**

1. The main disadvantages of most of personal protective clothing with the external cooling system is that they make structure bulky which makes garments heavy and uncomfortable to wear.
2. In addition, their cooling efficiency is not steady and reliable for personal clothing cooling devices. This demands the need for more advanced technological solutions in this field.
3. This necessitates the development of novel technical solutions to enhance clothing ventilation and comfort.
4. This chapter provides comprehensive information on subjects such as clothing insulation and the thermal comfort of the human body. It also discusses the use of computational fluid dynamics (CFD) for numerical simulation, as well as techniques for approximation and optimization of the results.

### 3. ANALYSIS OF THE STUDIED OBJECT (CLOTHING) AND FLUID FLOW MODEL: SOLIDWORKS FLOW SIMULATION

In order to analyze and understand the interaction of fluid flow, a simple cylindrical model of a solid body and jacket is being utilized. The model's schematic diagram is shown in figure 3. The dimensions of the model are selected randomly in this study, since the main aim is to understand the flow simulation process and study fluid interaction with the model. For the numerical analysis, SolidWorks flow simulation tool is used.

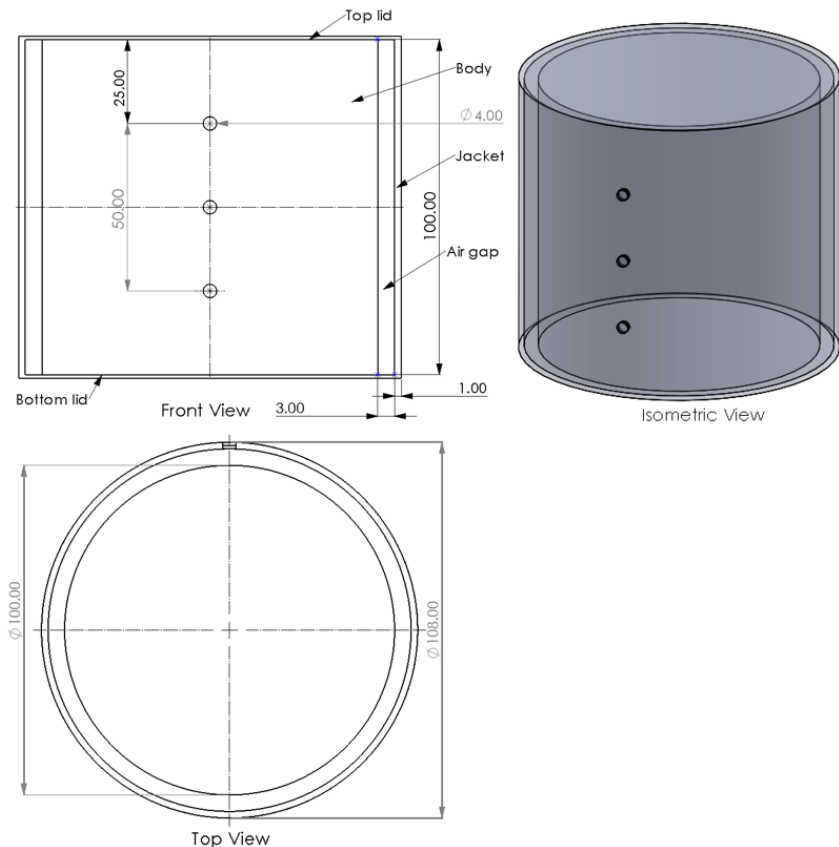


Figure 3. Schematic diagram of cylindrical model.

### 3.1. Boundary Conditions of Ventilation Model

This is a transient study. In the simulation study, heat conduction and convection are considered with physical time of 1 second. The physical time is selected smaller to save computation time. Furthermore, gravity is taken into consideration. The study fluid is the air with laminar and turbulent characteristics. The next step is to select initial boundary condition of the study. Here the inlet air velocity of 5 m/s is set for the study. Inlets are three ventilation holes of 4 mm diameters in this study, while outlet is assigned at the bottom lid with environmental pressure condition (figure 3.1.1). The air temperature of 20 °C and pressure of 101325 Pa is considered. The top part of the model is considered as air tight, means air can only pass through the bottom part of the model. Inlet velocity at the ventilation holes is shown with red arrows and outlet boundary condition with environment pressure is shown in blue arrow in figure 3.1.1. The heat generation rate of body is considered as 200W, under normal walking condition [125]. The normal average body temperature is taken as 36.5 °C.

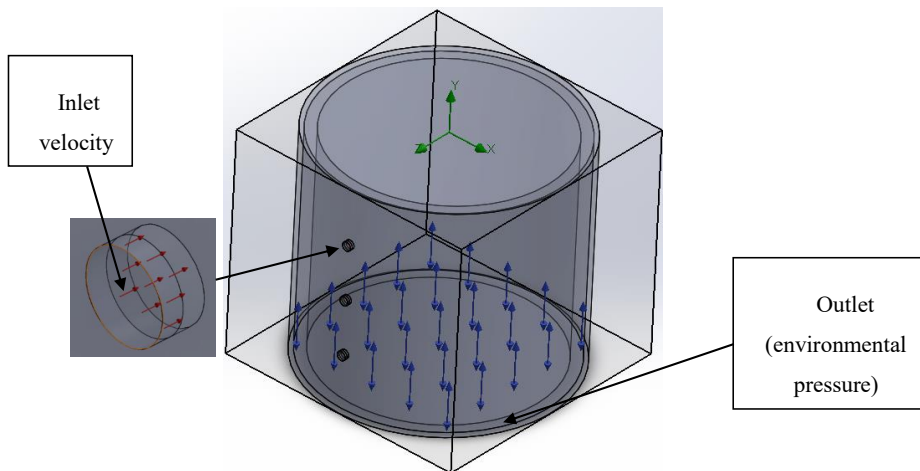


Figure 3.1.1. Computational domain with initial conditions (cylindrical model).

In the present study basic mesh of size ( $N_x=28$ ,  $N_y=24$ ,  $N_z=28$ ) is employed in the flow simulation study as using fine mesh extensively increases computational time. The model is simulated to obtain results for the flow pressure and the surface temperature of the body. Flow

pressure is calculated in the air gap between jacket and body, once air enters through the ventilation holes.

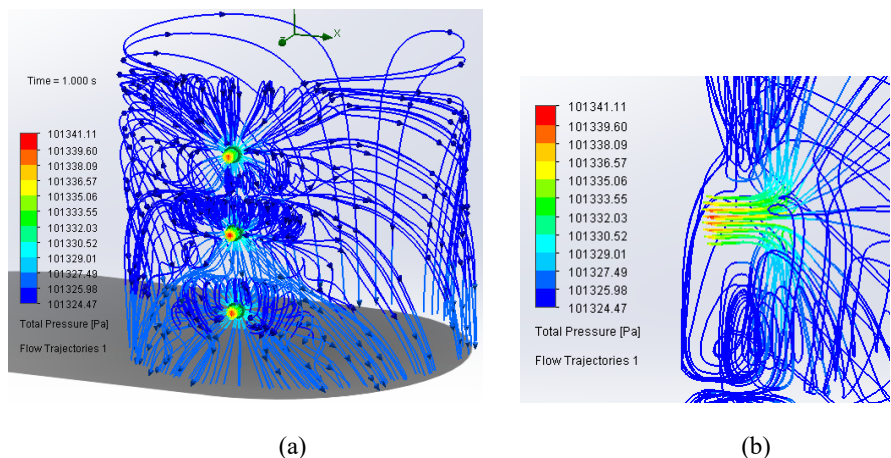


Figure 3.1.2. Flow pressure plot: Pressure distribution in air gap: (a); Pressure variation in over entire model. (b). Pressure variation near ventilation hole.

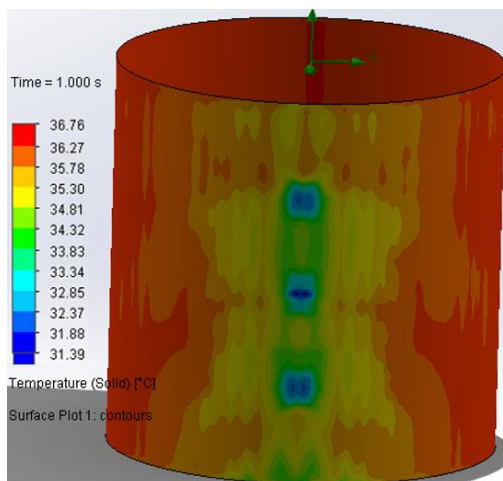
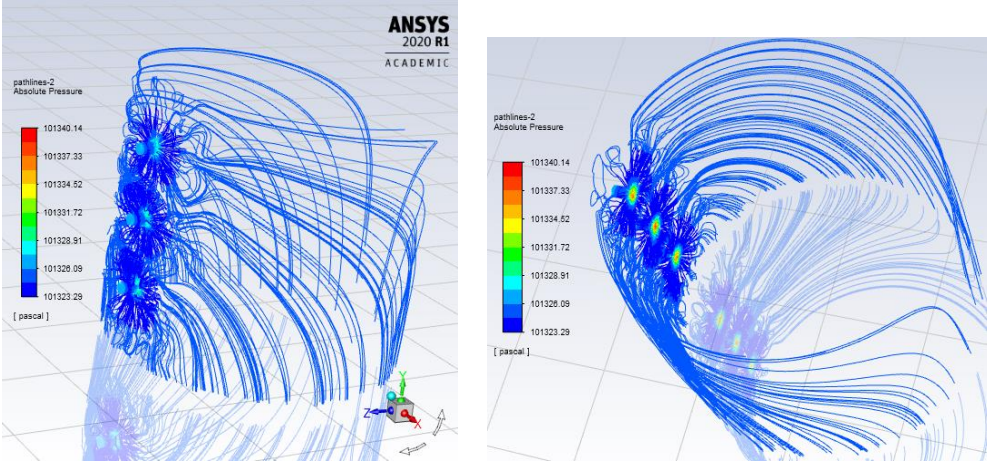


Figure 3.1.3. Surface temperature of body.

From the pressure plot in the figure 3.1.2 (a), it can be visible that air pressure is higher at the inlet which is decreases gradually once it enters into the gap between body and the jacket. This

pressure variation mostly occurs at the inlet which can be observed in figure 3.1.2 (b), while in rest of part it remains uniform, as observed in figure 3.1.2 (a). Figure 3.1.3 shows surface temperature variation over the body due to ventilation effect. The lowest temperature is at ventilation hole, though it's in very small area. The highest temperature observed is 36.76 °C, which is 0.26 °C higher than initially set body temperature of 36.50 °C. This is because we have applied heat generation rate of 200W in the study, which is excess heat generated due to normal walking condition. It is important to note here that the obtained results can be differ at different time intervals since this is a transient process. Moreover, it is also important at initial stage to understand and check reliability of the obtained results. To check the reliability of the results, the ANSYS software is used to perform the same analysis using the same model and boundary conditions. The outcomes derived from the ANSYS software are displayed below.



(a) (b)  
Figure 3.1.4. Flow pressure plots, ANSYS: (a) Front view. (b) Back view.

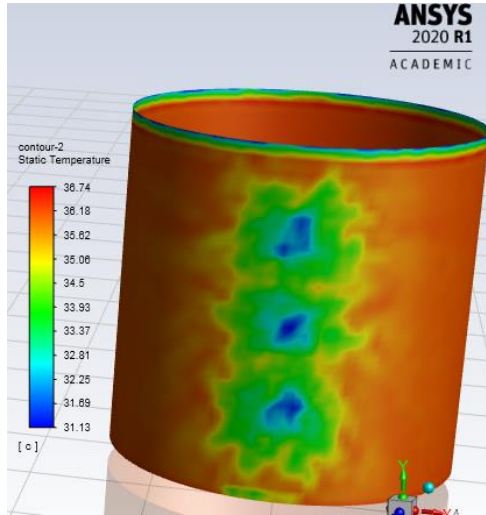


Figure 3.1.5. Surface temperature plot, ANSYS.

Figure 3.1.4 shows pressure plots from the front and side views. The results obtained here are similar to those of SolidWorks, with a difference in the value of  $\Delta P$  of only 0.21 Pa in both cases. It is visible from the pressure plots that the majority of pressure fluctuations occur at the inlets, while the pressure remains stable in the rest of the part in both scenarios. The detail numerical comparison of results obtained in the SolidWorks and ANSYS is shown in table 3.1.

Table 3.1.

Numerical results comparison; SolidWorks v/s ANSYS

	Pressure [Pa]			Body Surface Temperature [°C]		
	Minimum	Maximum	$\Delta P$	Minimum	Maximum	$\Delta T$
<b>ANSYS</b>	101323.29	101340.14	16.85	31.13	36.74	5.61
<b>SolidWorks</b>	101324.47	101341.11	16.64	31.39	36.76	5.37

In the table 3.1,  $\Delta P$  and  $\Delta T$  refers to pressure difference and temperature difference respectively. The achieved pressure range is very close with minor variation. The range of surface temperature

values obtained in ANSYS is also close to that in SolidWorks. The differences in the results obtained for  $\Delta P$  is 1.25% and for  $\Delta T$  is 4.37%, which is within an acceptable tolerance as the difference is less than 5%. This difference can be due to the method of discretization as it has higher impact on the simulation results. SolidWorks and ANSYS use different element types for the process of meshing. The element used in ANSYS is a 20-node hexahedral solid element, while the element in SolidWorks is cubic.

### **3.2. Analysis of Different Simple Shapes of Ventilation Elements**

Climate change has increased the need for more active cooling of the human body, even in the temperate climate zone. In hotter environments or during intense activity, the human body generates a significant amount of heat that needs to be removed to prevent potential danger of overheating of body [126]. When the human body temperature exceeds a certain threshold, sweating begins. This process is a result of the body's natural thermoregulation, where the heat emitted by the body is utilized through the evaporation of liquid [127]. The evaporation intensity is determined by the air circulation and the relative humidity at the body's surface. In order to enhance perspiration in the space between the body and clothing, it is necessary to remove moist air or fully saturated vapor from the body [128]. There are many venting methods for clothing [129], including various vents, the use of mesh fabric in various areas of clothing, and others, but they often do not fully ensure efficient air exchange and safety from several external environmental conditions. When a dense fabric is utilized to provide mechanical protection against harsh weather conditions such as sun radiation, dust, rain, insect access, and bites, the outer layer of the clothing may lack sufficient air permeability. Consequently, the accumulation of warm, humid air around the body can lead to discomfort or perhaps result in the body overheating.

The study involves the design of five ventilation elements, labeled E1 to E5. The pressure, temperature, and heat flux are determined using SolidWorks Flow Simulation tool. The calculations are performed at three distinct inlet air velocities: 2 m/s, 5 m/s, and 8 m/s. The results are evaluated and examined based on heat flux, pressure difference, and temperature difference. The primary goal is to determine which element's geometric shape results in the least amount of flow energy



loss in the flow channel of the element. Higher pressure differences result in increased flow energy losses, which may lead to a decrease in body cooling. The obtained results indicate that how different shapes of ventilation elements can affect the flow pressure difference and flow energy losses.

**Model and Components for the Analysis:**

In order to simplify the problem in this study, a basic elliptical shape model of the jacket and body is created. The body is positioned at the center, with the jacket placed over it, maintaining a consistent gap of 2.2 mm between them. Figure 3.2.1 displays the schematic illustration of the model. The jacket has one inlet ventilation hole with a diameter of 2 mm on the front side, and 10 outlet holes with a diameter of 4 mm on the back side.

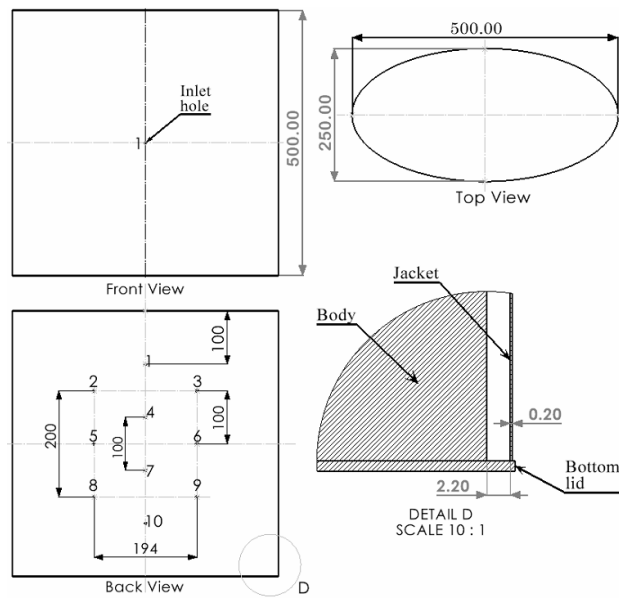


Figure 3.2.1. Elliptical model of body and jacket.

In this study, five different ventilation elements are utilized to examine and compare the efficiency of each shape. Figure 3.2.2 illustrates the shape and nomenclature of each ventilation component. The position of the ventilation element relative to the jacket's inlet hole is denoted by a circular symbol in figure 3.2.2. The shapes of element E4 and E5 are circular, but they have

different curvatures. The main difference is that E4 is attached tangent to the intake hole, whereas E5 is attached concentrically to the inlet hole.

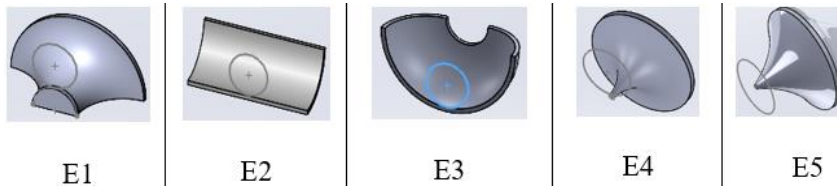


Figure 3.2.2. Different simple shapes of ventilation elements.

The study is conducted at intake air velocities of 2, 5, and 8 m/s. The investigation sets standard parameters for the initial boundary conditions as an air temperature of 20 °C and an atmosphere pressure of 101325 Pa. In the simulation study, the jacket and body are assigned separate materials with specific material properties. The analysis considers the same material properties as the jacket for all ventilation elements. The properties of these materials are presented in table 3.2.1. The initial boundary conditions in the study are same as described in section 3.1.

Table 3.2.1.

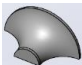
Material properties [130, 131]

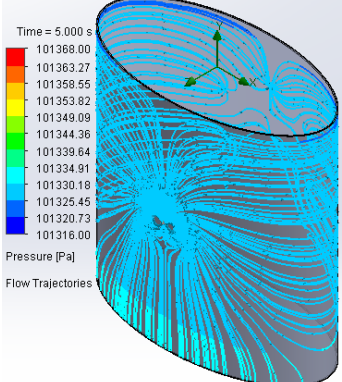
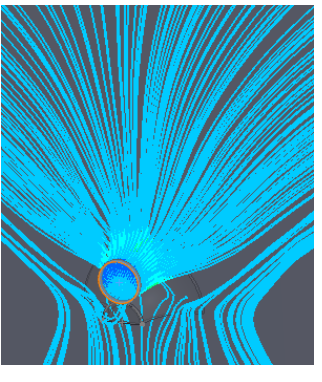
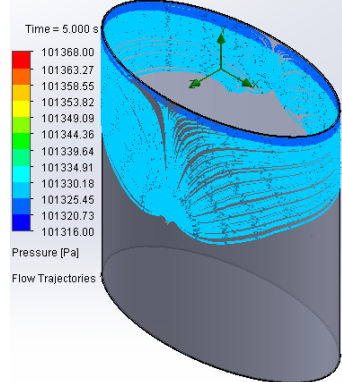
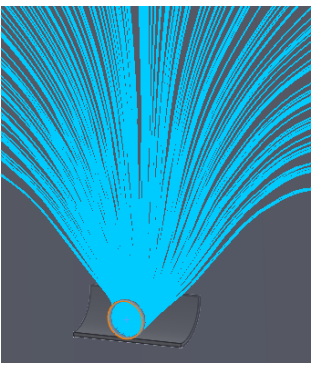
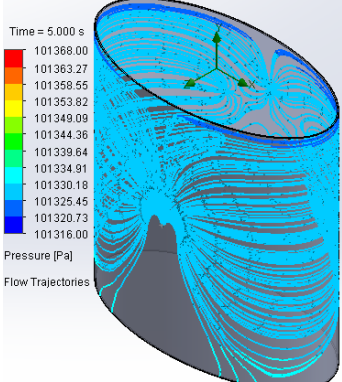
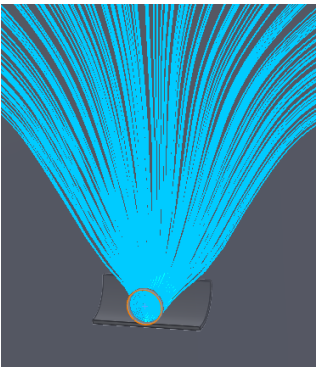
Material property	Human body	Jacket
Average density [kg/m <sup>3</sup> ]	985	1420
Specific heat [J/kg. K]	3600	1140
Thermal conductivity [W/m. K]	0.21	0.261

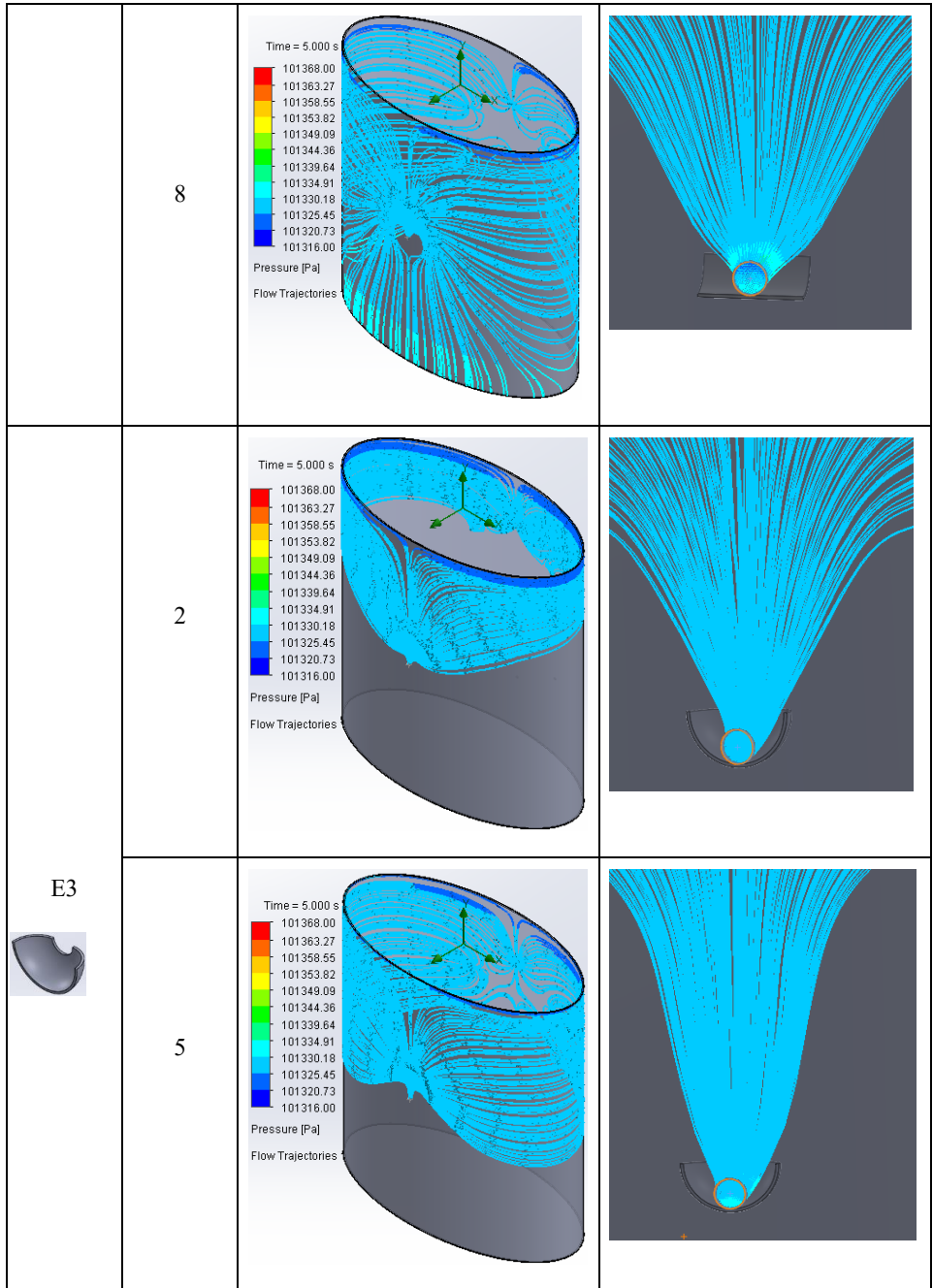
## Results and Discussion:

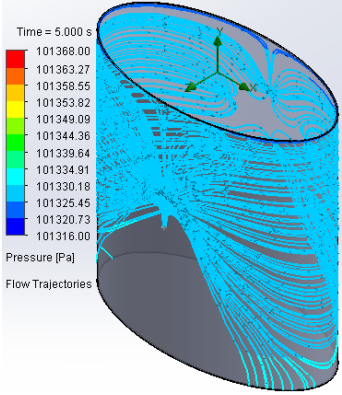
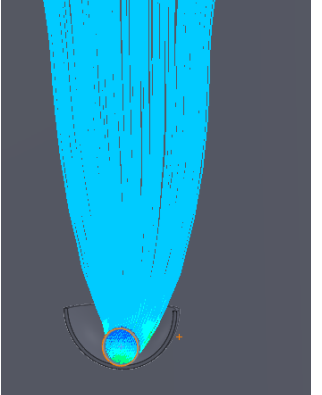
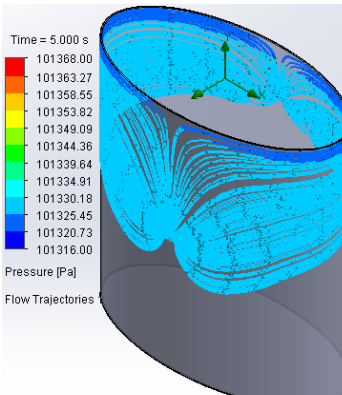
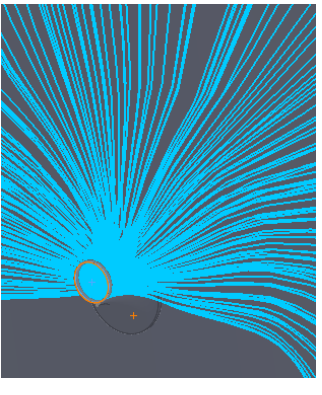

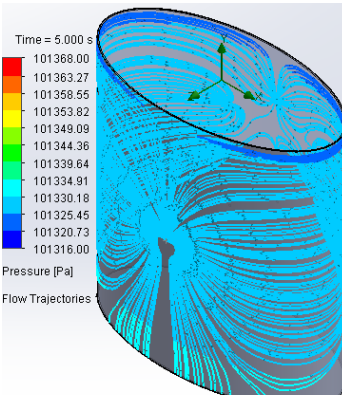
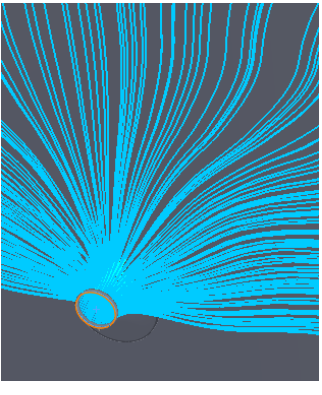
The results are presented for the physical time of 5 seconds. Moreover, difference in the obtained results for each element would be almost same at any specific time; hence, to reduce computational time, smaller physical time of 5 seconds is selected for the study. Here, the basic mesh is employed to save computational time. This study involves comparative analysis of five

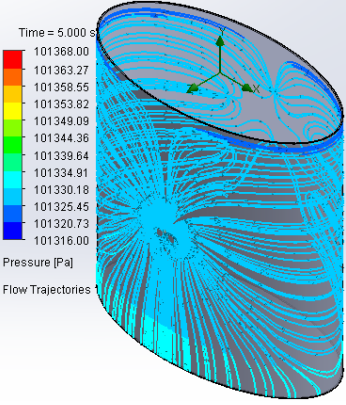
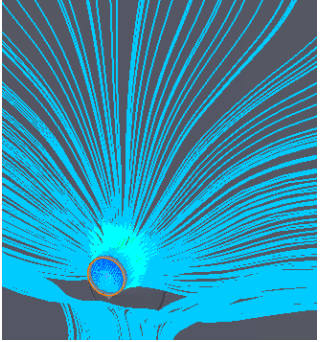
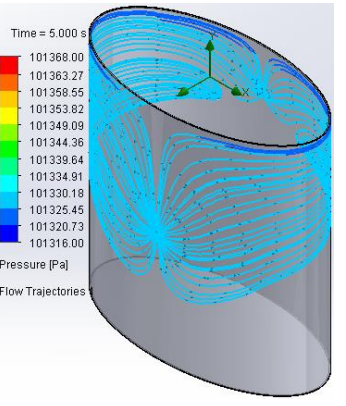
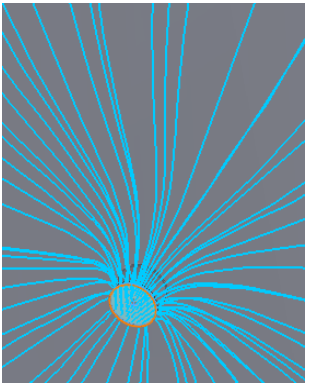

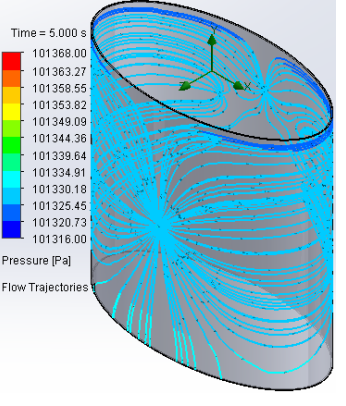
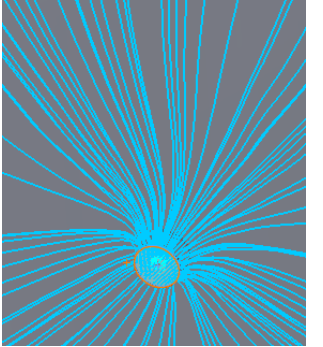
different elements that shares the same set of values in the numerical simulation. Thus, the difference in the results at a given mesh level would be almost same as we are using the same values and boundary conditions in each case. Therefore, the final outcome of the study will not be significantly influenced by it.

Element	Velocity [m/s]	Pressure Plots [Pa]	
E1 	2	<p>Time = 5,000 s</p> <p>101368.00 101363.27 101358.55 101353.82 101349.09 101344.36 101339.64 101334.91 101330.18 101325.45 101320.73 101316.00</p> <p>Pressure [Pa]</p> <p>Flow Trajectories</p>	
	5	<p>Time = 5,000 s</p> <p>101368.00 101363.27 101358.55 101353.82 101349.09 101344.36 101339.64 101334.91 101330.18 101325.45 101320.73 101316.00</p> <p>Pressure [Pa]</p> <p>Flow Trajectories</p>	

	8	<p>Time = 5.000 s</p>  <p>101368.00 101363.27 101358.55 101353.82 101349.09 101344.36 101339.64 101334.91 101330.18 101325.45 101320.73 101316.00</p> <p>Pressure [Pa]</p> <p>Flow Trajectories</p>	
	2	<p>Time = 5.000 s</p>  <p>101368.00 101363.27 101358.55 101353.82 101349.09 101344.36 101339.64 101334.91 101330.18 101325.45 101320.73 101316.00</p> <p>Pressure [Pa]</p> <p>Flow Trajectories</p>	
E2	5	<p>Time = 5.000 s</p>  <p>101368.00 101363.27 101358.55 101353.82 101349.09 101344.36 101339.64 101334.91 101330.18 101325.45 101320.73 101316.00</p> <p>Pressure [Pa]</p> <p>Flow Trajectories</p>	



	8	<p>Time = 5,000 s</p>  <p>101368.00 101363.27 101358.55 101353.82 101349.09 101344.36 101339.64 101334.91 101330.18 101325.45 101320.73 101316.00</p> <p>Pressure [Pa] Flow Trajectories</p>	
	2	<p>Time = 5,000 s</p>  <p>101368.00 101363.27 101358.55 101353.82 101349.09 101344.36 101339.64 101334.91 101330.18 101325.45 101320.73 101316.00</p> <p>Pressure [Pa] Flow Trajectories</p>	
<p>E4</p> 	5	<p>Time = 5,000 s</p>  <p>101368.00 101363.27 101358.55 101353.82 101349.09 101344.36 101339.64 101334.91 101330.18 101325.45 101320.73 101316.00</p> <p>Pressure [Pa] Flow Trajectories</p>	

	8	<p>Time = 5.000 s</p>  <p>Pressure [Pa]</p> <p>Flow Trajectories</p>	
E5	2	<p>Time = 5.000 s</p>  <p>Pressure [Pa]</p> <p>Flow Trajectories</p>	
	5	<p>Time = 5.000 s</p>  <p>Pressure [Pa]</p> <p>Flow Trajectories</p>	



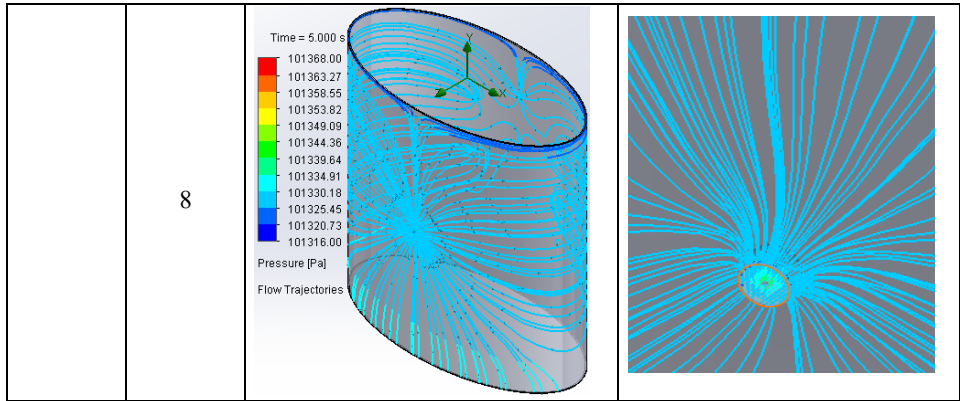
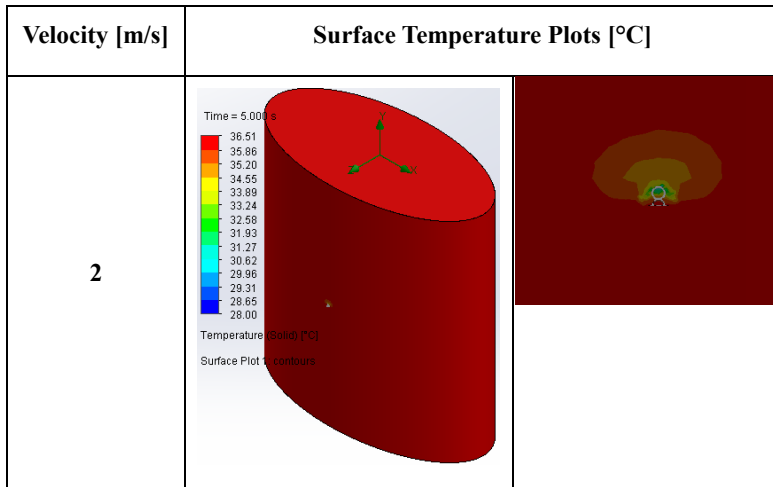


Figure 3.2.3. Flow pressure trajectories (E1 to E5).

The pressure distribution for each ventilation element at various inflow velocities is depicted in the figure 3.2.3. To ensure a fair comparison of the pressure distribution across all indicated cases, a uniform scale is employed in each pressure plot, and the associated pressure values are provided in Table 3.2.2. The image in the right column of figure 3.2.3 provides an enlarged views of the ventilation hole, specifically highlighting the impact of ventilation elements on the flow path and pressure distribution at different air velocities. The image in the left column depicts an isometric representation of the pressure distribution across the whole model. The same color scale is used in all the picture for easy comparison.





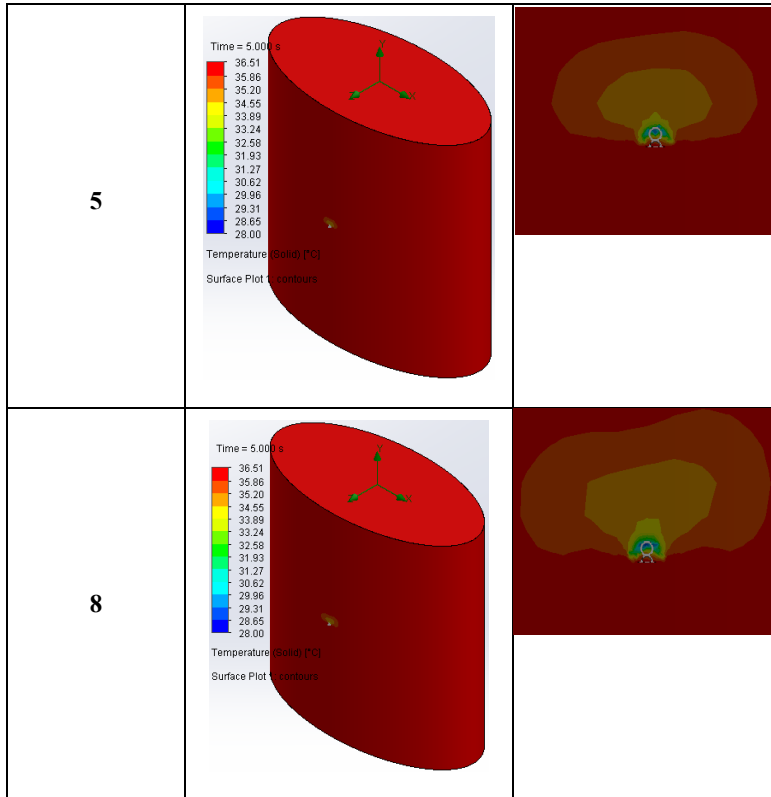


Figure 3.2.4. Surface temperature of body for E1.

The temperature plots for ventilation element E1 are displayed in figure 3.2.4. The left column illustrates the temperature distribution across the full solid body model, while the right column provides a zoomed-in view of the ventilation hole for a clearer perception of the temperature distribution in that area. Similarly, temperature plots for other ventilation elements are analyzed, and the resulting values are shown in Table 3.2.2. The temperature charts clearly demonstrate that as the inlet velocity increases from 2 to 8 m/s, the cooling coverage area increases further to the ventilation hole. This pattern is also applicable to other ventilation elements listed.

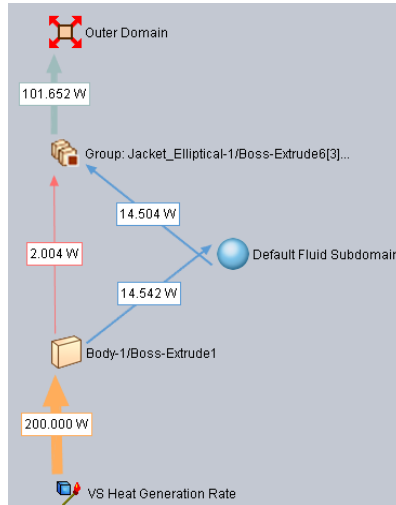


Figure 3.2.5. Flux plot for E1 at 2 m/s.

In the figure 3.2.5, Body-1/Boss-Extrude1 and Jacket\_Elliptical-1 are references to the human body and jacket model respectively, while the Default Fluid Subdomain refers to the study fluid (air). The Outer Domain, in the flux plot depicts the amount of heat lost into the environment. As illustrated in figure 3.2.5, the flux plots are used to compute the rate of heat transfer in each case.

Table 3.2.2.

Numerical values of results

Elements	Inlet Velocity [m/s]	Values	Pressure [Pa]	Surface Temperature [°C]
	2	Max	101329.45	36.50
		Min	101325.22	30.64
		Avg.	101328.06	36.50
		Max	101336.79	36.50

E1	5	Min	101325.25	29.30
		Avg.	101328.06	36.50
	8	Max	101349.03	36.50
		Min	101321.09	28.74
		Avg.	101328.09	36.50
E2	2	Max	101329.01	36.50
		Min	101325.22	32.78
		Avg.	101328.05	36.50
	5	Max	101333.80	36.50
		Min	101325.24	31.77
		Avg.	101328.04	36.50
	8	Max	101342.91	36.50
		Min	101323.10	31.17
		Avg.	101328.09	36.50
E3	2	Max	101329.28	36.50
		Min	101325.22	33.01
		Avg.	101328.05	36.50
	5	Max	101335.30	36.50
		Min	101325.16	31.86

		Avg.	101328.11	36.50
	8	Max	101344.94	36.50
		Min	101321.96	31.21
		Avg.	101328.12	36.50
E4	2	Max	101329.25	36.50
		Min	101325.19	32.69
		Avg.	101328.01	36.50
	5	Max	101335.55	36.50
		Min	101325.24	31.62
		Avg.	101328.03	36.50
	8	Max	101347.70	36.50
		Min	101322.24	31.22
		Avg.	101328.04	36.50
E5	2	Max	101329.28	36.50
		Min	101325.26	33.35
		Avg.	101328.04	36.50
	5	Max	101332.25	36.50
		Min	101325.27	32.89
		Avg.	101328.06	36.50

	8	Max	101338.54	36.50
Min		101325.14	32.77	
Avg.		101328.08	36.50	

Table 3.2.2 displays the detail values of obtained results. The terms "Max," "Min," and "Avg" in the table correspond to the maximum, minimum, and average values of the results, respectively. The provided temperature value represents the surface temperature of the body. The pressure and temperature difference are calculated from both the maximum and minimum values recorded in table 3.2.2, whereas the heat flux is determined based on the flux plot depicted in figure 3.2.5. The acquired values of heat transfer, pressure difference, and temperature difference are utilized to assess the efficiency of ventilation elements and to recommend the most effective element out of five.

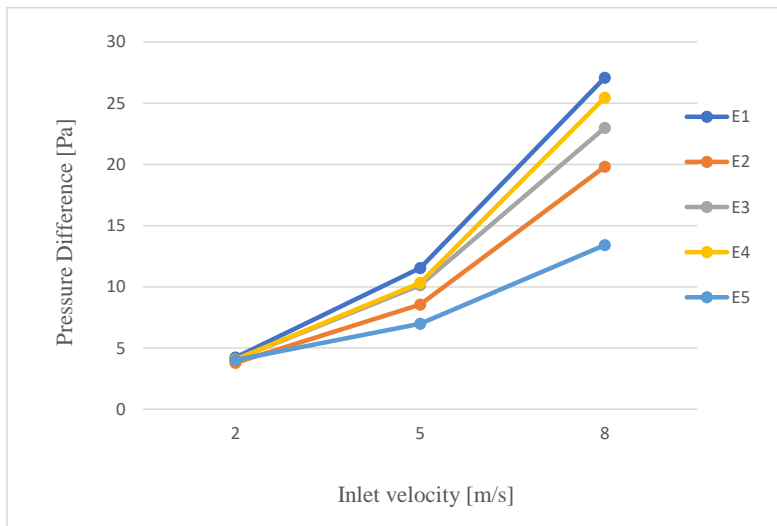


Figure 3.2.6. Pressure difference v/s velocity.

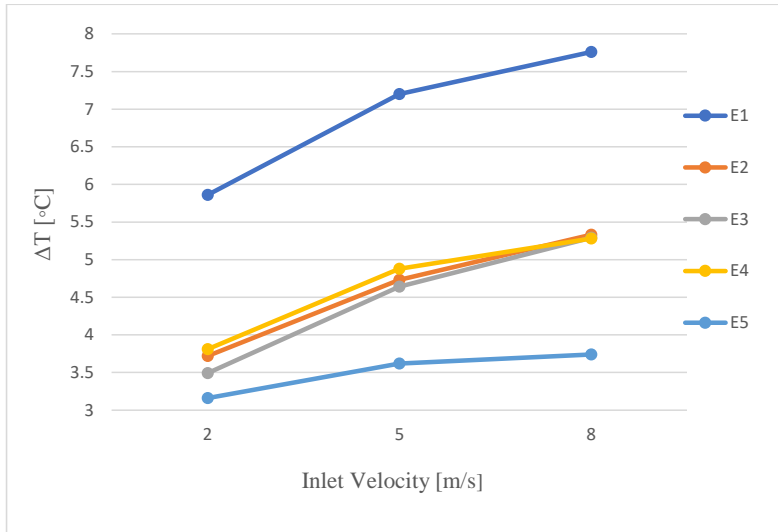


Figure 3.2.7. Surface temperature difference ( $\Delta T$ ) v/s velocity.

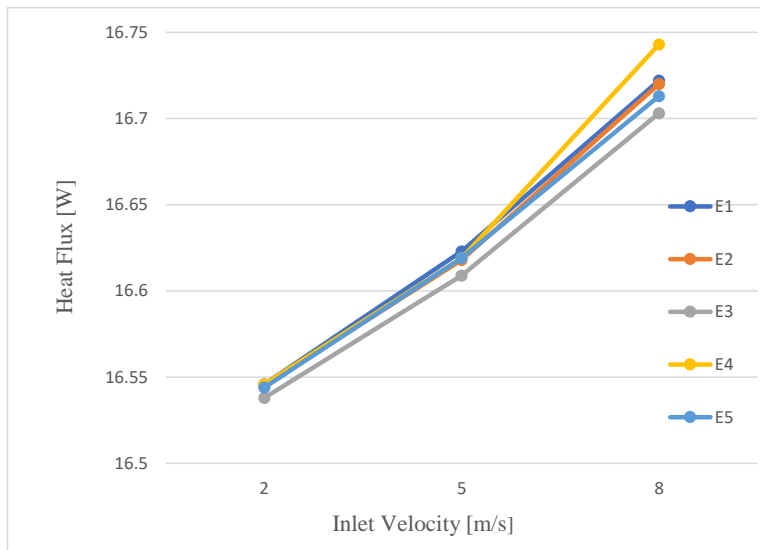


Figure 3.2.8. Heat flux v/s velocity.

Figure 3.2.6 demonstrates that the pressure difference increases consistently as the air velocity increase for all ventilation elements. Initially, all elements show almost equal pressure

differences at lower velocity of 2 m/s. However, with velocities of 5 and 8 m/s, the difference gradually rises. Furthermore, the outcomes obtained from element E5 show the most minimal difference in pressure among all the elements. This suggests better performance as it indicates a more consistent flow with lower pressure fluctuations. The element E5 exhibits a more gradual change in temperature as the velocity increases, as depicted in figure 3.2.7. As a result, this leads to lower temperature fluctuations caused by air turbulence and may provide better comfort of body. In the figure 3.2.8, the given heat flux values represent the overall heat transfer from the body to the jacket through the fluid for each ventilation element at distinct velocities. Due to the use of a single inlet ventilation system in this experiment, the heat transfer is roughly equal for all the scenarios. The rate of heat transmission is a critical aspect since it directly correlates with the level of cooling.

From the obtained results and its comparison, it can be said that it is very important to consider the system's operating parameters to select the appropriate component, because some elements may work well at lower speeds but may not perform effectively at higher velocities. It is evident from the results analysis that element E5 provides lowest pressure difference and smaller energy losses at the inlet flow channel than other mentioned elements in the study. A smaller pressure difference results in more uniform flow throughout the system and less flow fluctuations and when you have less fluctuations in the flow, energy losses are also small, which ultimately provide better cooling of the system. Moreover, E5 offers more gradual temperature difference at different inlet velocities, resulting in less variations of temperature due to air fluctuation. As a person moves in different directions, the air intake through the protective jacket's vents may come from various sides and angles, which may result in flow fluctuations. If there are higher temperature variations at different air velocities, it may cause higher temperature at one point and lower at other, which may create discomfort of the body.

Considering all the results and analysis points, element E5 is the most suitable out of all the mentioned ventilation elements in the present study, which could provide better cooling and comfort of the body. Predicting fluid flow and selecting effective element design is a complex task but it is possible through proper optimization and simulation analysis as mentioned in this study.

### **3.3. Comparative Analysis of Complex Shape Ventilation Elements**

This research investigates the effectiveness of ventilation element by designing three distinct types of ventilation elements, namely E1, E2, and E3. The study is conducted using two different wind inlet velocities. The ventilation elements vary in their geometric dimensions, with the main difference being the size of the outlet through which the inlet air enters the system, as well as the height of the element. The objective is to identify the geometric shape of the element that results in the least amount of flow energy losses in the flow channel of the cell, which occurs from the inlet to the outlet. This energy loss can be measured by the pressure difference ( $\Delta P$ ). Greater pressure difference ( $\Delta P$ ) may results in increased flow energy losses. If there is a drop in the flow's energy, the cooling of the body decreases. SolidWorks Flow Simulation is utilized to compute the pressure, temperature, and heat flux for a simplified elliptical model of the human body covered with a protective jacket. The obtained outcomes are compared and analyzed in order to provide the most optimal geometric configuration of the ventilation element. The pressure and temperature differences for each ventilation element have been determined for comparison. The findings indicate that element E1 has a lower pressure difference than E3, whereas E2 has the lowest pressure difference among E1 and E3.

#### **Model Design and Components:**

The same elliptical model design is used in the study as it is mentioned in section 3.2, the main difference here is that there are four inlet ventilation holes of 2 mm diameter in the front side comprising in a single ventilation element and ten outlet holes of 4 mm diameter at the back side of the jacket. The schematic drawing of the model is shown in the figure 3.3.1.



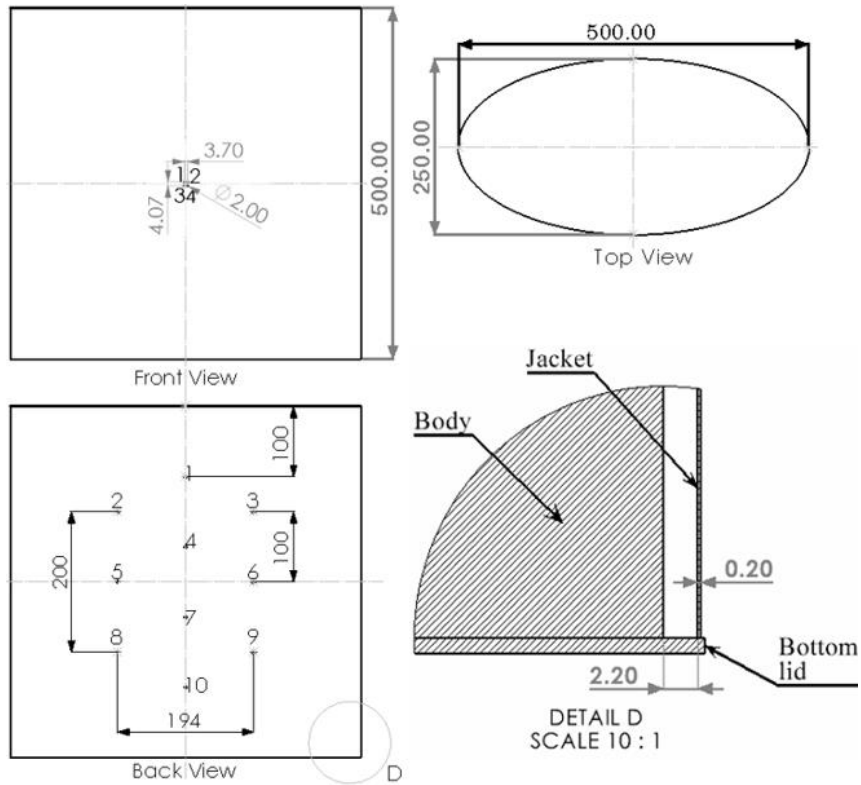


Figure 3.3.1. Elliptical model design with single ventilation element comprising four ventilation holes.

The study utilizes three distinct designs of the ventilation element, as shown in the figure 3.3.2 (a), (b), and (c). The elements have identical shapes but vary in geometric dimensions, allowing for the investigation of the optimal geometric shape of the ventilation element. A ventilation element consists of four inlet ventilation holes, which together create a unit ventilation system. Figure 3.3.2 (d) illustrates the position of the ventilation element in relation to the ventilation holes. The element is attached at the interior side of the jacket. The same initial boundary conditions and material properties are applied in simulation study as mentioned in the section 3.2. Here, the results are computed for two different air velocity of 2 and 5 m/s.

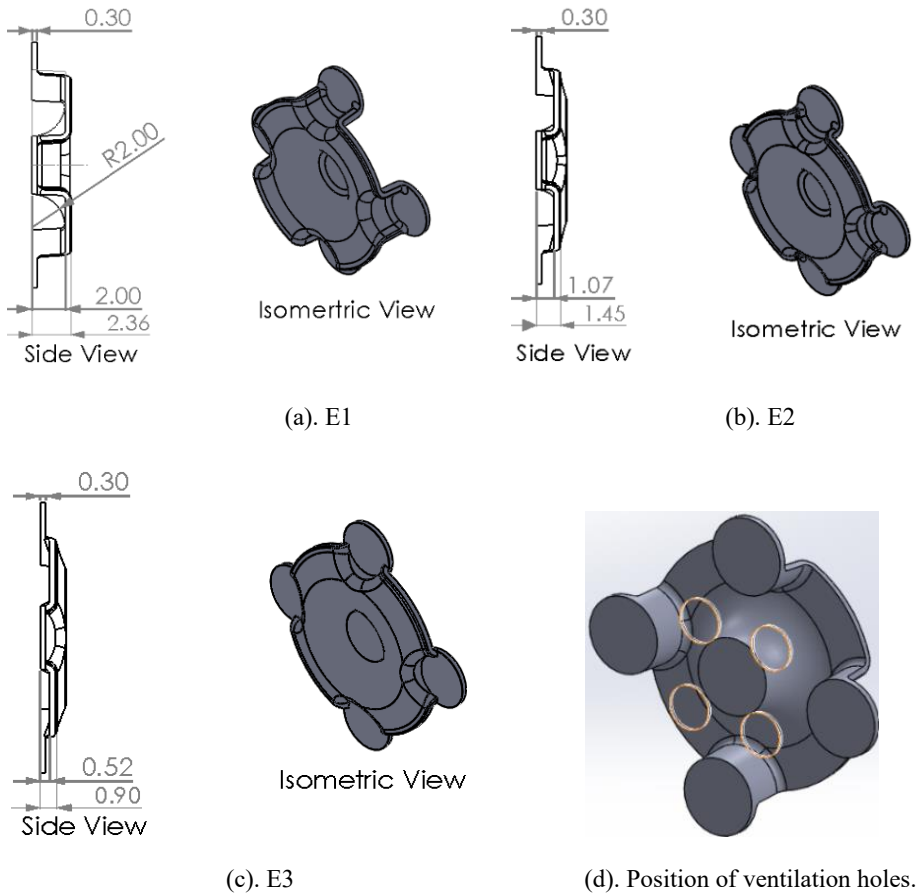


Figure 3.3.2. Three different geometric dimensions of a ventilation element.

Assumptions considered in the Flow Simulation study:

- The top and bottom part of the jacket are closed to study the effectiveness of the ventilation, which means air can only move outside from back side ventilation holes (outlets).
- Radiation is not considered as the heat loss by radiation will be the same in all cases.
- Heat transfer through conduction and convection from the body to the jacket and to outer environment.

### Results and Discussion:

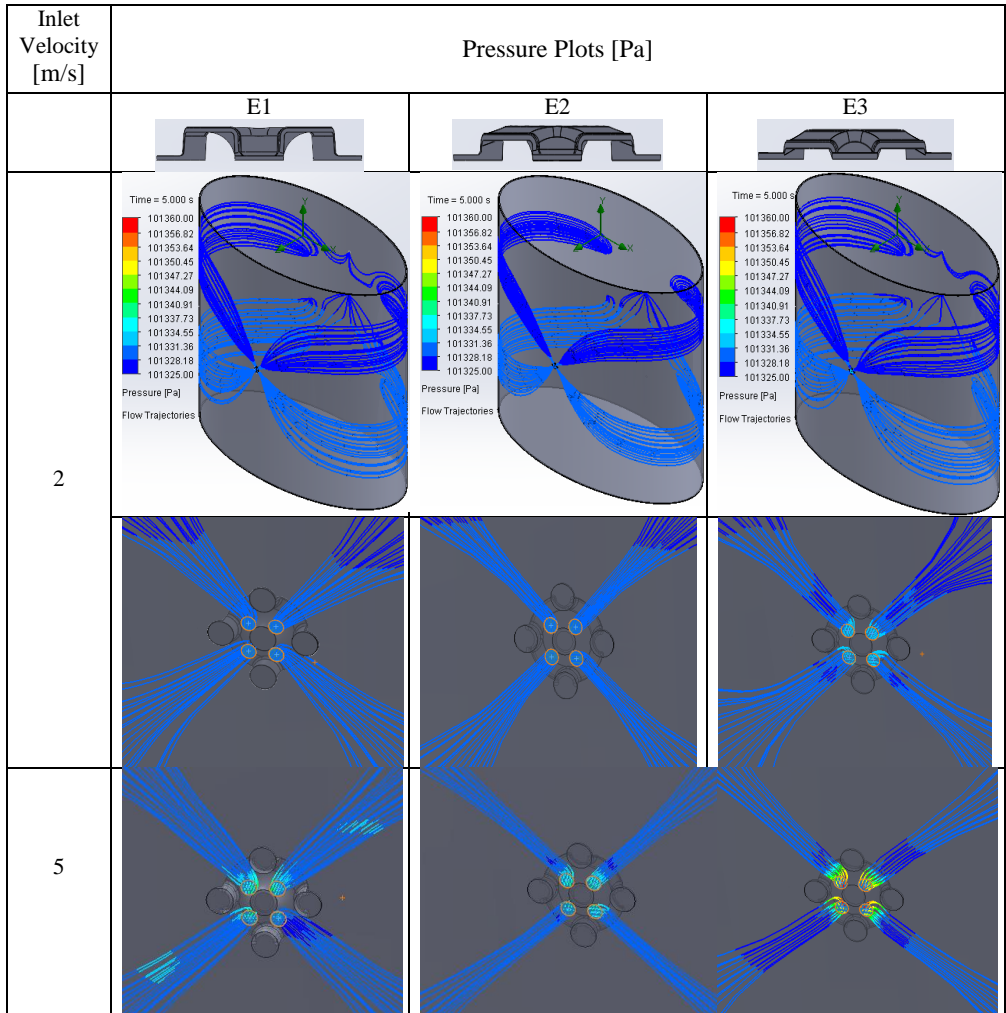


Figure 3.3.3. Pressure plots for E1, E2 and E3.

In the figure 3.3.3, the first row images display an axonometric view of the pressure distribution across the entire model, using the same color scale for all columns. The subsequent images in the second and third rows provide a closer view near the ventilation hole, allowing for the visualization of how the ventilation elements impact the flow path and pressure distribution at different velocities of 2 and 5 m/s. In order to compare the pressure distribution in each scenario, a uniform scale is used for all the plots. The corresponding pressure values are provided in Table 3.3. Based on the

pressure plots, it can be noticed that element E2 exhibits the lower energy losses compared to E1 and E3, particularly at a higher velocity of 5 m/s. Consequently, element E2 has the potential to offer better cooling while minimizing pressure fluctuations.

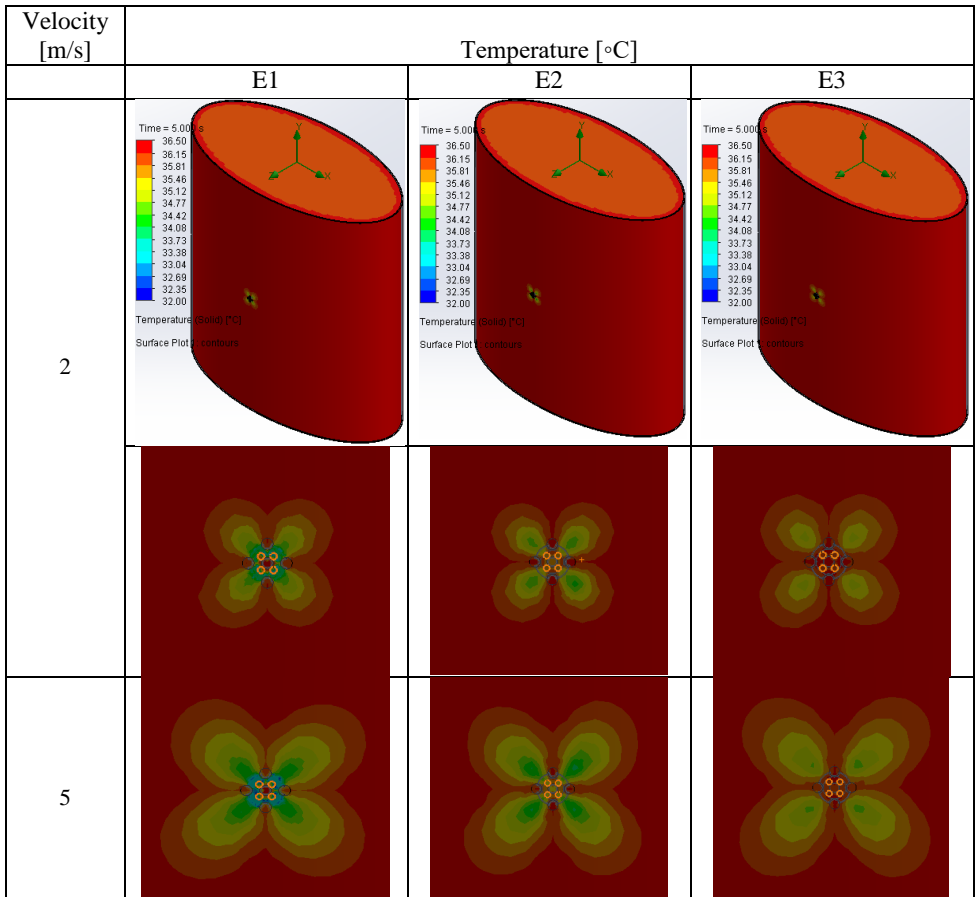


Figure 3.3.4. Surface temperature plots of body for E1, E2 and E3.

In the figure 3.3.4, the first row shows pictures of temperature distribution over the complete model, while the next rows show pictures with the zoom view near the ventilation holes to visualize the cooling effect. Detailed values of the obtained temperatures in all three cases are shown in table 3.3. It is clearly seen from the temperature plots that the cooling coverage area extends near the ventilation with the increasing inlet velocity from 2 to 5 m/s, in all cases. Here, equal scale is taken for easy comparison and visualization.

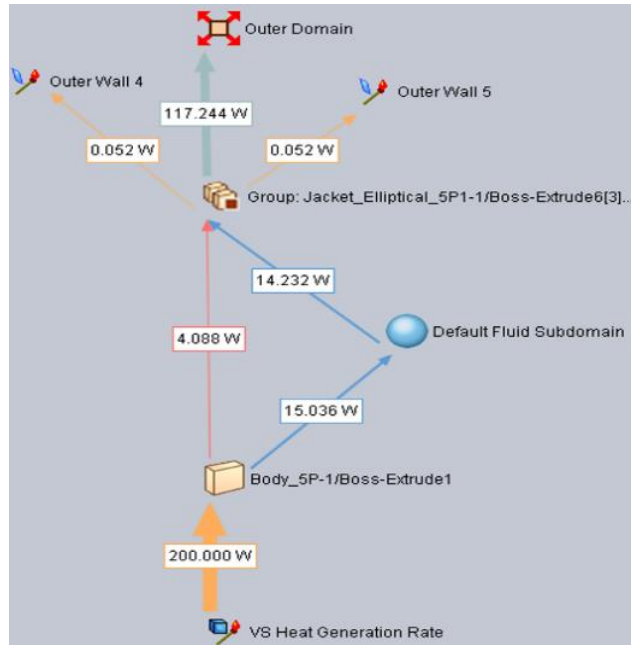


Figure 3.3.5. Heat flux for element E1 at 2 m/s.

In the figure 3.3.5, Body\_5P-1/Boss-Extrude1 refers to the human body model, jacket\_elliptical-5P1 to the jacket and default fluid subdomain is air. The amount of heat released to the atmosphere is represented by Outer Domain in the plot. The rate of heat transfer in all cases is calculated from the flux plots as shown in the figure 3.3.5, similarly the values of heat fluxes are calculated for other ventilation elements at different velocities, which are mentioned in the table 3.3.

Table 3.3.

Numerical values of the results (E1 – E3)

Element	Inlet velocity [m/s]	Values	Pressure [Pa]	$\Delta P$ [Pa]	Temperature [°C]	$\Delta T$	Heat transfer from body to fluid [W]
E1	2	Max	101330.12	4.2	36.50	3.87	18.64
		Min	101325.92		32.63		14.563
		Ave	101328.03		36.50		-
	5	Max	101344.28	18.41	36.50	4.45	19.124
		Min	101325.87		32.05		15.036
		Ave	101328.08		36.50		-
E2	2	Max	101330.36	4.18	36.50	2.28	18.612
		Min	101326.18		34.22		14.586
		Ave	101328.06		36.50		-
	5	Max	101339.31	12.84	36.50	2.6	19.087
		Min	101326.47		33.90		15.061
		Ave	101328.06		36.50		-
E3	2	Max	101333.97	8.18	36.50	1.53	18.616
		Min	101325.79		34.97		14.590
		Ave	101328.05		36.50		-
	5	Max	101359.92	34.04	36.50	1.88	19.103
		Min	101325.88		34.62		15.077
		Ave	101328.04		36.50		-

The results are compared based on the pressure difference, temperature difference, and heat transfer, as indicated below. Figure 3.3.6 clearly illustrates that element E2 exhibits the lowest pressure difference. The results indicate that element E2 exhibits a pressure difference that is 5.57 Pa lower than element E1 at a wind velocity of 5 m/s, representing a reduction of 30.26% compared to E1. In addition, E2 exhibits a pressure difference that is 4 Pa lower than E3 when the wind velocity is 2 m/s, resulting in a decrease of approximately 48.90%. Similarly, at a wind velocity of 5 m/s, E2 demonstrates a pressure difference that is 21.2 Pa lower than E3, corresponding to a reduction of 62.28%. The rate at which the temperature difference changes in relation to the velocity is more gradual in E2, as depicted in the figure 3.3.7. This implies that there are less fluctuations in the temperature due to changes in air movement. Due to the presence of a single ventilation element in the current investigation, heat transport is nearly same in all three elements.

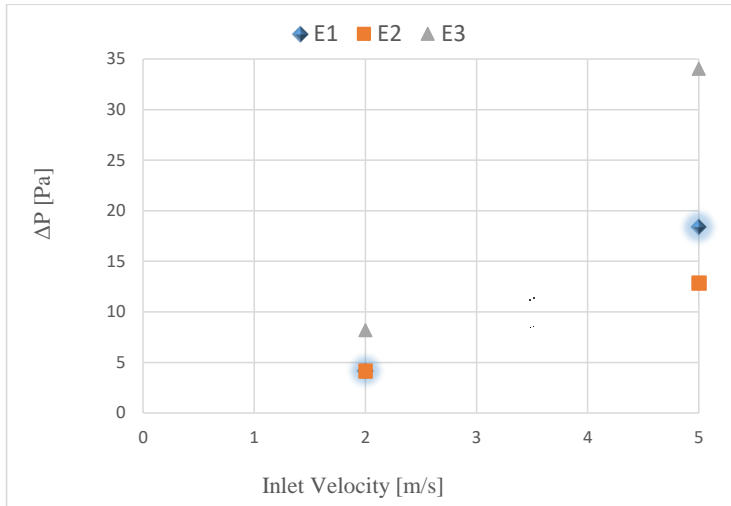


Figure 3.3.6. Pressure difference ( $\Delta P$ ) v/s velocity.

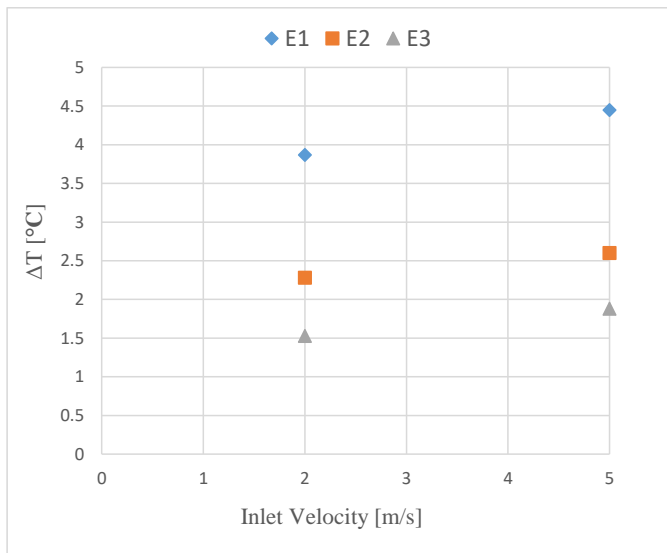


Figure 3.3.7. Temperature difference ( $\Delta T$ ) v/s velocity.

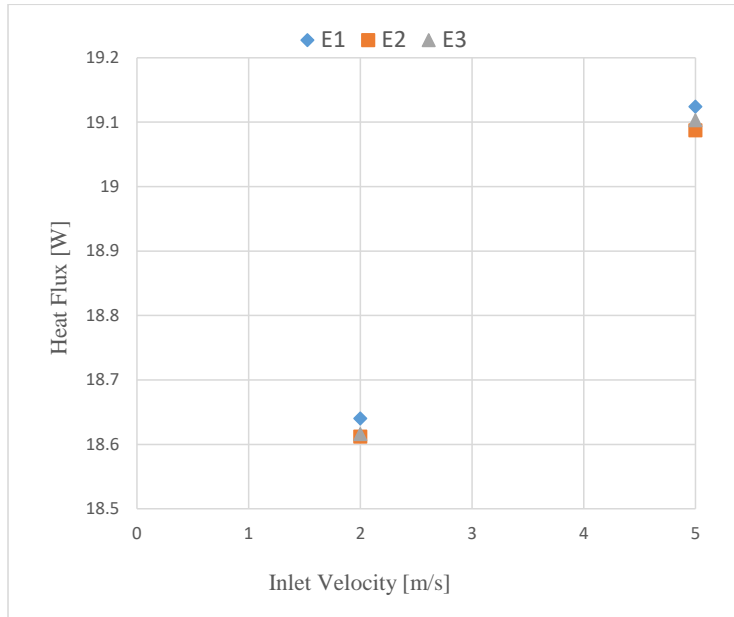


Figure 3.3.8. Heat flux v/s velocity.

The results indicate a gradual increase in pressure differential across all ventilation elements as the inlet velocities increase from lower to higher values. At an initial velocity of 2 m/s, elements E1 and E2 exhibit nearly identical pressure differences, whereas E3 demonstrates more pressure fluctuations at the intake, suggesting subpar performance. The pressure differential gradually grows at air velocity of 5 m/s in all three element. It is crucial to observe that certain elements may function effectively at lower velocity but may exhibit poor performance at higher velocities. Therefore, it is crucial to understand the operating parameters of the system and select the appropriate element accordingly.

From the obtained results, it can be concluded that for smaller inlet velocity of 2 m/s element E1 is more appropriate but it shows higher pressure difference and energy losses in the cell flow channel at higher inlet velocity of 5 m/s. This is an important point to notice because some element may work well at smaller velocity but may not provide good performance at higher velocities, hence it is important to choose proper element according to working parameters. Considering overall performance at smaller and higher inlet velocity, element E2 is more appropriate than the



other mentioned element designs in the study, which provides the lowest pressure difference and the smallest flow energy losses in the cell flow channel that could provide better cooling.

This study shows that it is important to choose proper dimensions of the element opening, as very small dimensions may provide higher pressure difference and a larger opening size may provide higher temperature difference, while selecting a proper dimension in between may improve the performance. Selecting proper dimensions can be a difficult task, but it can be achieved through proper optimization and simulation study. At the same time the developed models are usable for the comparative ventilation effectivity analysis that will allow proceed with further investigations, for example, optimization of the location points of the multiple ventilation elements on protective clothing.

### **3.4. Conclusions of the Analysis of Different Shape Ventilation Elements**

1. It is evident from the results analysis in section 3.2, that the element E5 provides lowest pressure difference and smaller energy losses at the inlet flow channel than other mentioned elements in the study. A smaller pressure difference results in more uniform flow throughout the system and less flow fluctuations and when you have less fluctuations in the flow, energy losses are also small, which ultimately provide better cooling of the system.
2. From the obtained results in section 3.3, it can be concluded that for smaller inlet velocity of 2 m/s element E1 is more appropriate but it shows higher pressure difference and energy losses in the cell flow channel at higher inlet velocity of 5 m/s. This is an important point to notice because some element may work well at smaller velocity but may not provide good performance at higher velocities, hence it is important to choose proper element according to working parameters.
3. Considering overall performance at smaller and higher inlet velocity, element E2 is more appropriate than the other mentioned element designs in the study, which provides the lowest pressure difference and the smallest flow energy losses in the cell flow channel that could provide better cooling.

4. Based on the results analysis in chapter 3.4, it can be concluded that element E1 provides overall better results both at lower and higher air velocities. Moreover, E1 provides smallest energy losses in the element flow channel and shows lower fluctuations in pressure and temperature difference with the change in air velocity than other mentioned elements. This makes element E1 more suitable over other mentioned elements, which could provide better cooling at different inlet air velocity.

## **4. FORMATION OF THE INPUT DATA FOR THE MODELING OF THE RESEARCH OBJECT (CLOTHING) MODEL**

### **4.1. Formulation of Task of Shape Optimization of Ventilation Element**

In the chapter 3, we observed how the design of a ventilation element can impact flow distribution, pressure, and temperature variations, highlighting the importance of selecting the correct shape of ventilation element. This chapter concentrates on optimizing the shape of ventilation element for protective clothing using a metamodeling approach.

The software KEDRO [119] is utilized in this study for shape optimization of ventilation elements. It enables experiment planning, metamodel construction, and global optimization using these metamodels. The direct parameterization approach of CAD-based geometry [132] is increasingly effective and broadly applicable because of the advancement of automated design software and very efficient metamodeling methodologies [133, 134]. In this work metamodeling approach with different order polynomial local and global as well as Kriging approximations are compared for the shape optimization of ventilation elements. The primary objective is to determine the geometric shape of the element that minimizes flow energy losses in the cell flow channel, as shown by the pressure difference. A multistep approach was implemented to attain optimal results.

1. Strategizing the placement of control points for Non-Uniform Rational B-Splines (NURBS) to achieve elements with a smooth shape.
2. Constructing geometric models using SolidWorks, in accordance with the design of experiments.
3. Calculating responses for a comprehensive model utilizing (CAE) software, (SolidWorks Flow Simulation).
4. Creating metamodels for responses, derived from the computer experiment.
5. Employing metamodels for optimizing shape of element.
6. Validating the optimal design of the entire model using (CAE) software.

#### **Model Design and Boundary Conditions:**

In prior investigations (section 3.2) revealed that ventilation elements with a torus shape cut-out in the core [135] are the most efficient in terms of smallest flow losses. This study focuses on

further shape optimization of the outer ring of the ventilation element. Two design variables, the length of straight lines R60 and R90, are presented with specified lower and higher bounds as shown in the figures 4.1.1 and 4.1.2.

(1)  $0.36 \leq R60 \leq 2$ ; (2)  $0.01 \leq R90 \leq 2.5$ . The lower endpoints of these lines serve as control points for NURBS that determine the smooth shape of the outer ring of the ventilation element. Metamodel construction utilizes the Mean Square Distance Latin Hypercube (MSDLH) design of experiment with 2 components, as shown in the figure 4.1.3.

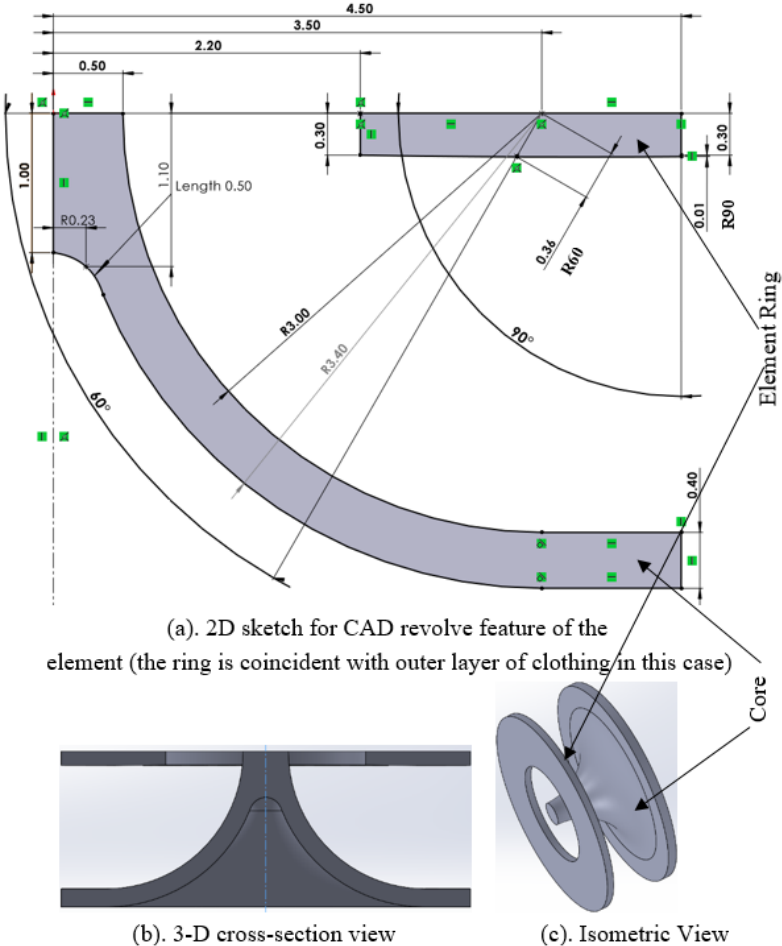


Figure 4.1.1. Ventilation element CAD model with lower bounds of design variables.

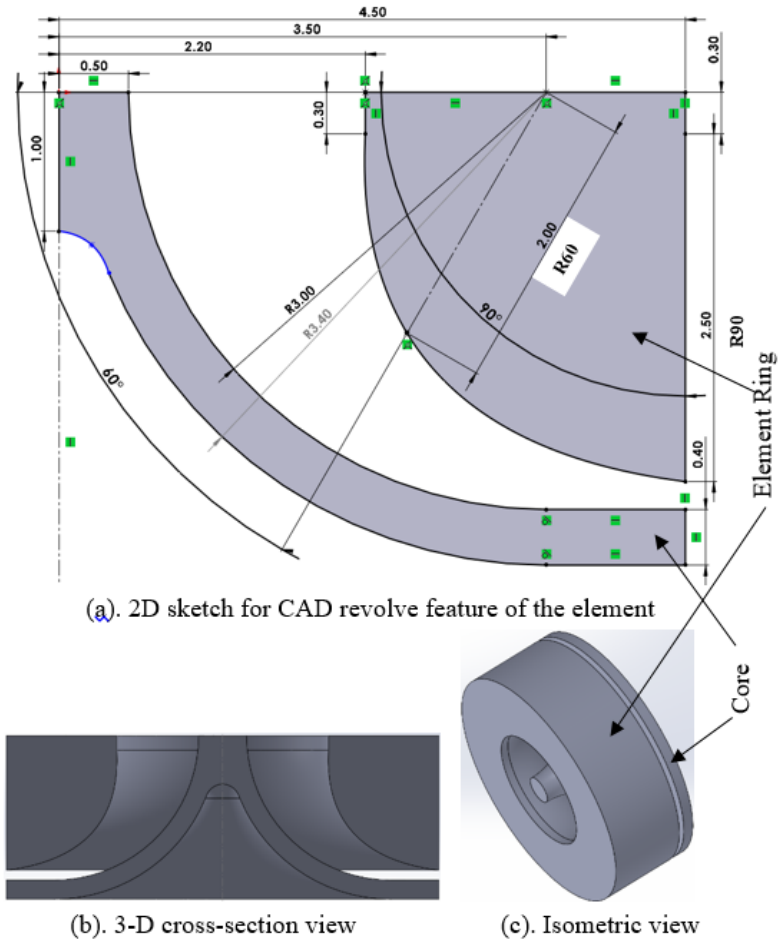


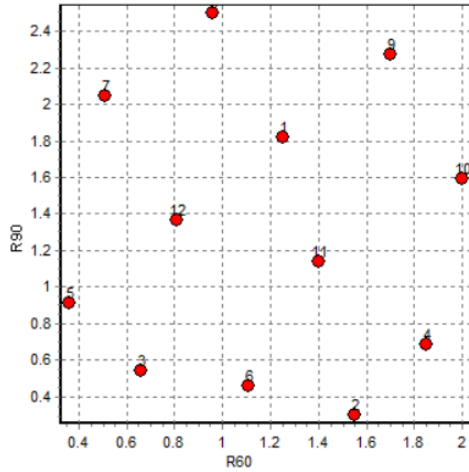
Figure 4.1.2. Ventilation element CAD model with upper bounds of design variables.

Figures 4.1.1 and 4.1.2 display the smallest and largest dimensions of the element ring. Figure 4.1.3 (a) illustrates the Design of Experiment (DOE) with 12 numerical design values within a specified range. In this DOE, factors  $X1=R60$  and  $X2=R90$  represent the coordinates of the element ring, where R60 corresponds to points at  $60^\circ$  and R90 corresponds to points at  $90^\circ$  with the horizontal axis in the 2D sketch. Using KEDRO, this Design of Experiments (DOE) is constructed, resulting in the generation of 12 geometric model of elements by SolidWorks using these DOE.

The model of body and jacket are designed in a basic elliptical form, with the body at the center and the jacket around it with a consistent 3.4 mm gap. This is depicted in figure 4.1.4.

Input Factor Values by Experimental Design		
Total No. of Runs= 12		Factors= 2
Factor_N_1_to_2		
Mne-	X 1	X 2
monic	R60	R90
Levels	12	12
Min	0.36	0.01
Max	2	2.5
1)	1.25454545454545	1.82090909090909
2)	1.55272727272727	0.01
3)	0.658181818181818	0.236363636363637
4)	1.85090909090909	0.689090909090909
5)	0.36	0.915454545454545
6)	1.10545454545455	0.462727272727273
7)	0.509090909090909	2.04727272727273
8)	0.956363636363636	2.5
9)	1.70181818181818	2.27363636363636
10)	2	1.59454545454545
11)	1.40363636363636	1.14181818181818
12)	0.807272727272727	1.36818181818182

(a). Numerical values



(b). Graphical representation

Figure 4.1.3. MSDLH DOE with 12 trials for 2 factors generated by KEDRO.

Figure 4.1.4 displays a schematic representation of the model design of the body and jacket. It includes a single inlet with a diameter of 4.4 mm at the front and 10 outlets with a diameter of 4 mm at the back of the jacket. A ventilation element is positioned to the inlet hole in the space between the body and the jacket, with no elements attached to the outlets. A simulation study was conducted using 12 ventilation elements created with a metamodel. The results gained from the simulation study were utilized as input in KEDRO for optimization. The flow simulation inquiry uses a base air temperature of 20 °C and an air pressure of 101325 Pa as standard parameters. Two different inlet air speeds of 4 and 8 m/s are utilized in the study. Initially, several materials with certain qualities are allocated to the jacket and body as mentioned in table 3.2.1 (chapter 3.2).

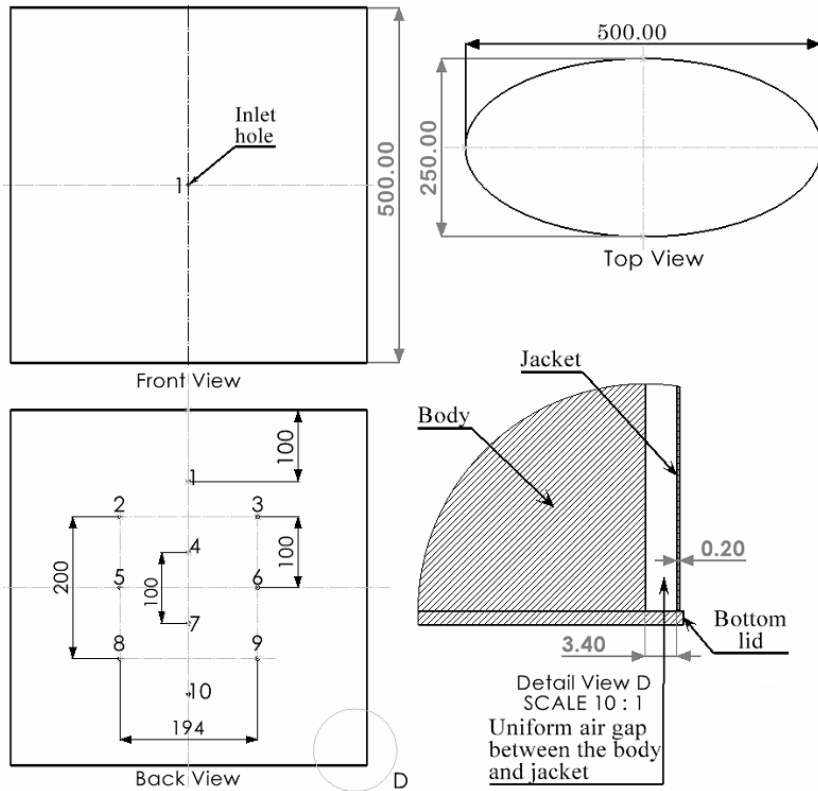


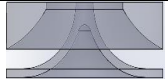
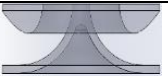
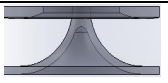
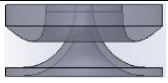
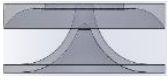
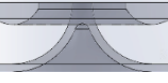



Figure 4.1.4. Elliptical model design (with an air gap of 3.4 mm).

### Results and Discussion:

After setting all the input parameters and boundary conditions as mentioned in the previous section, a flow simulation study is conducted for a physical time of 5 seconds. The results are then assessed in terms of flow pressure and surface temperature. The results for each case are displayed in table 4.1.

Table 4.1.

Simulation results of 12 elements generated using DOE

Element cross section shape	Inlet Velocity [m/s]	Values	Pressure [Pa]	$\Delta P$ [Pa]	Temperature [°C]	$\Delta T$ [°C]
 1	4	Max	101331.16	5.55	36.50	7.5
		Min	101325.61		29.00	
	8	Max	101338.00	17.48	36.50	8.24
		Min	101320.52		28.26	
 2	4	Max	101331.07	6.17	36.50	6.2
		Min	101324.90		30.30	
	8	Max	101337.54	21.96	36.50	7.13
		Min	101315.58		29.37	
 3	4	Max	101331.51	6.06	36.50	8.05
		Min	101325.45		28.45	
	8	Max	101342.51	22.20	36.50	8.54
		Min	101320.31		27.96	
 4	4	Max	101332.92	8.49	36.50	7.24
		Min	101324.43		29.26	
	8	Max	101345.29	29.05	36.50	8.36
		Min	101316.24		28.14	
 5	4	Max	101331.59	5.89	36.50	7.38
		Min	101325.70		29.12	
	8	Max	101340.49	21.55	36.50	8.14
		Min	101318.94		28.36	
 6	4	Max	101331.23	5.74	36.50	6.91
		Min	101325.49		29.59	
	8	Max	101341.61	22.52	36.50	8.44
		Min	101319.09		28.06	
 7	4	Max	101333.92	8.25	36.50	7.04
		Min	101325.67		29.46	
	8	Max	101347.83	22.87	36.50	8.54
		Min	101324.96		27.96	
 8	4	Max	101359.86	34.4	36.50	6.64
		Min	101325.46		29.86	
	8	Max	101444.59	119.28	36.50	7.61
		Min	101325.31		28.89	
 9	4	Max	101341.56	18.83	36.50	6.91
		Min	101322.51		29.59	
	8	Max	101372.52	51.32	36.50	7.83
		Min	101321.20		28.67	



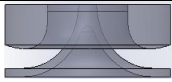
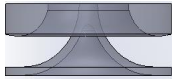
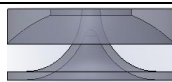
	4	Max	101336.65	13.92	36.50	7.27
		Min	101322.73		29.23	
	8	Max	101360.79	45.42	36.50	8.4
		Min	101315.37		28.10	
 11	4	Max	101331.09	5.7	36.50	6.76
		Min	101325.39		29.74	
	8	Max	101334.51	17.87	36.50	8.3
		Min	101316.64		28.20	
 12	4	Max	101331.08	5.56	36.50	6.68
		Min	101325.52		29.82	
	8	Max	101338.09	17.74	36.50	8.16
		Min	101320.35		28.34	

Table 4.1 shows the calculated pressure and temperature differences, denoted as  $\Delta P$  and  $\Delta T$ , respectively. These values are derived from the results of the flow simulation study. The estimated values of  $\Delta P$  and  $\Delta T$  are utilized as data inputs in KEDRO for further approximation and optimization. The Kriging method is utilized for the approximation in this study. In the figures 4.1.5 to 4.1.8, the symbol  $dP$  refers to  $\Delta P$  and  $dT$  refers to  $\Delta T$ .

Functions Yr:	dP	dT
Sigma Cross	4.526287	0.225006
Sigma Cross%	52.529536%	46.762349%
R2 adjusted		
F-Crit 99%		
Sigma	0.000000	0.000003
Sigma%	0.000001	0.000727
MeanExpValue	10.370000	7.048333
StDev of Exp	8.616651	0.481170
Exp. Range	28.960000	1.850000
MaxError	0.000000	-0.000008
Bad Point No.	11	12
Max Rel Error	0.00%	0.00%
BadRelPointNo.	11	12
Max Cook Dist.		
Suspicious point	0	0
No. of Actual Exp	12	12
Filtered STD		

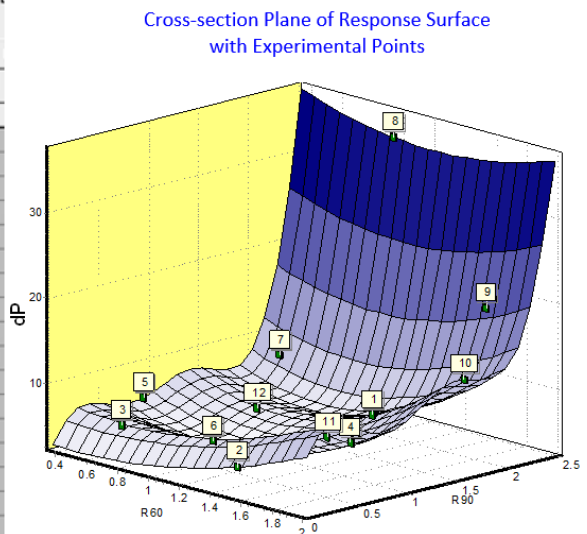


Figure 4.1.5. Response Surface  $\Delta P = f(R60, R90)$  using experiment with 12 trials for Kriging approximation for case of wind velocity 4 m/s.

Cross-section Plane of Criterion Surface

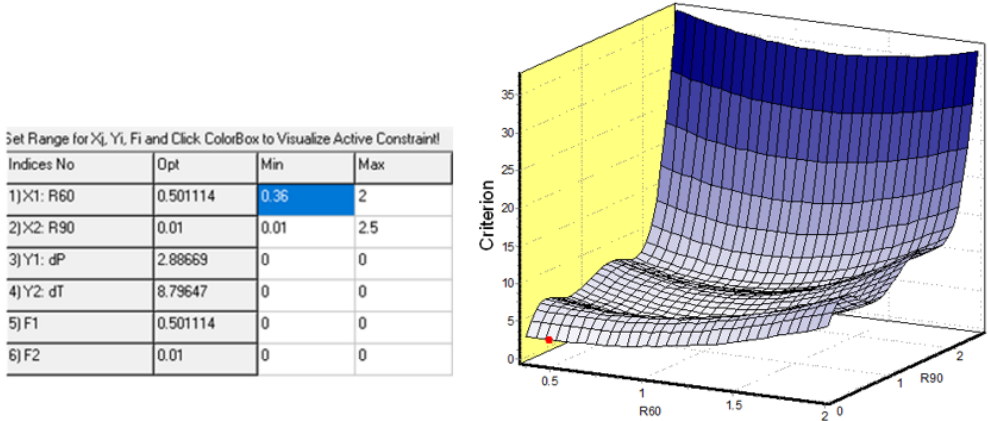


Figure 4.1.6. Optimization results for case of wind velocity 4 m/s (red point indicate global minimum of  $\Delta P$ ).

Figure 4.1.5 shows Kriging approximation by response surface with experimental points. There are two main indicators to check the quality of approximation: Sigma Cross% and Max Rel Error. Here, Sigma Cross is the leave-one-out-cross-validation error and Max Rel Error is maximum relative error (in relation to the experimental values).

$$\text{Sigma Cross} = \sqrt{\frac{\sum_{i=1}^n (y_i - \hat{y}_{i(-i)})^2}{n}} \quad (4.1.1)$$

Where,  $\hat{y}_{i(-i)}$  is the value of the approximated function for input factor value  $x_i$ , if the approximation does not use the  $i$ -th experiment point;  $n$  – the total number of experiment points. A more informative indicator for the approximation quality is relative cross-validation error (Sigma Cross%) as a percentage of Standard Deviation:

$$\text{Sigma Cross}\% = \sqrt{\frac{\sum_{i=1}^n (y_i - \hat{y}_{i(-i)})^2}{n}} \times \frac{100}{STD} \quad (4.1.2)$$

where,  $STD$  is Standard Deviation:

$$STD = \sqrt{\frac{\sum_{i=1}^n (y_i - \bar{y})^2}{n-1}} \quad (4.1.3)$$

and  $\bar{y}$  is the mean value of the response in the experimental points:

$$\bar{y} = \frac{\sum_{i=1}^n y_i}{n} \quad (4.1.4)$$

Your approximation's quality will be severely lacking if the value of Sigma Cross% is closer or greater than 100%. A smaller value of Sigma Cross% will result in a better approximation. The approximation is also considered better when the value of Max Rel Error percentage is smaller or close to zero. A Sigma Cross% of 52.52% and a Max Rel Error of 0.001% are indicative of an acceptable level of approximation in this case. Results of optimization according to the minimal pressure difference as a criterion are displayed in the figure 4.1.6. The obtained results are verified using a flow simulation study conducted at an inlet velocity of 8 m/s. The results are then utilized for approximation and optimization by repeating the same process.

Approximation of Response Surface: ELOp\_8.prj

Runs: Total=12

Approx Order:  Custom  Kriging

Third  Second  First-linear

Functions Yi:	dP	dT
Sigma Cross	11.128550	0.173858
Sigma Cross%	38.320989%	41.196844%
R2 adjusted		
F-Crit 99%		
Sigma	0.000001	0.000000
Sigma%	0.000004	0.000021
MeanExpValue	33.962500	8.140833
StDev of Exp	29.040352	0.422018
Exp. Range	102.410000	1.410000
MaxError	-0.000002	0.000000
Bad Point No.	11	12
Max Rel Error	0.00%	0.00%
BadRelPointNo.	11	12
Max Cook Dist.		
Suspicious point	0	0
No. of Actual Exp	12	12
Filtered STD		

Cross-section Plane of Response Surface with Experimental Points

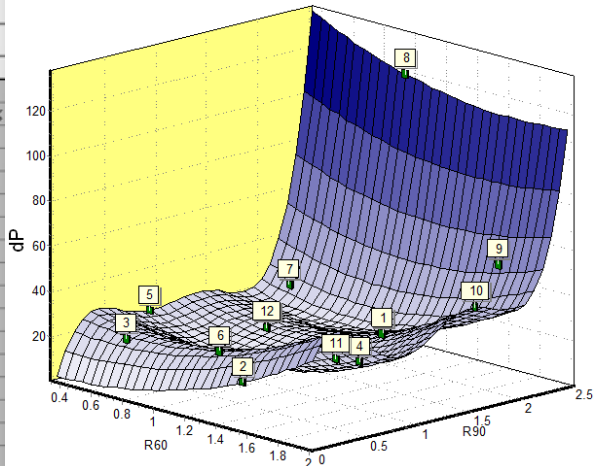


Figure 4.1.7. Approximation of response surface at 8 m/s.

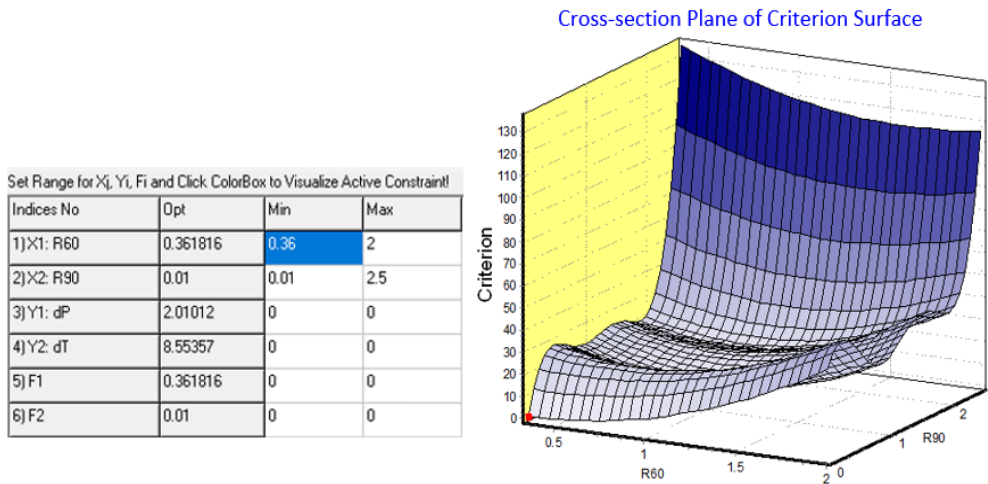


Figure 4.1.8. Optimization results for case of wind velocity 8 m/s (red point indicate global minimum of  $\Delta P$ ).

The value of Sigma Cross% obtained from the figure 4.1.7 is 38.32%, indicating a better quality of approximation compared to results at 4 m/s (52.53%). The optimum design of ventilation element obtained from the results at wind speeds of 4 and 8 m/s is same, indicating the method's reliability. From the results, the optimal design variables for ventilation element's design are  $R60=0.36$  and  $R90=0.01$ , as shown in the figure 4.1.8. The last step involves validating the optimized design using SolidWorks Flow Simulation to compare the simulation and optimization outcomes. The calculated  $\Delta P$  value for the optimal design with a wind velocity of 4 m/s is 5.39 Pa, which deviates from the optimization results by 2.5 Pa. The difference is primarily caused by the level of approximation quality; enhancing this quality will yield more precise optimization results.

Specific optimal design points for the element ring were determined based on the criteria of minimum pressure difference at wind velocities of 4 m/s and 8 m/s. A very small difference was also observed in obtained values of optimum design points at 4 and 8 m/s. The coordinate value for R90 remains the same in both cases, with a slight variation for R60. The metamodel's quality for the approximation of results at 8 m/s were better based on obtained values of Sigma Cross%. It can be concluded from the obtained results that optimum design variables for the element ring can provide minimum pressure difference and ultimately better cooling. The ring is practically

nonexistent at the optimal design points, suggesting that the element without an outside ring will provide the best results. The study demonstrates that employing a metamodeling approach with CFD simulation can significantly decrease the computing time required for optimization.

## **4.2. Analysis of Ventilation Element with and without Constant Cross-Section Area Opening**

In this study we are using a ventilation element which can be positioned at a ventilation hole in protective clothing to provide mechanical strength to the clothing and to improve air exchange. In this study we have designed a ventilation element with a constant arc length and an outer ring to investigate its efficiency. Moreover, different coordinate values are used in the design of the element and the results are compared and analyzed to propose an optimum design.

This work presents the design of a ventilation element with a constant cross-sectional area of  $3.14 \text{ mm}^2$ , including an outside ring. The paper analyzes five distinct scenarios, four of which involve varying coordinate values for the outer ring and core, while the fifth scenario consists of the ventilation element without an outer ring. The efficiency of the ventilation element design is assessed by analyzing and comparing the outcomes of all five scenarios. These ventilation elements are attached at the ventilation hole on the inner side of the protective jacket. The attached ventilation element enhances the structural strength of the clothing by covering the ventilation hole and preventing dust, insects, etc. from directly contacting the body. Furthermore, the ventilation elements facilitate the smooth circulation of air within the jacket. The goal is to identify the element's geometric configuration that leads to the lowest energy losses in the flow channel of the cell, which are shown by the pressure difference. The energy losses in the flow increase as the pressure difference ( $\Delta P$ ) increases, and the cooling of the body decreases when the flow is weakened or loses energy. CFD is utilized to compute the pressure, temperature, and heat flow for a reduced elliptical model of the human body equipped with a protective jacket. The acquired outcomes are compared and analyzed to examine the concept of a consistent cross-sectional area in the configuration of ventilation elements, both with and without an outer ring. The pressure and temperature differences are computed for each scenario to facilitate comparison. The results

indicate that the element design without an outer ring yields better overall results and reduced flow energy losses in the cell flow channel, as compared to the element design having an outer ring.

**Model Design and Boundary Conditions:**

Here, same model design and boundary conditions are used as it is mentioned in the section 3.2. Simulation study is carried out at three different inlet air velocity of 2, 5 and 8 m/s.

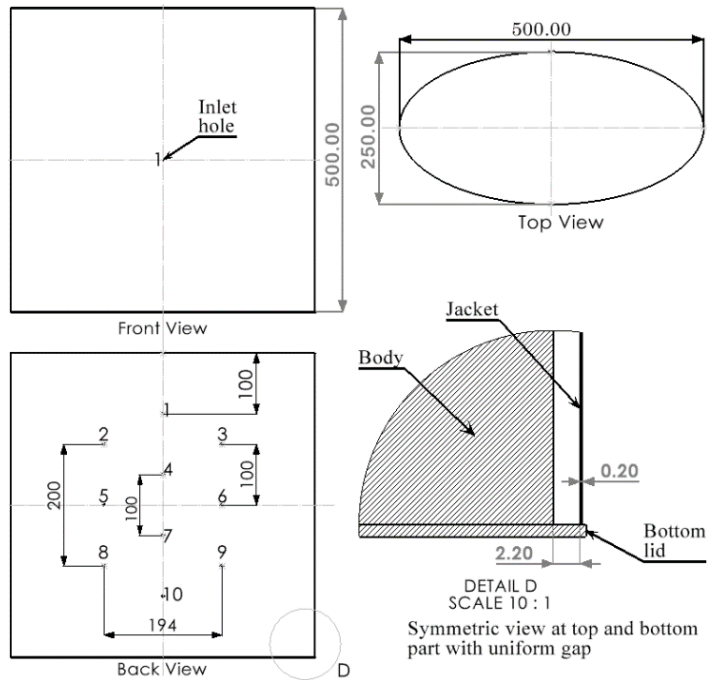


Figure 4.2.1. Elliptical model design.

There are four ventilation element design with outer ring named as E0-30, E0-45, E0-60 and E0-90, while fifth case is consisting of a core without outer ring which is named as E1. Figure 4.2.2 represents design of element E0-90 with core and outer ring. The coordinate values used in all cases of ventilation element design are mentioned in the table 4.2.1. All mentioned dimensions are in millimeters.

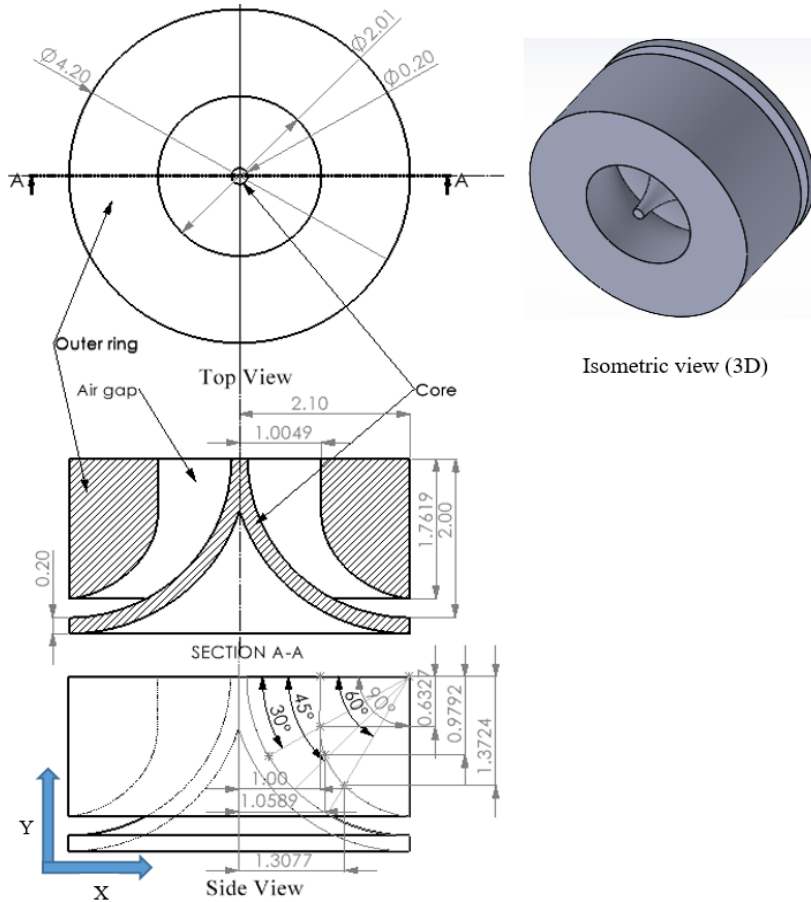


Figure 4.2.2. Design of element E0-90.

In the following table 4.2.1, the symbol  $\alpha$  indicates the reference coordinate angle ranging from  $0$  to  $90^\circ$ . The coordinates for the ring are denoted by  $X1$  and  $Y1$ , while the coordinates for the core are denoted by  $X2$  and  $Y2$ . The letter  $S$  denotes the constant cross-sectional area of the air gap in the element. Therefore, the cross-sectional area between the core and outer ring remains constant at all specified angles. The intricate details of the element's design is shown in the figure 4.2.2.

Table 4.2.1.

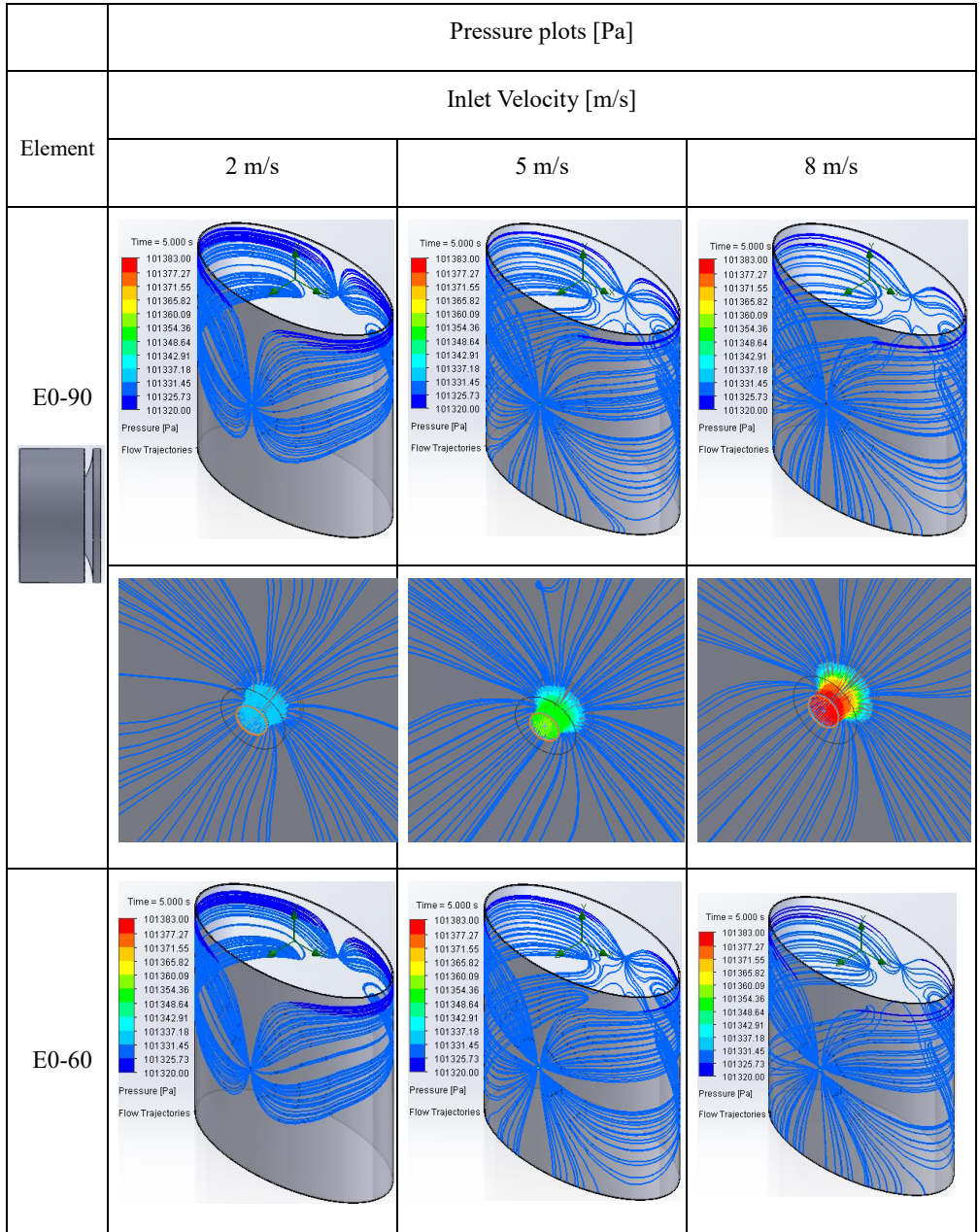
Coordinate Design Values of Elements

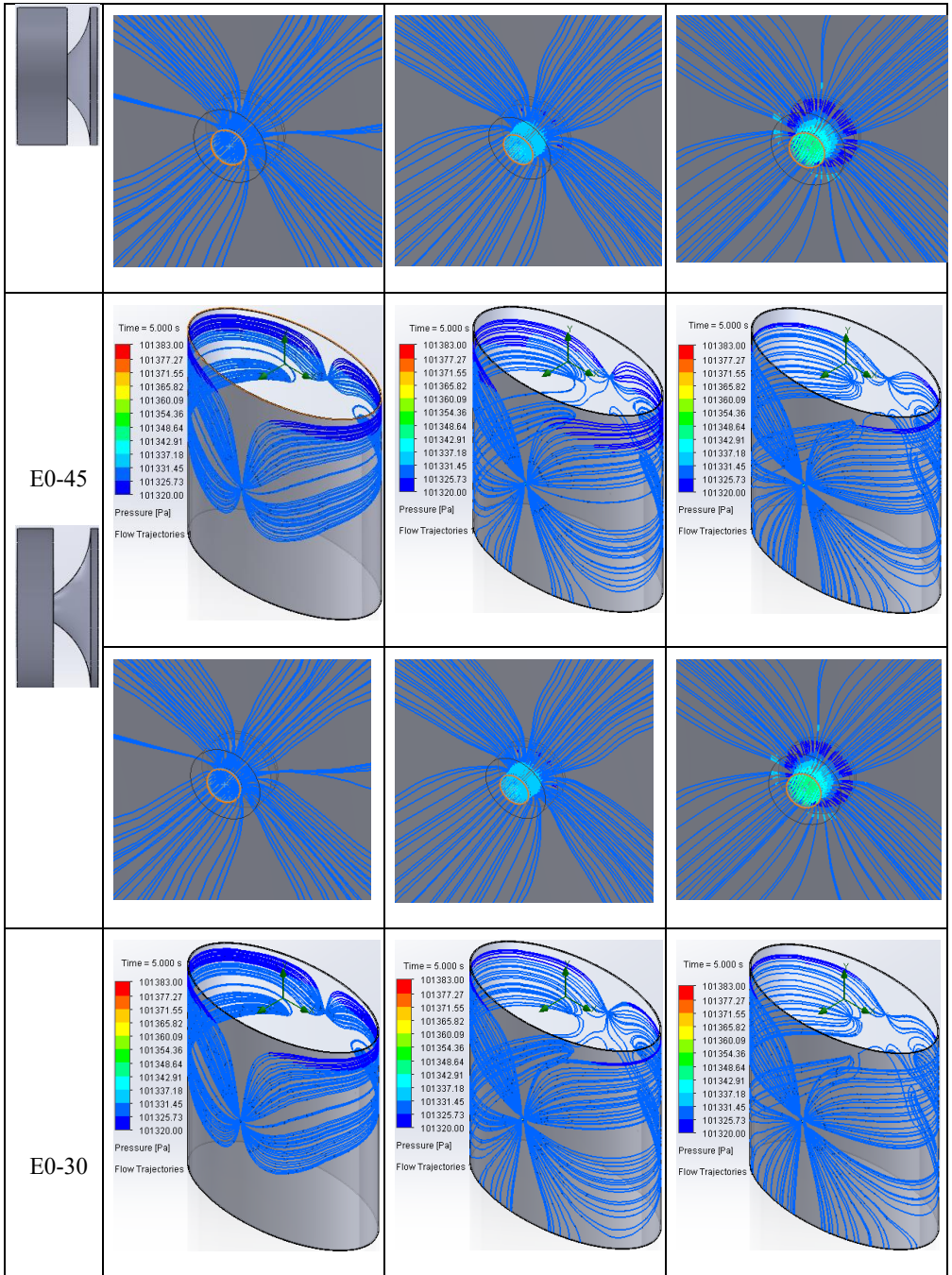
$\alpha$	X1	Y1	X2	Y2	S
0°	1.0049	0	0.1	0	3.14
30°	1	0.6327	0.3679	1	
45°	1.0589	0.9792	0.6857	1.4140	
60°	1.3077	1.3724	1.1	1.7320	
90°	2.10	1.7619	2.1	2	

### Results Analysis and Discussion:

The results provided are computed under the condition where the incoming air enters the inlet ventilation perpendicular to the front face. The simulation analysis presents results for a duration of 5 seconds, where all elements are subjected to same boundary conditions and values as specified in the preceding chapter 3.2.







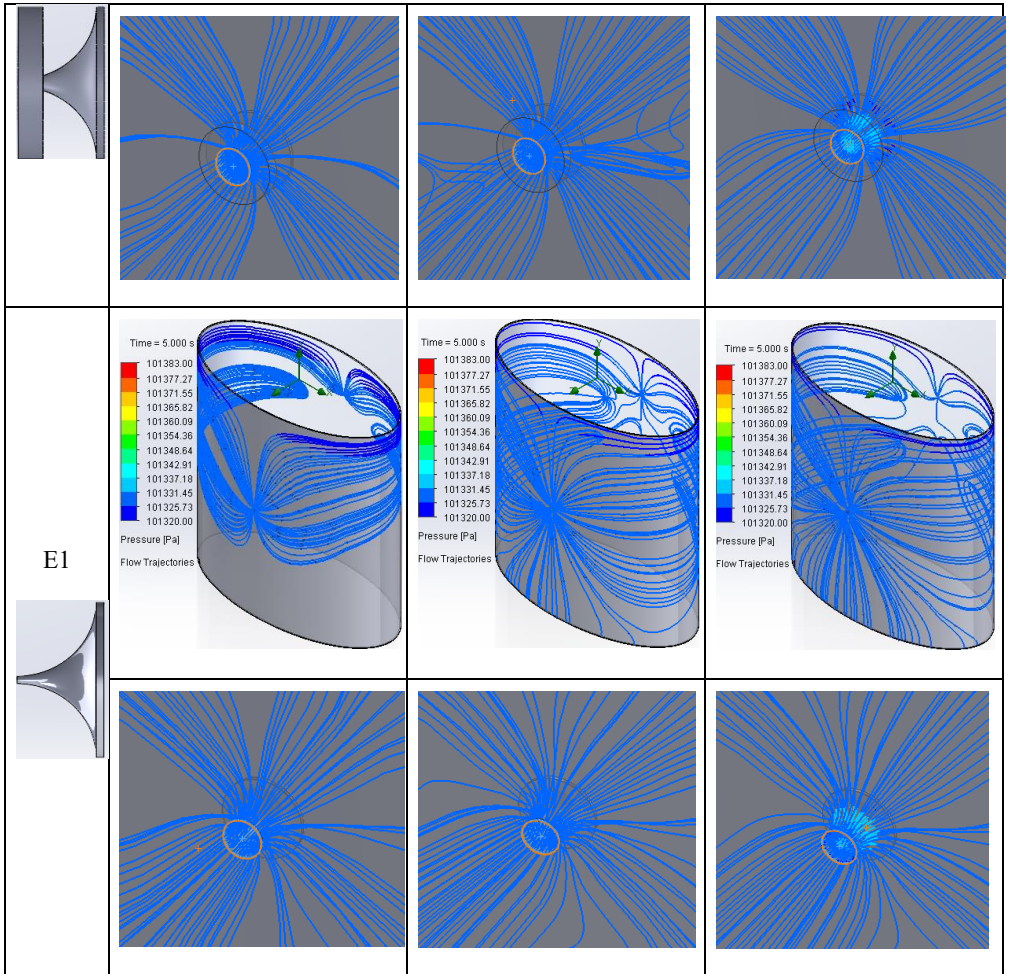


Figure 4.2.3. Flow pressure plots.

The figures 4.2.3 clearly demonstrate that the majority of fluctuations occur near the inlet of the flow channel at the ventilation element. The related numerical values are provided in table 4.2.2. Furthermore, the findings indicate that the fluctuations in pressure increase proportionally with the rise in air velocities. The results show that when the size of the outer ring reduces, there is a decrease in pressure difference.

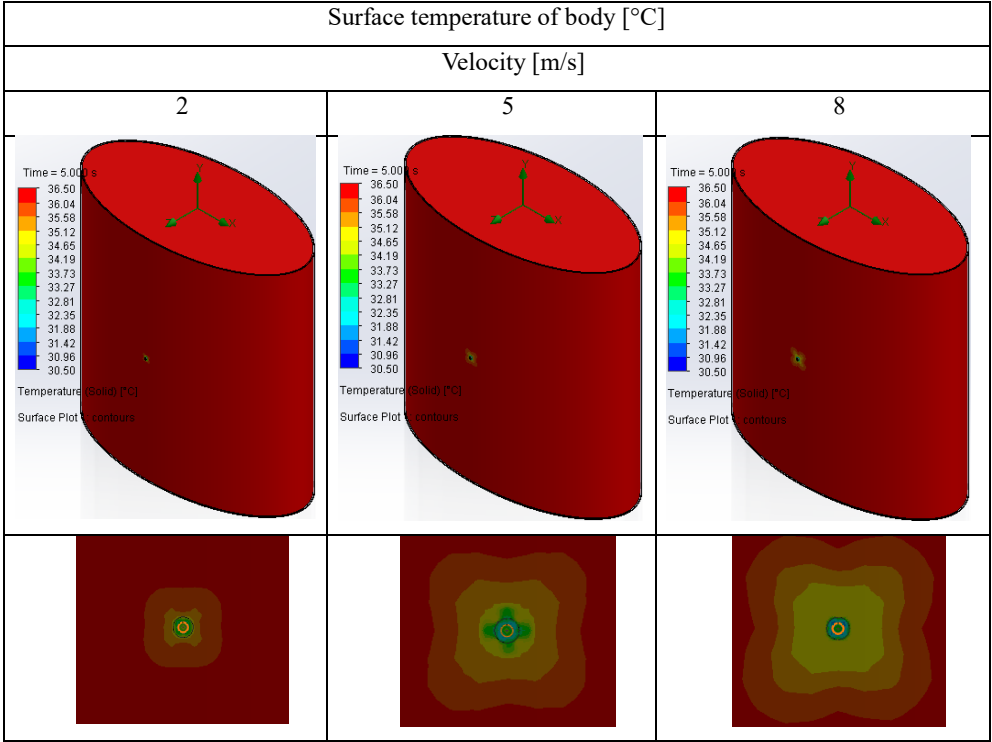


Figure 4.2.4. Surface temperature plots for element E0-90.

In the figure 4.2.4, the top row displays the surface temperature across the entire model, while the bottom row shows the temperature distribution near the ventilation with an enlarged view. Furthermore, temperature plots for other ventilation scenarios are examined, and the corresponding results are presented in the table 4.2.2. The cooling range increases as the inflow velocity increases from 2 to 8 m/s, as observed from the temperature plots. This is logical because it is evident that a higher air velocity results in increased heat transfer, hence enhancing the cooling capacity. This is also true for other cases of mentioned ventilation elements.

Table 4.2.2.

## Numerical Values of Simulation Results

Element	Inlet Velocity [m/s]	Values	Pressure [Pa]	$\Delta P$	Surface Temperature of body	$\Delta T$
E0-90	2	Max	101335.71	10.41	36.50	3.39
		Min	101325.30		33.11	
	5	Max	101354.00	28.60	36.50	4.75
		Min	101325.40		31.75	
	8	Max	101382.94	57.53	36.50	5.03
		Min	101325.41		31.47	
E0-60	2	Max	101331.06	5.69	36.50	3.53
		Min	101325.37		32.97	
	5	Max	101337.41	12.54	36.50	4.94
		Min	101324.87		31.56	
	8	Max	101345.44	25.44	36.50	5.31
		Min	101320.00		31.19	
E0-45	2	Max	101329.67	4.41	36.50	2.9
		Min	101325.26		33.60	
	5	Max	101334.64	9.96	36.50	5.39
		Min	101324.68		31.11	
	8	Max	101343.53	20.34	36.50	5.84
		Min	101323.19		30.66	
E0-30	2	Max	101329.12	3.79	36.50	3.07
		Min	101325.33		33.43	
	5	Max	101331.64	6.16	36.50	5.29
		Min	101325.48		31.19	
	8	Max	101336.87	13.53	36.50	5.73
		Min	101323.34		30.77	

E1	2	Max	101329.30	4.01	36.50	3.34
		Min	101325.29		33.16	
	5	Max	101331.82	6.6	36.50	5.14
		Min	101325.22		31.36	
	8	Max	101337.87	13.01	36.50	5.88
		Min	101324.86		30.62	

Table 4.2.2 displays obtained values of results and from these values, pressure difference and temperature difference are calculated for each case. These measured pressure and temperature differences are used to compare the efficiency of mentioned ventilation element designs to suggest the most efficient element design. The comparison is described in the figures 4.2.5 and 4.2.6 below, in form of graphical representation.

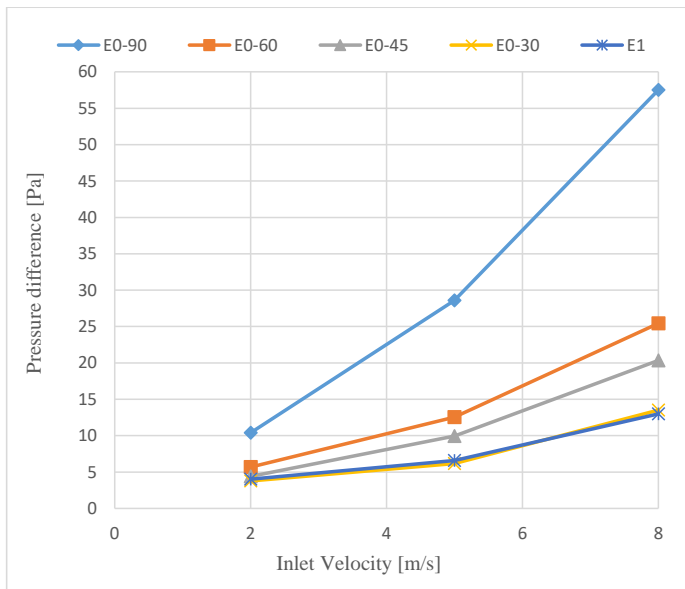


Figure 4.2.5. Pressure difference at different air velocities.



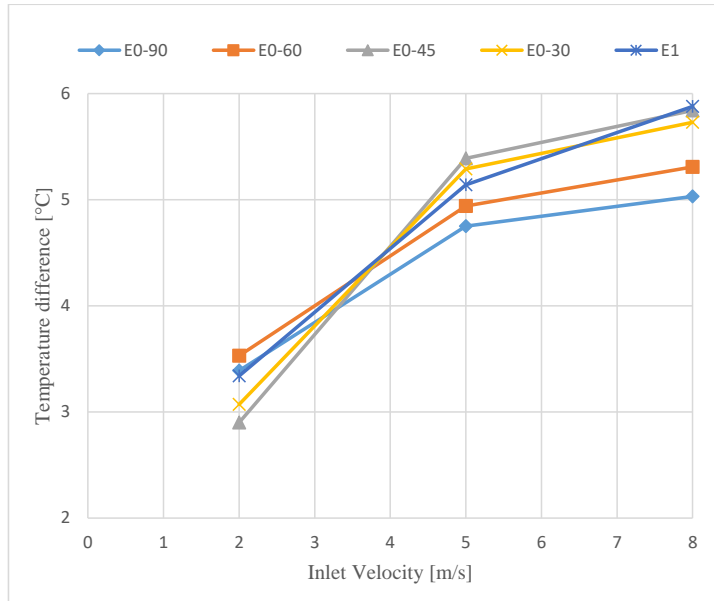


Figure 4.2.6. Temperature difference at different air velocities.

The pressure difference for five separate scenarios can be seen in figure 4.2.5 at three distinct air velocities. The pressure difference is highest at E0-90, as shown by the graphical representations. The element E0-30 and E1 exhibit the lowest pressure differential among all elements, with a minor disparity in pressure between them. It is worth noting that as the angle ( $\alpha$ ) lowers from  $90^\circ$  to  $30^\circ$  in outer ring design, the pressure difference also decreases. Lower pressure difference may result in less flow energy losses, hence enhancing the cooling efficiency of the system.

Figure 4.2.6 illustrates the comparison of all the described scenarios in terms of temperature difference. Contrary to pressure difference, a larger temperature difference suggests better cooling. Upon observing figure 4.2.6, it is evident that at a velocity of 2 m/s, element E0-60 and E0-90 exhibit the highest difference in temperature. However, with velocities of 5 and 8 m/s, both elements display the smallest temperature difference. This implies that E0-60 and E0-90 may offer better cooling performance when the air velocity is low, but they are less effective when the inlet velocities are larger. This is due to the fact that energy losses and pressure difference increase

in these elements as velocity increases, as shown by figure 4.2.5. The elements E0-60 and E0-90 exhibit higher energy losses and pressure differences, which increase with the increase in velocity. This indicates the low efficiency of these elements. Regarding element E0-45 and E0-30, both exhibit the smallest temperature difference at a velocity of 2 m/s, but the largest difference at 5 m/s. This suggests that they may not be particularly efficient at lower speeds, but can deliver better results at higher air velocities.

Although choosing the right design can be challenging, it can be done with careful optimization and simulation analysis. CAD design and CFD software are crucial tools for these reasons, as they significantly reduce the time and cost associated with production and physical experiments.

### **4.3. Selection of Appropriate Criteria for Optimization of Ventilation Element**

This work aims to determine suitable criteria for optimizing the shape of ventilation elements in protective garments using a metamodeling approach. Complex models generally need computationally demanding algorithms, hence metamodels, sometimes called approximations, response surfaces, or surrogate models, are utilized to expedite the optimization process. The Efficient Global Optimization (EGO) method, principally utilizing Kriging, is commonly employed for solving deterministic optimization problems with complex models. Kriging, or Gaussian Process (GP) regression, is utilized as a metamodeling tool for computationally expensive simulations due to its ability to create surfaces of varying complexity, potentially interpolating, within a probabilistic framework.

Ensuring thermal comfort is essential for individuals in hot climates or challenging work environments to mitigate heat stress. Heat stress can lead to mental and physical fatigue, causing health issues and decreased productivity at work [136, 137]. In recent years, there has been increased focus on developing personal cooling garments due to the rise of innovative textiles and the global need for energy-efficient solutions. Researchers are exploring various new materials, cooling techniques, and structural optimizations for these garments. Various ventilation methods include electric cooling, liquid cooling, and air cooling with and without an external power source



[10]. Our work focuses on ventilation without an external power source by integrating a ventilation element into protective clothing. The design of the ventilation element used may significantly affects the efficiency of air exchange between the outside environment and the microclimate within the clothes. We reached this conclusion in our prior research investigation with various ventilation element shapes [135]. We determined an effective shape for the ventilation element in this work and optimized its shape based on criteria of minimal pressure difference [138]. This study aims to expand our research by choosing several potential criteria to determine optimal parameters for ventilation element optimization and assess the method's reliability. The software KEDRO is utilized for shape optimization of ventilation elements, facilitating experiment preparation, metamodel generation, and global optimization using these metamodels. SolidWorks is utilized to generate models based on design of experiments derived from metamodels, and its flow simulation tool is used to compute values of required criteria.

**Model and Boundary Conditions:**

Here the same optimization technique is used as it is described in the chapter 4.1. The model design, material properties and boundary conditions are also same as it is mentioned in the chapter 4.1. The experiments are conducted at an air velocity of 4 m/s. The twelve ventilation element created based on DOE are shown in the figure 4.3.1.

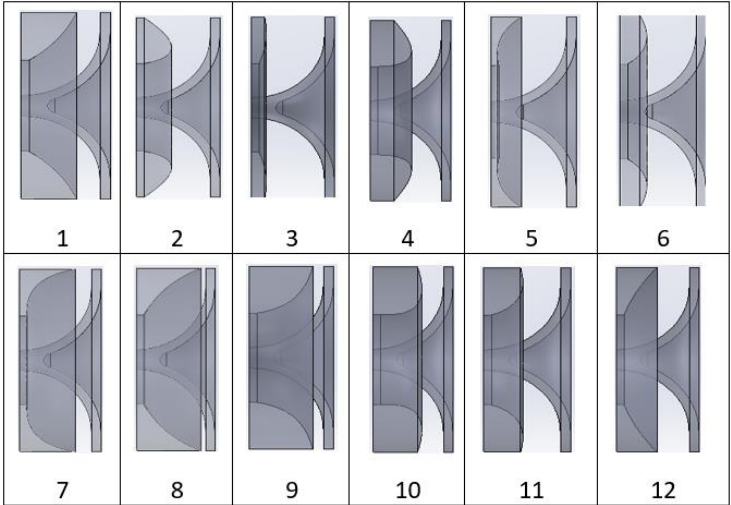


Figure 4.3.1. Twelve geometrical design of element constructed using DOE.

The different criteria considered in flow simulation study are as under:

1. HTR – Heat Transfer Rate [W]
2. H - Absolute Total Enthalpy (average) [J/kg]
3.  $\Delta H$  - Absolute Total Enthalpy Rate [W]
4. HF – Surface Heat Flux (average) [W/m<sup>2</sup>]
5. dP – Pressure Difference (from flow trajectories) [Pa]
6. dT - Surface Temperature Difference (body) [°C]

### Results and Discussion:

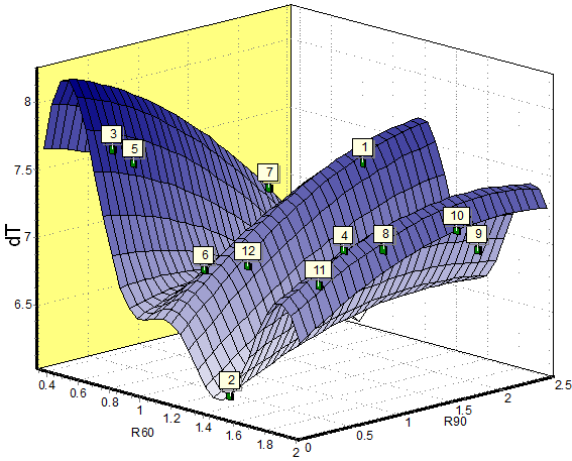
Each of the 12 elements is analyzed individually, and the resulting data is assessed to obtain required values. The results obtained for each criteria are displayed in table 4.3.1. Here all the mentioned parameters values in table 4.3.1 are with respect to body, except  $\Delta H$  and dP. Where,  $\Delta H$  represents heat transfer through ventilation holes and negative sign shows that heat is releasing from the system. The parameters dP gives the pressure difference particularly in a space between body and jacket where air flows entering through ventilation element.

Table 4.3.1.

Numerical values of simulation results

Element	HTR [W]	H (avg.) [J/kg]	$\Delta H$ [W]	HF (avg.) [W/m <sup>2</sup> ]	dP [Pa]	dT [°C]
1	17.655	312509.94	-0.997	29.682	5.55	7.5
2	17.644	312509.58	-1.00	29.663	6.17	6.2
3	17.622	312509.25	-0.997	29.693	6.06	7.7
4	17.693	312509.84	-0.997	29.746	8.49	7.24
5	17.650	312509.43	-0.997	29.674	5.89	7.38
6	17.599	312509.65	-1.00	29.587	5.74	6.91
7	17.617	312510.01	-0.997	29.617	8.25	7.04
8	17.612	312510.09	-0.997	29.584	34.4	6.64
9	17.692	312510.21	-0.997	29.744	18.83	6.91
10	17.689	312509.84	-0.997	29.739	13.92	7.27
11	17.687	312509.94	-0.997	29.725	5.7	6.76
12	17.632	312509.62	-0.997	29.643	5.44	6.68

It is evident from the results that only dP and dT exhibit sufficient sensitivity in values for further approximation and optimization, whereas the other parameters provide nearly identical values for all 12 DOE, which are not very beneficial for quality approximation. In the chapter 4.1, we discussed the process of optimization of element using minimum pressure difference (dP) as a criterion. This study revealed that dT could be another valuable parameter for optimization, as other mentioned parameters lack sufficient sensitivity. Further approximation and optimization based on the criteria of maximum temperature difference (dT) is described below. A greater temperature difference results in better cooling due to the increased heat transfer rate with higher temperature difference.



(a)

Functions Yr:	dP	dT
Sigma Cross	4.316561	0.195112
Sigma Cross%	50.095577%	44.620717%
R2 adjusted		
F-Crit 99%		
Sigma	0.000000	0.000000
Sigma%	0.000000	0.000000
MeanExpValue	10.370000	7.027500
StDev of Exp	8.616651	0.437267
Exp. Range	28.960000	1.600000
MaxError	0.000000	0.000000
Bad Point No.	11	11
Max Rel Error	0.00%	0.00%
BadRelPointNo.	11	11
Max Cook Dist.		
Suspicious point	8	2
No.ofActualExp	12	12
Filtered STD		

(b)

Figure 4.3.2. Response surface  $dT = f(R60, R90)$  using 12 DOE for Kriging approximation: (a) Cross-section plane of response surface; (b) Indices of approximation quality.

Figure 4.3.2 displays the Kriging approximation performed with the response surface showing experimental points. Two primary metrics for evaluating approximation quality are Max Rel Error and Sigma Cross%. Here, Max Rel Error is the maximum relative error (in proportion to the experimental values).

The quality of your approximation is severely lacking if the Sigma Cross% is close or greater than 100%. On the other hand, a smaller Sigma Cross% yields better approximation quality. A lower value of Max Rel Error % also indicates a better approximation. In this case, the Max Rel Error is 0.0% and the Sigma Cross% is 50.09% for dP and 44.62% for dT (figure 4.3.2 (b)), both of which show that the approximation is of good quality, though there is a scope for improvement.

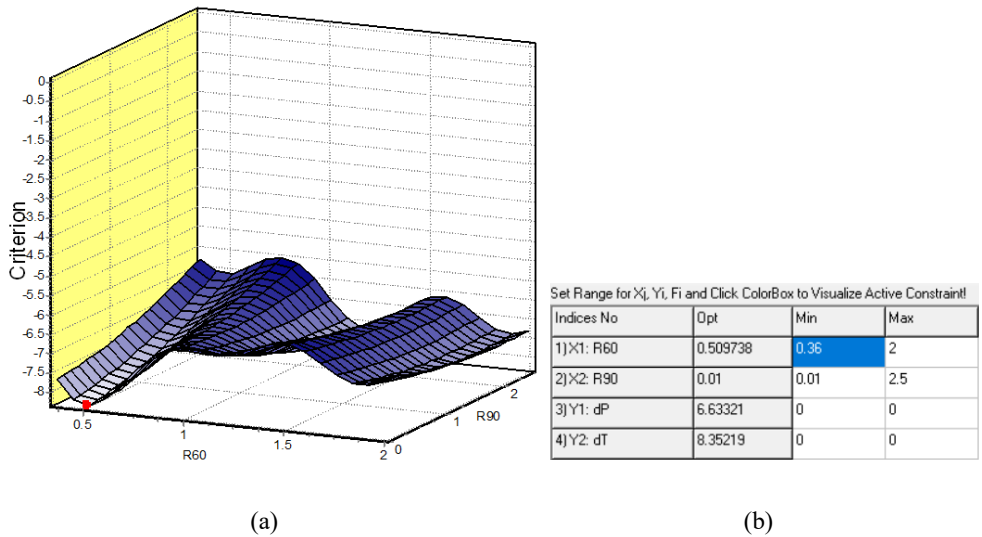


Figure 4.3.3. Optimization result (red point indicates global minimum of -dT): (a) Cross-section plane of criterion surface; (b) Optimum values.

The optimization results obtained using -dT as a criterion are shown in figure 4.3.3. The negative (-) sign indicates that the maximum value of dT leads to better performance and 8.52 °C is the maximum value of dT that we can achieve by the optimal design of ventilation element. Figure 4.3.3 (a) shows a cross-sectional plane of the criterion surface, with a red point representing the optimal coordinate position of the element design. The optimal coordinate values for element design are shown in figure 4.3.3 (b), represented by X1: R60 and X2: R90. The indices Y1: dP and Y2: dT represent the relative values of flow pressure difference and surface temperature difference that can be achieved by the optimal design of a ventilation element. Once the optimum values for the coordinates are determined, a geometric model of the ventilation element is generated

in SolidWorks using the optimal values of R60 and R90 depicted in figure 4.3.3. Given that the coordinate values of R90 for both dP and dT are the same and very small (0.01), it can be concluded that there is no outer ring exist and the geometrical shape of the element remains same in both the scenarios. After creating the CAD model of the ventilation element, it is positioned to the inlet hole of the model that includes the jacket and body depicted in chapter 4.1. The entire model is subsequently simulated in SolidWorks flow simulation to determine the flow pressure and surface temperature for the optimal design of the ventilation element. The values of dP and dT are calculated from obtained results, which are shown in figure 4.3.4 and 4.3.5 respectively.

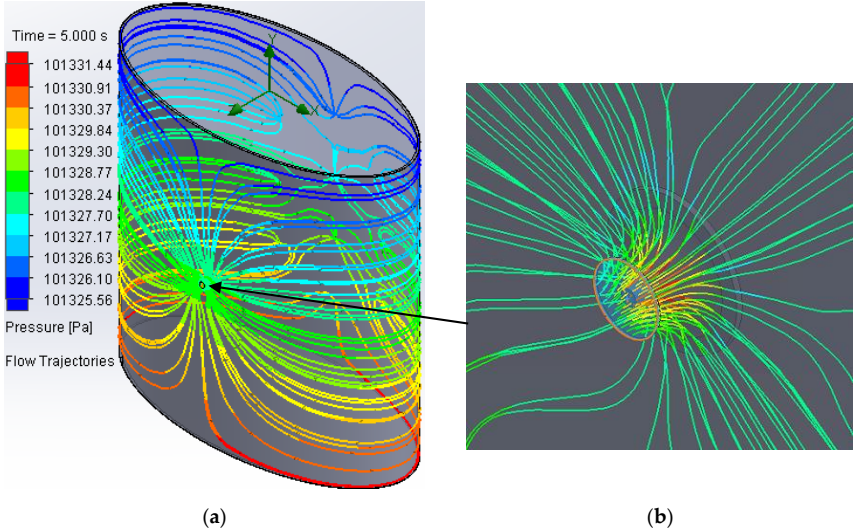


Figure 4.3.4. Flow pressure plots for optimum element design: (a) Flow pressure over entire model; (b) Zoomed view near ventilation hole.

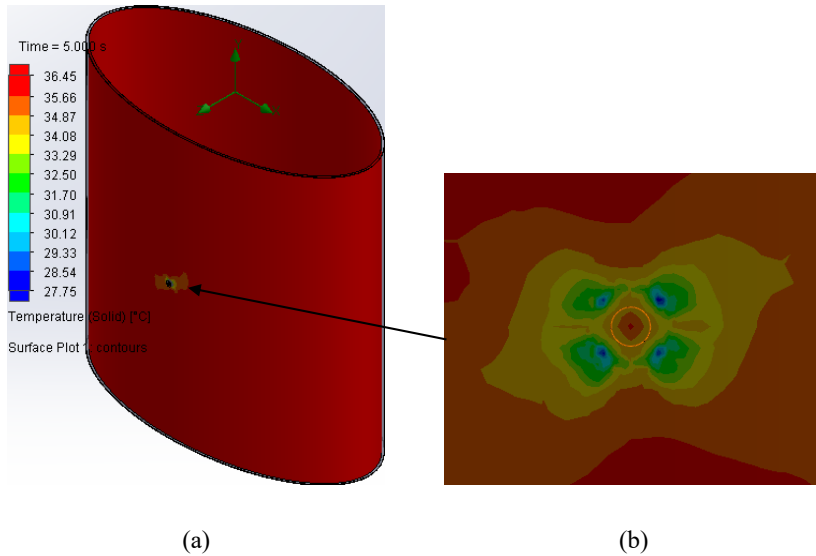




Figure 4.3.5. Surface temperature of body: (a) Surface temperature plot of whole model; (b) Enlarged view near ventilation hole.

Table 4.3.2.

Results comparison

Title 1	dP [Pa]	dT [°C]
Optimum shape of element	R60=0.50;	R60=0.40;
	R90=0.01	R90=0.01
		
Sigma Cross%	42.73	39.82
Optimum values from KEDRO	4.80 (Min)	8.52 (Max)
Value from flow simulation results	5.88	8.70

The values obtained through optimization using KEDRO and SolidWorks flow simulation are close with minor deviation. The difference depends mostly on the quality of approximation and

CFD model. By improving the quality of approximation, it is possible to acquire values that are very close with very slight variance. Furthermore, implementing a fine mesh in a CFD simulation can decrease the variation in the resulting values, but it also leads to a substantial increase in calculation time as the mesh level increases. The analysis indicates that the quality of the approximation for dT (Sigma Cross%=44.62) is slightly better than that of dP (Sigma Cross%=50.09). However, in both the cases quality of approximation is good enough to provide results with minor deviation. This can be said as the obtained results of the flow simulation and optimization show a minor difference of 0.2 °C (8.55 – 8.35) for dT and 0.12 Pa for dP (6.75 – 6.63). The percentage difference between the obtained values is 1.7% for dP and 2.34% for dT. The error falls within the permissible tolerance as it is less than 5%.

#### **4.4. Conclusions of Shape Optimization of Ventilation Element**

1. It can be concluded from the obtained results in chapter 4.1, that the ring is practically nonexistent at the optimal design points, suggesting that the element without an outside ring will provide the best results. The study demonstrates that employing metamodeling approach with CFD simulation can significantly decrease the computing time required for optimization.
2. In the chapter 4.3, different criteria were considered for the optimization of ventilation element and the results indicates that not all parameter values will show enough sensitivity for the approximation and optimization of element.
3. From the results it is clear that dP and dT are most appropriate and sensitive criteria for the optimization of ventilation element out of all mentioned criteria in this study. Moreover, these both parameters provide same optimal shape of ventilation element.
4. However, dT shows slight better approximation quality than dP which makes dT most appropriate parameter for the optimization of ventilation element. This is also true as the ventilation elements are to be used in protective clothing to provide efficient cooling of human body in case of warm environment or heavy work load conditions and temperature is the best indicator to predict the efficiency of cooling.

## **5. ANALYSING THE EFFICIENCY OF THE STUDIED OBJECT (CLOTHING) AND VENTILATION ELEMENT BY SOLIDWORKS FLOW SIMULATION**

### **5.1. Analysing Efficiency of Ventilation Element with Simplified Model**

The foundational work of researchers like Richardson [139] and Courant, Friedrichs, and Lewy [140] laid the groundwork for computational fluid dynamics (CFD). Their pursuit of understanding fluid motion led to the creation of robust numerical methods that have improved the numerical representation of various forms of fluid flow [141]. CFD is rapidly becoming into an influential and prevalent tool across numerous sectors; every solution embodies a complex web of mathematical physics, numerical methodologies, user interfaces, and cutting-edge visualization approaches [142]. For both experimental and computational fluid dynamics (CFD) purposes, it is necessary to precisely simulate the properties of the atmospheric boundary layer (ABL) in order to accurately anticipate the wind's effect on built objects [143]. Thermal modelling of structures will also be affected by the flow characteristics [144]. The best approach for accurately representing turbulence is to maintain the spectral characteristics of the input flow [145]. It is ideal to match velocity spectra with those obtained at full-scale, including the complete frequency range. Yet, accomplishing this goal through small-scale experiments and simulations is challenging. One reason for inaccurate pressure predictions in reduced scale experiments is the occurrence of small-scale turbulence that causes the shedding of immature vortices. These experiments are both economically expensive and difficult to handle [146]. On the other hand, full-scale computational fluid dynamics (CFD) simulations need a significant amount of processing time and resources [147].

This study aims to assess the efficacy of ventilation elements E1 and E2 with a focus on reducing computation time. The ventilation elements are designed for use in protective clothing to provide effective cooling and prevent insects, rain, and dust from directly reaching the human body [17]. Therefore, selecting the correct element is crucial. Using a fine mesh in simulations is crucial for obtaining accurate findings, but it significantly increases computing time. On the other hand, a coarse mesh may not provide precise values but might be useful for comparing results when using



the same parameters to estimate efficiency. This study compares ventilation elements E1 and E2 in two separate scenarios to determine the most efficient element with respect to optimal computational time. The first scenario uses a simplified elliptical model of the human body and jacket. In the second case, the model is simplified into two square plates, where one plate refers to the jacket surface and the other represents the body. This study utilizes SolidWorks flow simulation to provide results with an inlet air velocity of 2 m/s. The specific model dimensions and boundary conditions are explained in the next section.

## **5.2. Simplified Model Design and Boundary Conditions**

Here the same elliptical model design is considered as it is mentioned in previous chapter 3.2. The ventilation element E1 and E2 are individually attached at inlet ventilation hole shown in front view of the figure 5.2.1, to obtain simulation results. These results are then compared to analyze efficiency of both the ventilation elements. These ventilation elements are shown in the figures 5.2.2 and 5.2.3. The boundary conditions and material properties are also kept same as of previous study in the chapter 3.2.

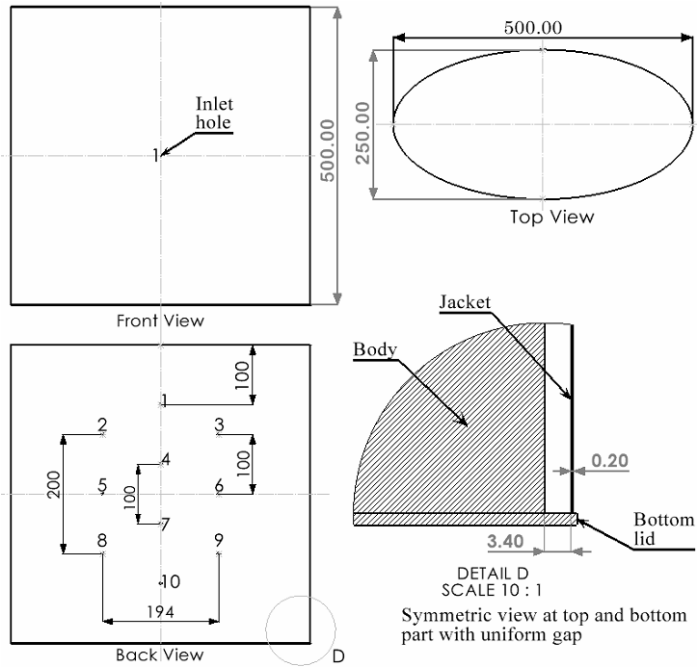


Figure 5.2.1. Case 1: Simplified elliptical model of human body and jacket.

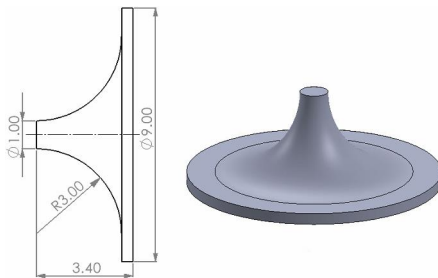


Figure 5.2.2. Ventilation element E1.

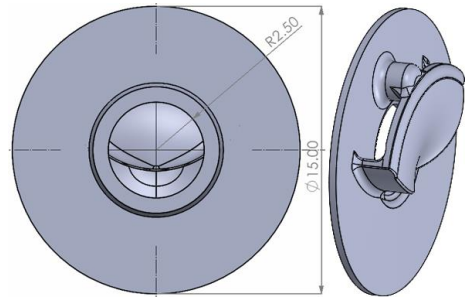


Figure 5.2.3. Ventilation element E2.

For case 2, the model design is simplified to two square plates with reduced area, where one plate represents the jacket and the other represents the body. Figure 5.2.4 displays the design of this model. The same parameters are utilized in the flow simulation study as previously mentioned.

In this scenario, the only variation lies in the fact that external flow simulation is being conducted while taking into account the enclosed boundary to the model dimensions. The computational domain's length is 73.40mm. Figure 5.2.5 displays the computational domain, with a red arrow indicating the inlet velocity at the front and a blue arrow representing the environmental condition at the backside.

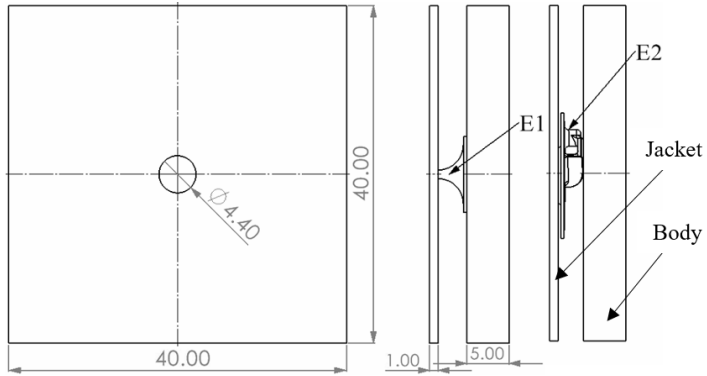


Figure 5.2.4. Case 2: Simplified model with two square plates.

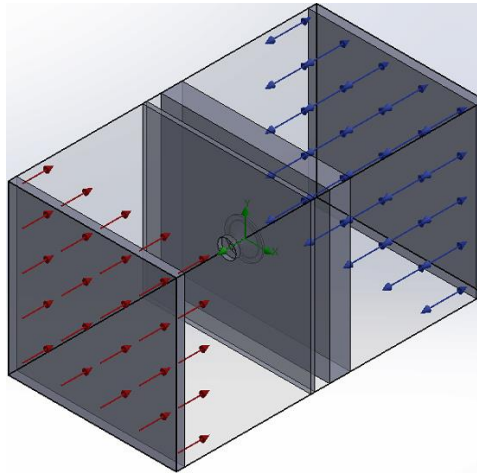


Figure 5.2.5. Case 2: Computational domain.

The following are the criteria that were considered in the analysis of the flow simulation study:

1. HTR – Heat Transfer Rate [W]

2. HF (avg.) – Surface Heat Flux (average) [ $\text{W}/\text{m}^2$ ]
3. dP - Pressure Difference [Pa]
4. dT - Surface Temperature Difference (body) [ $^{\circ}\text{C}$ ]
5. T (avg.) – Average Surface Temperature (body) [ $^{\circ}\text{C}$ ]

**Results and Discussion:**

All the results mentioned here are simulated for physical time of 10 seconds and since this study is transient in nature, results may get influenced by the set physical time of the study.

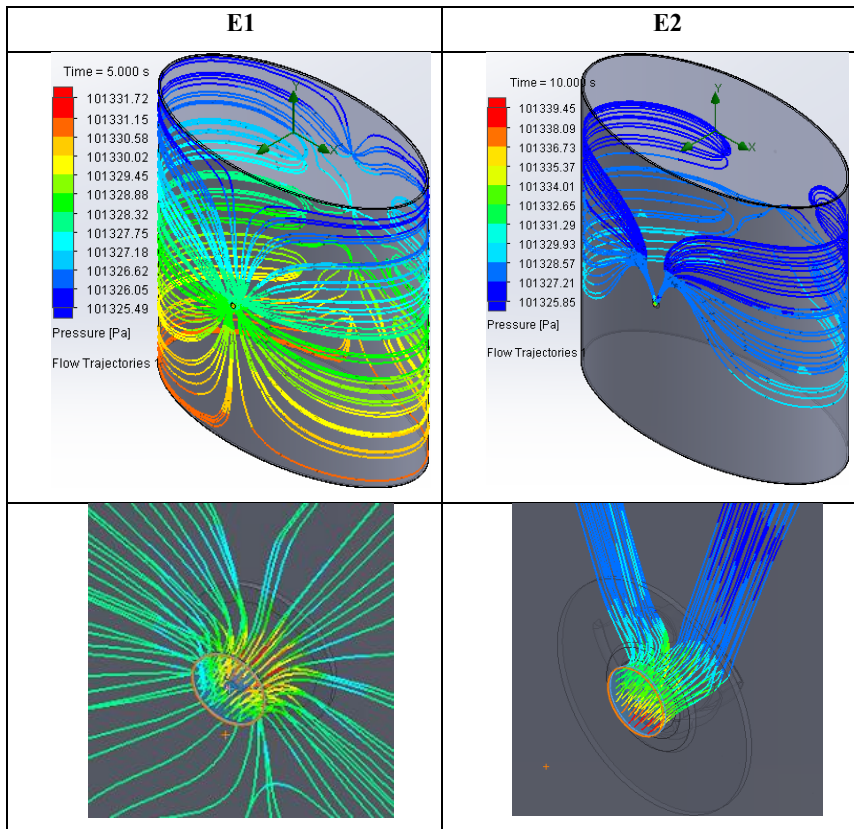


Figure 5.2.6. Flow pressure trajectories in case 1.

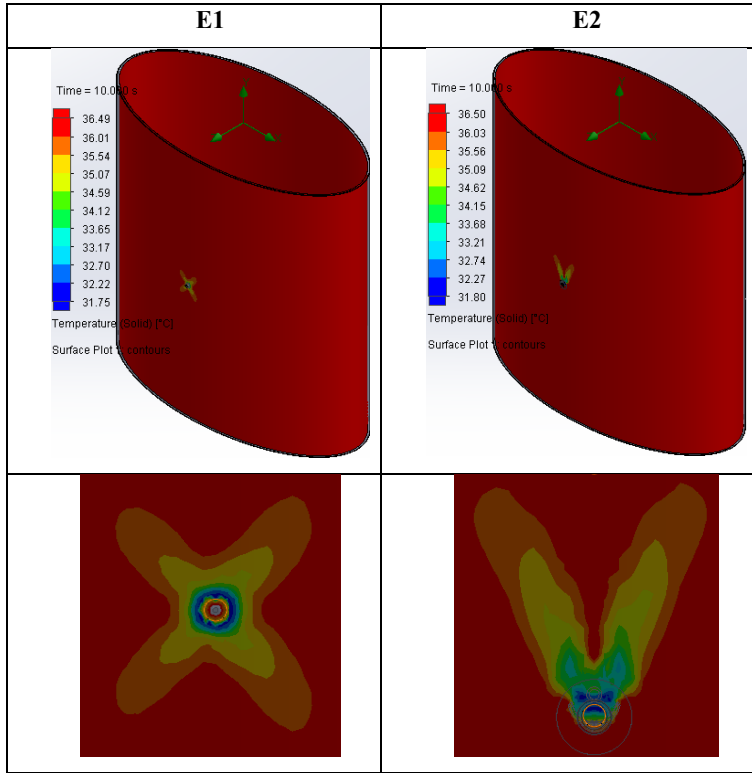


Figure 5.2.7. Surface temperature plots of body in case 1.

Table 5.2.1.

Numerical values of results for case 1.

Parameters	E1	E2	$\Delta$
HTR. [W]	8.739	8.702	0.037
HF (avg.) [W/m <sup>2</sup> ]	12.154	12.065	0.089
dP [Pa]	6.23	13.6	7.37
dT [°C]	4.75	4.70	0.05
T (avg.) [°C]	36.44	36.44	0

Table 5.2.1 shows that there is minimal sensitivity in the results for E1 and E2, except for criteria  $dP$ , for predicting the efficiency of the elements. This is due to the larger surface area of the model compared to ventilation and the presence of only one inlet ventilation. One way to achieve comparable results is by increasing the number of ventilation units, however this will significantly increase computational time, making it less ideal option. Another alternative is to decrease the model's area in proportion to the ventilation element, which can yield sensible results and greatly reduce computing time. This option we have considered for the model used in case 2 (figure 4.2.4). Same set of criteria were considered in case 2, and the detailed values of obtained results are mentioned in table 5.2.2. In the table 5.2.1 and 5.2.2,  $\Delta$  refers to the difference in value between E1 and E2.

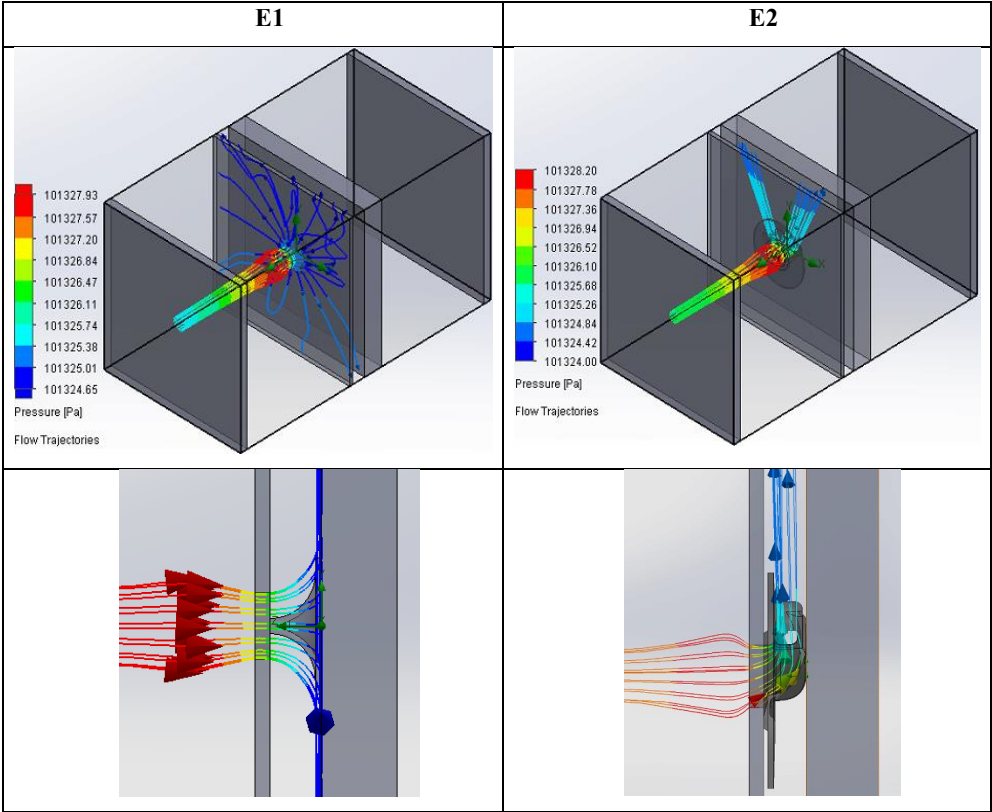


Figure 5.2.8. Flow pressure trajectories in case 2.

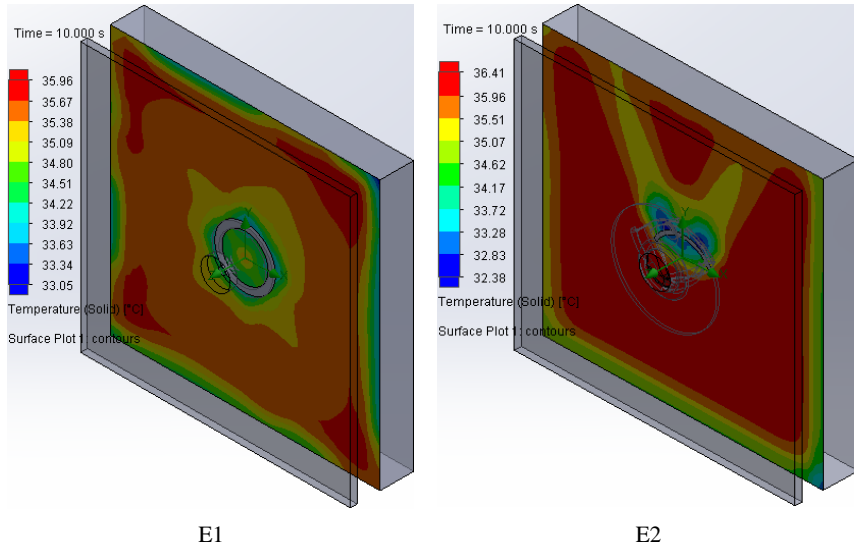


Figure 5.2.9. Surface temperature plots in case 2.

Table 5.2.2.

Numerical values of results for case 2.

Parameters	E1	E2	$\Delta$
HTR [W]	0.328	0.196	0.132
HF (avg.) [W/m <sup>2</sup> ]	207.097	124.507	82.59
dP [Pa]	3.28	4.2	0.92
dT [°C]	2.91	4.03	1.12
T (avg.) [°C]	35.34	35.90	0.56

Table 5.2.2, shows that the sensitivity of the Surface heat flux (HF) and average body temperature T (avg.) increases in case 2. Element E1 provides higher value of HF compared to E2, indicating that the heat transfer rate of E1 is better. A higher heat transfer rate refers to a higher cooling efficiency. Therefore, the average body temperature for E1 (35.34 °C) is lower than that of

E2 (35.90 °C). Based on these two criteria, it can be concluded that element E1 offers better cooling efficiency compared to E2.

From the result analysis, it can be concluded that the results in the first case do not provide sensitive values for predicting the efficiency of element E1 and E2. This is due to the larger surface area of the model in comparison to the ventilation. However, the value of pressure difference in case 1 is comparable but since this value is in Pascal (Pa) the difference is very small and it does not provide much idea for predicting efficiency of ventilation elements. In order to solve this issue, the model is simplified into two square plates with significantly less surface area in the second case. As a result, the sensitivity of the obtained results is enhanced in this case. The most significant criterion for comparison is the HF and T (avg.), indicating that element E1 offers better cooling efficiency compared to E2.

### **5.3. Selection of Appropriate Criteria for Analysing the Efficiency of Ventilated Clothing**

The efficient design and management of ventilation systems are crucial for maintaining indoor air quality and improving building energy efficiency [148]. The characteristics of the airflow within a building have a significant impact on the effectiveness of ventilation systems in removing pollutants from that space [149]. The same is true for ventilated protective clothing. Computational Fluid Dynamics (CFD) has been extensively utilized for the design and implementation of building ventilation systems. This approach is also increasingly being adopted in other areas of fluid dynamics research, such as the ventilation of protective clothing. For designing systems involving fluid flows, CFD simulations are frequently used as the base. In order to ensure human thermal comfort, it is necessary to maintain a heat balance between the human body and the surrounding environment. This involves regulating the heat generated within the body and the heat transferred to or from the body. The heat dissipation/gain process is influenced by multiple factors, and it involves different types of heat transport, such as conduction, convection, radiation, and evaporation. When the body absorbs more heat than it can release, it leads to thermal discomfort



as the body's core temperature and heat storage grow. Normally, the body's core temperature is around 36.5 °C (+ or - 1 °C) in thermal comfort conditions. Experiencing an excessive increase in body heat may cause a serious threat to one's health and lead to heat stress. In order to alleviate heat stress or attain thermal comfort in such circumstances, it is imperative to implement efficient exterior cooling methods [30]. Utilizing personal cooling systems to provide individualized cooling can be an effective method to reduce heat stress or achieve thermal comfort in situations when implementing widespread air conditioning is not possible [150]. Personal cooling systems (PCS) are specifically developed to reduce the risks posed by elevated core body temperatures, while also enhancing the overall job performance of individuals. Various personal cooling systems are available, such as a cooling chair [151], wrist-band devices [152], radiant cooling desk [153], desk fan [154], and personal cooling clothing [155 - 158], and so on. Clothes creates its own atmosphere and is our most personal space, according to Watkins [159].

The present study focuses on the crucial task of selecting suitable criteria in a flow simulation analysis aimed for predicting the cooling efficiency of ventilated protective clothing. This study examines three different cases of a simplified elliptical model of the human body with a protective jacket comprising 11, 48 and 105 ventilation elements. SolidWorks Flow Simulation is used to simulate all three models individually to calculate values of eight different criteria. It is assumed that increasing the number of ventilation units would result in an enhancement of cooling efficiency. However, it is crucial to understand how the values of various criteria change in flow simulation studies under different situations, and which criteria are crucial for the analysis. The criteria values for three cases are recorded and compared. The analysis results indicate a gradual increase in values of heat transfer rate, pressure and temperature differences as the number of ventilation unit increases. However, certain parameter values like flow pressure difference do not provide sufficiently information to predict efficiency of the system, whereas parameter like average temperature shows low sensitivity. The study suggests that the heat transfer rate and heat flux are most appropriate criterion to be examined in such a situation. This is because a higher amount of heat being transferred from the body indicates a better cooling efficiency.

#### **Model Design and Boundary Conditions:**

Figures 5.3.1 to 5.3.3 display the model design with three distinct cases. To ease the research, basic elliptical models of the body and jacket are created and aligned with the body at the center

and the jacket placed over it. A ventilation hole with a diameter of 4.4 mm is used in all instances, and an optimum circular ventilation element is connected to all ventilation locations. Figure 5.3.4 displays the schematic diagram of the ventilation element. All dimensions shown in the figures are in millimeters. In this study, an inlet air velocity of 4 m/s is used. The boundary conditions and material properties used in flow simulation study are same as it is described in chapter 3.2.

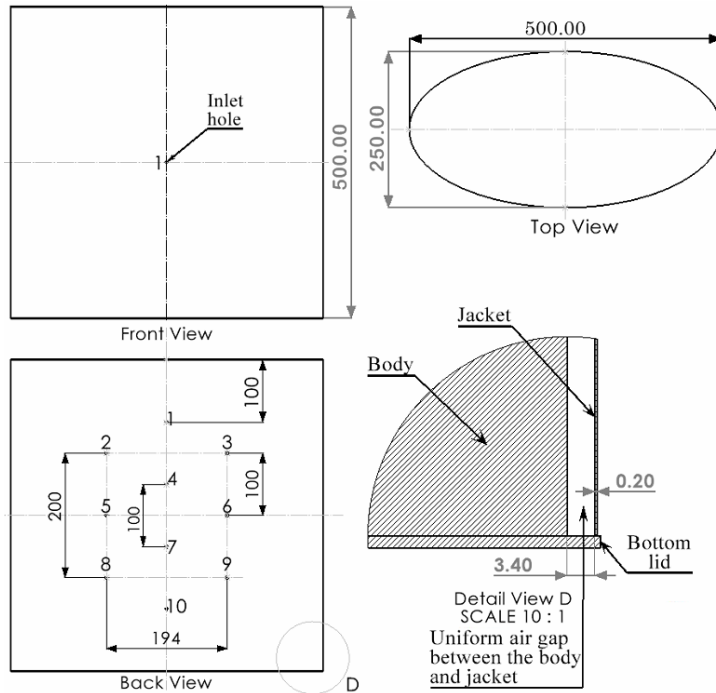


Figure 5.3.1. Case 1: model design with 11 ventilation holes.

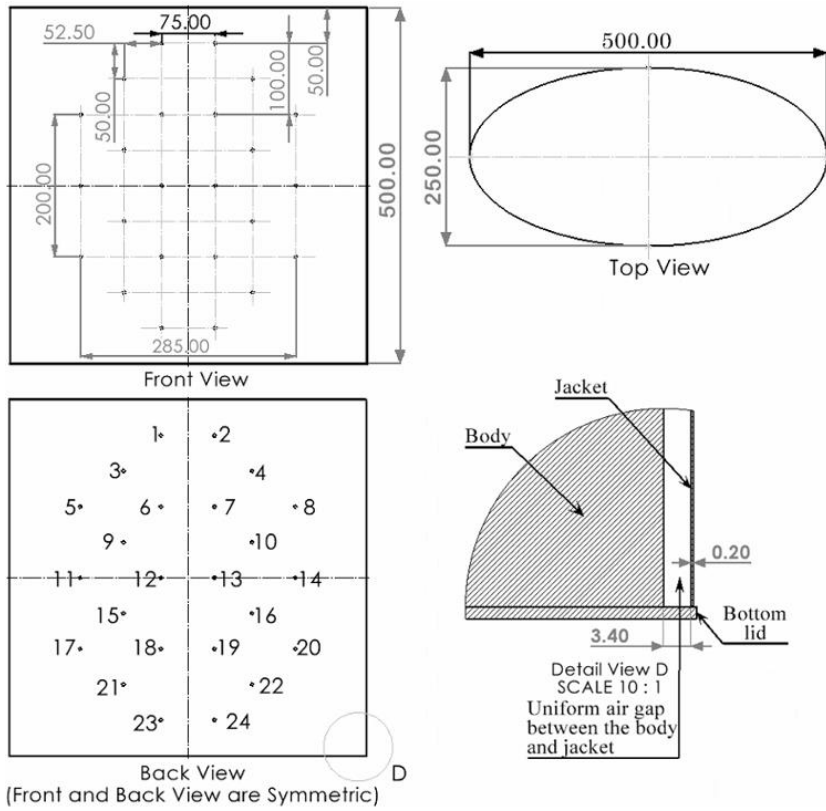


Figure 5.3.2. Case 2: model design with 48 ventilation holes.

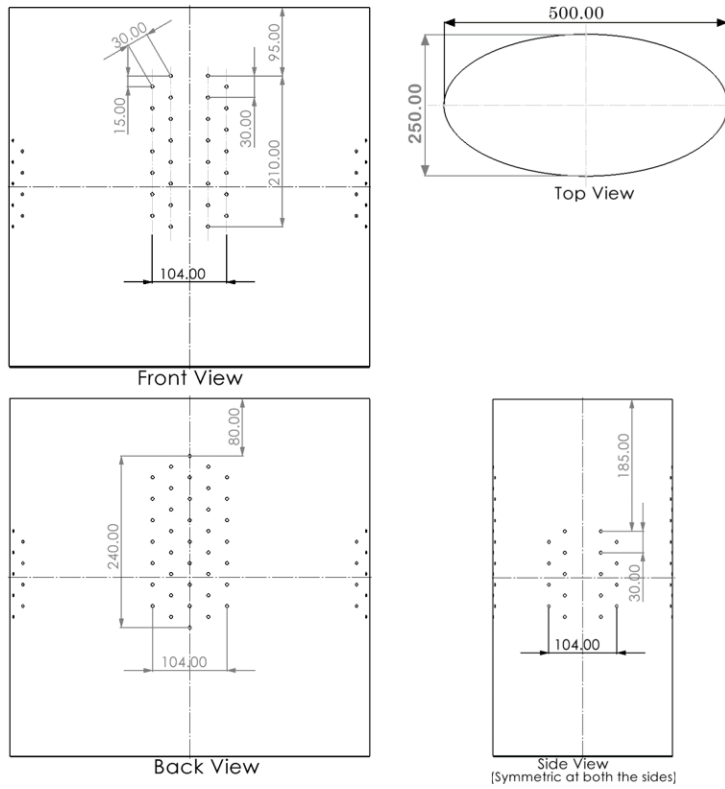


Figure 5.3.3. Case 3: model design with 105 ventilation holes.

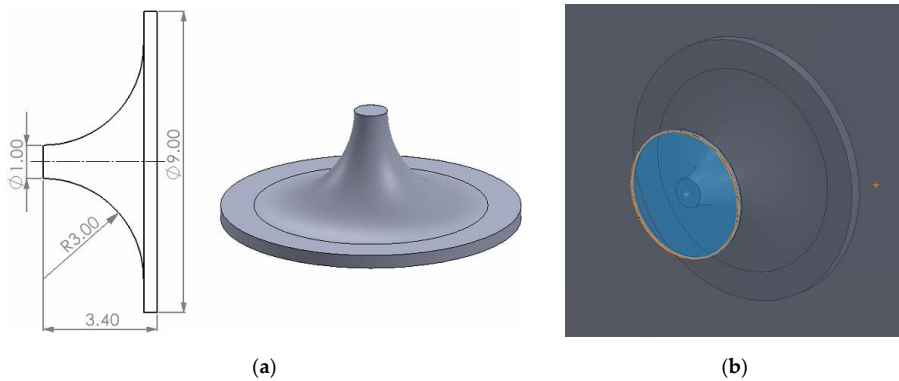


Figure 5.3.4. Ventilation element: (a) geometric dimensions of element; (b) position of ventilation element (highlighted orange circle shows ventilation hole).

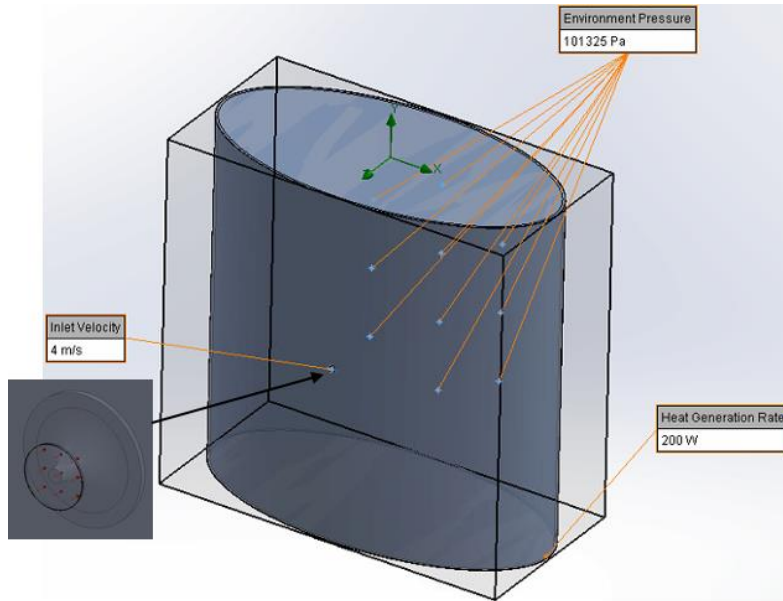


Figure 5.3.5. Computational domain and boundary conditions in case 1.

Figure 5.3.5 shows computational domain with set boundary conditions in the case 1. Inlet air of 4 m/s is visible at the front side, which enters into the air gap between the body and jacket and moves out through backside ventilations which are assigned to environmental pressure. The direction of air is perpendicular to the front face in all three cases. The same boundary conditions are assigned to model in case 2 and 3, the only difference is the numbers of inlet and outlet ventilation holes in each case.

The criteria analysed in the flow simulation study are as under:

1. HTR – Heat Transfer Rate [W].
2.  $\Delta H$  - Absolute Total Enthalpy Rate [W].
3. HF (avg.) – Surface Heat Flux (average) [ $\text{W}/\text{m}^2$ ].
4. dP - Pressure Difference [Pa].
5. dT - Surface Temperature Difference [ $^{\circ}\text{C}$ ].
6. T (avg.) – Average Surface Temperature [ $^{\circ}\text{C}$ ].
7. PMV (avg.) – Predicted Mean Vote.
8. PPD (avg.) – Predicted Percentage Dissatisfied (average) [%].

**Results and Discussion:**

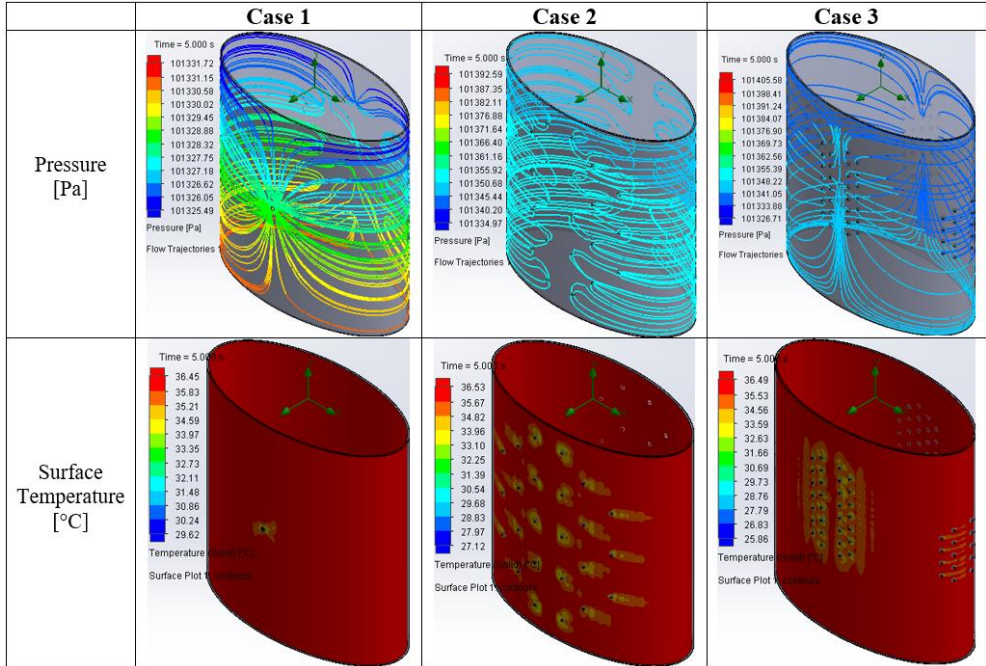


Figure 5.3.6. Flow pressure and surface temperature plots in each case.

The flow simulation study using SolidWorks is conducted for 5 seconds of physical time to determine values of eight specified criteria. Figure 5.3.6 displays pressure and surface temperature plots for all three cases. All parameter values derived from the simulation study are listed in table 5.3 below.

Table 5.3.

Numerical values of analysed criteria.

<b>Criteria</b>	<b>Case 1</b>	<b>Case 2</b>	<b>Case 3</b>
HTR [W]	17.637	32.288	43.714
$\Delta H$ [W]	-1.021	-23.490	-43.140
HF (avg.) [ $W/m^2$ ]	29.651	54.284	73.491
dP [Pa]	6.23	57.62	78.87
dT [ $^{\circ}C$ ]	6.83	9.41	10.63
T (avg.) [ $^{\circ}C$ ]	36.31	36.15	36.03
PMV (avg.)	3.05	2.95	2.93
PPD (avg.) [%]	99	98.8	98.5

Closely analysing results in table 5.3, it is known that all parameters values increases gradually with the increase in number of ventilations, except average surface temperature T (avg.), PMV and PPD. The value of average temperature decreases with the increase in number of ventilations, which makes sense as with higher number of ventilation more heat can transfer from the body that lowers body temperature. Moreover, with higher temperature difference, value of average temperature decreases as more heat can transfer when we have higher temperature difference. Though the sensitivity of average temperature obtained is very low as there is very small difference in the values, which may not be very useful in the analysis when there is small difference in the number of ventilations. The same is true for PMV and PPD. If we look on pressure difference, it does not provide much ideas on the cooling efficiency as the most of pressure variation take place near the ventilation holes and in very small area which can be negligible. Furthermore, the pressure difference is measured in Pascals (Pa), and the difference between the obtained values in the three cases are too small to draw any conclusions regarding the cooling efficiency of the model, based on these values. This can also be true for temperature difference, as lower temperature exists at very small region (represented in dark blue colour in figure 5.3.7 (b)). Typically, a higher temperature difference results in a faster rate of heat transfer, resulting in higher cooling efficiency. However, in certain cases (such as present), the area experiencing the lowest temperature is quite small and can be considered insignificant. Therefore, in such instances, it is essential to take into account additional relevant criteria in order to ensure the reliability of the results. These both trends of pressure and temperature variations can be visible in the figure 5.3.7 (a) and (b) respectively.

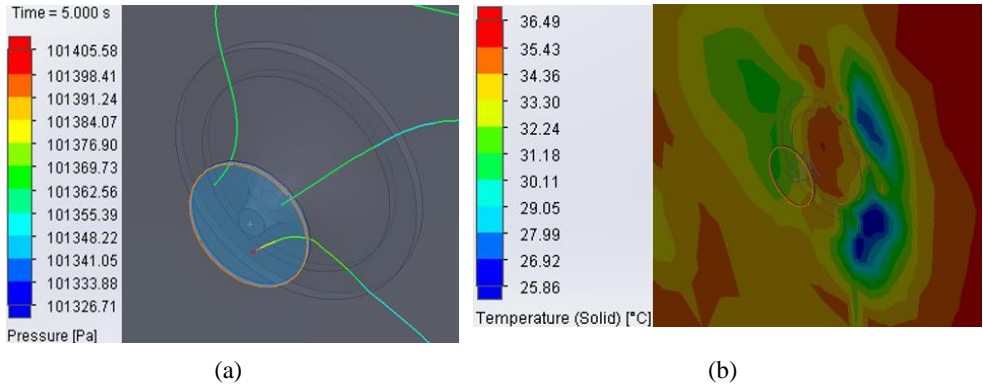


Figure 5.3.7. Flow pressure and surface temperature variation near ventilation hole: (a) Flow pressure variation; (b) Surface temperature variation near ventilation hole.

The analysis of the results suggests that the most suitable criteria for evaluating the heat dissipation from the system (body) in this study are HTR and HF. Given that the objective is to forecast cooling efficiency, either of the criteria can be advantageous, as cooling efficiency rises in accordance with an increase in heat transfer rate.

#### 5.4. Conclusions of Appropriate Criteria for Analysing the Efficiency of Ventilated Clothing

1. Based on the result analysis, it can be concluded that HTR and HF are the most appropriate criteria for analysing the heat removal from the system (body) in this study. Since the goal is to predict cooling efficiency, either of the criteria can be helpful because cooling efficiency increases with increase in heat transfer rate.
2. While the temperature difference can be following criteria for the analysis but in certain cases it might not provide enough sensitivity for the analyses, which is why it is better to use it in combination with other relevant criteria as HTR or HF in this case, to ensure the reliability of results.



3. This study demonstrates variations in parameter values in CFD simulations in different instances and identifies criteria that are helpful for forecasting cooling efficiency in the analysis. It is evident that certain criteria, such as pressure, may not be very useful in predicting cooling efficiency of the system. Moreover, parameters like average temperature can show less sensitivity in certain scenarios.
4. In the future, it allows the formulation of more realistic and complex CFD problems for ventilated protective clothing, taking into consideration uncertainty introduced, for instance, by varying wind direction and ventilation position.

## CONCLUSIONS

1. This thesis work provides a detail analysis of the flow simulation study using a simplified model of the human body with a protective jacket. SolidWorks flow simulation is utilized for numerical simulation, offering a concise understanding of simulation studies and the interaction of fluid flow with the ventilated model.
2. Furthermore, various ventilation elements of simple and complex shapes are created and analyzed in detail by positioning each element at the corresponding ventilation hole in the ventilated jacket. The conducted numerical analysis provides insights into the impact of different shapes of ventilation elements on fluid flow and identifies that the toroidal cut-out shape of element is the most efficient out of other presented in the study.
3. A methodology was developed to optimize the shape of a toroidal cut-out ventilation element. In order to accomplish the objective, a metamodeling technique was employed, using different order polynomial local and global approximations, as well as Kriging approximations. Numerical simulation results were approximated and optimized to obtain optimum values of element design.
4. Numerical simulation was conducted using the optimized ventilation element to check the reliability of the method and optimization results. The difference between the obtained numerical and optimization results is 2.34%. The error is within acceptable tolerance since it is below 5%.
5. The optimization study effectively demonstrates that combining the metamodeling approach with CFD simulation can greatly reduce the computational time required for the optimization. It takes about 4 hours of processing time on a multicore computer with i9 processor to conduct a CFD simulation for calculating a single criterion point for the stated problem. However, by utilizing metamodels, the entire optimization process can be completed in just a few minutes.
6. In the future, it allows for the development of a more accurate shape optimization problem for ventilation elements, taking into account numerous positions of inlets and uncertainty caused by factors such as varying wind direction. Also, this technique is useful in solving other similar optimization problems.

7. Furthermore, various criteria are analysed to predict most suitable one for the shape optimization of ventilation element and predicting cooling efficiency of ventilated clothing in the numerical simulation. The results indicate that the flow pressure ( $dP$ ) and temperature difference ( $dT$ ) are the most sensitive criteria for optimizing ventilation elements, while the heat transfer rate (HTR) is the most appropriate for predicting cooling efficiency. This enables the selection of right criteria for the future studies.

## REFERENCES

- [1] Jiale Chai, Zhanxiao Kang, Yishu Yan, Lun Lou, Yiyang Zhou, Jintu Fan. Thermoregulatory clothing with temperature-adaptive multimodal body heat regulation. *Science Direct*. Volume 3, Issue 7, 20 July 2022, 100958.
- [2] Udayraj, Prabal Talukdar, Apurba Das, Ramasamy Alagirusamy. Heat and mass transfer through thermal protective clothing – A review. *International Journal of Thermal Sciences*. Volume 106, August 2016, 32-56.
- [3] Hancock PA, Vasmatazidis I. (2003). Effects of heat stress on cognitive performance: the current state of knowledge. *Int J Hyperthermia*; 19: 355–372.
- [4] McMorris T., Swain J., Smith M., Corbett J., Delves S., Sale C., Harris R., and Otter J. 2006. Heat stress, plasma concentrations of adrenaline, noradrenaline, 5-hydroxytryptamine and cortisol, mood state and cognitive performance. *International Journal of Psychophysiology*. 61(2), 204–215.
- [5] Cheung, S.S. (2008). Neuromuscular Response to Exercise Heat Stress. *Med. Sport. Sci.*, 53, 39–60.
- [6] U.S. Department of Labor. Overview: Working in Outdoor and Indoor Heat Environments. Occupational Safety and Health Administration. <https://www.osha.gov/heat-exposure>
- [7] ElSayed A. ElNashar, Hanaa H. Sidhom, and Zlatina Kazlacheva. New Approach of Technical Criticism of Egyptian Ancient Clothes with Vitruvius Aesthetics Theory for Fashion Design. *Applied Researches in Technics, Technologies and Education, Journal of the Faculty of Technics and Technologies, Trakia University*. Vol. 3, No. 1, 2015 ISSN 1314-8788 (print), ISSN 1314-8796 (online), doi: 10.15547/artte.2015.01.003, pp. 11-31.
- [8] Kelly Olson. Roman Underwear Revisited. *The Classical World (ISSN 0009-8418) journal of the Classical Association of the Atlantic States*. Published by: The Johns Hopkins University Press. Vol. 96, No. 2 (winter, 2003), pp. 201-210.
- [9] Heitor Luiz Ornaghi Júnior, Roberta Motta Neves, Francisco Maciel Monticeli, Lucas Dall Agnol. Smart Fabric Textiles: Recent Advances and Challenges. *MDPI Journal of Textiles* 2022. Volume 2, 21 November 2022. *Textiles* 2022, 2(4), 582-605; <https://doi.org/10.3390/textiles2040034>
- [10] Song Ren, Mengyao Han, and Jian Fang. Personal Cooling Garments: A Review. *MDPI Journal of Polymers*, 2022 Dec; 14(24): 5522. doi: [10.3390/polym14245522](https://doi.org/10.3390/polym14245522)
- [11] Chao Sun, Joe Sau-chuen Au, Jintu Fan, Rong Zheng. Novel ventilation design of combining spacer and mesh structure in sports T-shirt significantly improves thermal comfort. *Volume 48, May 2015, Pages 138-147*.
- [12] Knut Jaeger, Stuttgarter Strasse 82, D-73230 Kirchheim-Teck (DE). VENTILATION SYSTEM FOR CLOTHING. United States Patent. Patent No.: US 7,043,767 B2. Date of Patent: May 16, 2006.
- [13] Justin De Sousa, Christopher Cheatham, Matthew Wittbrodt. The effect of a moisture-wicking fabric shirt on the physiological and perceptual responses during acute exercise in the heat. November 2014, *Applied Ergonomics* 45(6):1447-1453.
- [14] Russ Clarke-Wildeman. Wicking fabric. *Olorun-sports.com*. Published online on August 15, 2018.
- [15] Mengmeng Zhao, Chuansi Gao, Faming Wang, Kalev Kuklane, Ingvar Holmér, Jun Li. A study on local cooling of garments with ventilation fans and openings placed at different torso

- sites. *International Journal of Industrial Ergonomics*. Volume 43, Issue 3, May 2013, pages 232-237.
- [16] Mengsheng Zhang, Zijun Li, Qiaoli Wang, Yu Xu, Pengyu Hu, Xiuzhi Zhang. Performance investigation of a portable liquid cooling garment using thermoelectric cooling. *Applied Thermal Engineering*. Volume 214, September 2022, 118830.
- [17] Motahareh Mokhtari Yazdi, Mohammad Sheikhzadeh. Personal cooling garments: a review. *The Journal of the Textile Institute*. Volume 105, 2014 - Issue 12, pp. 1231-1250.
- [18] Tinghui Guo, Bofeng Shang, Bin Duan, Xiaobing Luo. Design and testing of a liquid cooled garment for hot environments. *Journal of Thermal Biology*. Volumes 49–50, April–May 2015, Pages 47-54.
- [19] R. G Revaiah, T. M. Kotresh, Balasubramanian Kandasubramanian. Technical textiles for military applications. *The Journal of the Textile Institute*. Volume 111, 2020 - Issue 2, pp. 273-308.
- [20] Al Sayed, C.; Vinches, L.; Hallé, S. Towards optimizing a personal cooling garment for hot and humid deep mining conditions. *Open Journal of Optimization*. Vol. 05, No. 01, March 2016, pp. 35-43.
- [21] Cvetanović S.G.; Rutić S.Z.; Krstić D.D.; Florus S.; Otrisal P. The influence of an active microclimate liquid-cooled vest on heat strain alleviation. *Thermal Science* 2021, Volume 25, Issue 5 Part B, Pages: 3837-3846.
- [22] Teunissen L.P.J.; Wang L.-C.; Chou S.-N.; Huang C.-h.; Jou G.-T.; Daanen H.A.M. Evaluation of two cooling systems under a firefighter coverall. *Applied Ergonomics*. Volume 45, Issue 6, November 2014, Pages 1433-1438.
- [23] Bartkowiak G.; Dabrowska A.; Marszalek A. Assessment of an active liquid cooling garment intended for use in a hot environment. *Applied Ergonomics*. Volume 58, January 2017, Pages 182-189.
- [24] Peng Y.; Cui Y. *Advanced Textiles for Personal Thermal Management and Energy*. Joule. Volume 4, Issue 4, 15 April 2020, Pages 724-742.
- [25] Ni X.; Yao T.; Zhang Y.; Zhao Y.; Hu Q.; Chan A.P. Experimental study on the efficacy of a novel personal cooling vest incorporated with phase change materials and fans. *MDPI Journal of Materials* 2020, 13(8), 1801; <https://doi.org/10.3390/ma13081801>
- [26] Choudhary B.; Wang F.; Ke Y.; Yang J. Development and experimental validation of a 3D numerical model based on CFD of the human torso wearing air ventilation clothing. *International Journal of Heat and Mass Transfer*. Volume 147, February 2020, 118973.
- [27] Heqing L.; Liying G.; Bo Y.; Tianyu L.; Congying O. Experimental Study on the Effect of Air Cooling Garment on Skin Temperature and Microclimate. In *Proceedings of the 11th International Mine Ventilation Congress, Xi'an, China, 14–20 September 2018*; Springer: Singapore, 2019; pp. 742–752
- [28] Hadid A.; Fuks Y.; Erlich T.; Yanovich R.; Heled Y.; Azriel N.; Moran D. Effect of a personal ambient ventilation system on physiological strain during heat stress wearing body armour. In *Proceedings 13th International Conference on Environmental Ergonomics, Boston, MA, USA, 2–7 August 2009*; pp. 252–254.
- [29] Wu G.; Liu H.; Wu S.; Liu Z.; Mi L.; Gao L. A study on the capacity of a ventilation cooling vest with pressurized air in hot and humid environments. *International Journal of Industrial Ergonomics*. Volume 83, May 2021, 103106.
- [30] Choudhary B.; Udayraj. A coupled CFD-thermoregulation model for air ventilation clothing. *Energy and Buildings*. Volume 268, 1 August 2022, 112206.

- [31] Yang J.; Wang F.; Song G.; Li R.; Raj U. Effects of clothing size and air ventilation rate on cooling performance of air ventilation clothing in a warm condition. *International Journal of Occupational Safety and Ergonomics*. Volume 28, 2022 - Issue 1, pp. 354-363.
- [32] Erkan G. Enhancing the thermal properties of textiles with phase change materials. *Research Journal of Textile and Apparel*, May 2004, Volume 8 Issue 2, pp. 57-64.
- [33] Lou L.; Wu Y.S.; Zhou Y.; Fan, J. Effects of body positions and garment design on the performance of a personal air cooling/heating system. *International Journal of Indoor Environment and Health*, January 2022, Volume32, Issue1.
- [34] Lou L.; Shou D.; Park H.; Zhao D.; Wu Y.S.; Hui X.; Yang R.; Kan E.C.; Fan J. Thermoelectric air conditioning undergarment for personal thermal management and HVAC energy saving. *Energy and Buildings*. Volume 226, 1 November 2020, 110374.
- [35] Yang B.; Ding X.; Wang F.; Li A. A review of intensified conditioning of personal micro-environments: Moving closer to the human body. *Energy and Built Environment*. Volume 2, Issue 3, July 2021, Pages 260-270.
- [36] Valant M. Electrocaloric materials for future solid-state refrigeration technologies. *Progress in Materials Science*. Volume 57, Issue 6, July 2012, Pages 980-1009.
- [37] Ma R.; Zhang Z.; Tong K.; Huber D.; Kornbluh R.; Ju Y.S.; Pei Q. Highly efficient electrocaloric cooling with electrostatic actuation. *Science*, Vol 357, Issue 6356, 15 Sep 2017, pp. 1130-1134.
- [38] Gottschall T.; Gracia-Condal A.; Fries M.; Taubel A.; Pfeuffer L.; Manosa L.; Planes A.; Skokov K.P.; Gutfleisch O. A multicaloric cooling cycle that exploits thermal hysteresis. *Nature Materials*. Volume 17, September 2018, pages929–934.
- [39] Ding J.; Zhao W.; Jin, W.; Di C.-a.; Zhu D. Advanced Thermoelectric Materials for Flexible Cooling Application. *Advanced Functional Materials*. Volume31, Issue20, May 17, 2021, 2010695.
- [40] Sun W.; Liu W.-D.; Liu Q.; Chen Z.-G. Advances in thermoelectric devices for localized cooling. *Chemical Engineering Journal*. Volume 450, Part 4, 15 December 2022, 138389.
- [41] Chen W.-Y.; Shi X.-L.; Zou J.; Chen Z.-G. Thermoelectric Coolers: Progress, Challenges, and Opportunities. *Small Methods*. Volume6, Issue2, February 18, 2022, 2101235.
- [42] He W.; Zhang G.; Zhang X.; Ji J.; Li G.; Zhao X. Recent development and application of thermoelectric generator and cooler. *Applied Energy*. Volume 143, 1 April 2015, Pages 1-25.
- [43] Lv S.; Qian Z.; Hu D.; Li X.; He W. A comprehensive review of strategies and approaches for enhancing the performance of thermoelectric module. *MDPI Journal of Energies*. Volume 13, Issue 12, June 2020.
- [44] Yang Z.; Zhu C.; Ke Y.J.; He X.; Luo F.; Jianl W.; Wang J.F.; Sun Z.G. Peltier effect: From linear to nonlinear. *Acta Physica Sinica*. Volume 70, Issue 10 - May 20, 2021.
- [45] Zhao D.; Tan G. A review of thermoelectric cooling: Materials, modeling and applications. *Applied Thermal Engineering*. Volume 66, Issues 1–2, May 2014, Pages 15-24.
- [46] Alaoui C. Peltier thermoelectric modules modeling and evaluation. *International Journal of Engineering (IJE)*, Volume 5, Issue 1, 2011, pp. 114-121.
- [47] Xu Y.; Li Z.; Wang J.; Zhang M.; Jia M.; Wang Q. Man-portable cooling garment with cold liquid circulation based on thermoelectric refrigeration. *Applied Thermal Engineering*. Volume 200, 5 January 2022, 117730.

- [48] Lou L.; Shou, D.; Park H.; Zhao D.; Wu Y.S.; Hui X.; Yang R.; Kan E.C.; Fan J. Thermoelectric air conditioning undergarment for personal thermal management and HVAC energy saving. *Energy and Buildings*. Volume 226, 1 November 2020, 110374.
- [49] Suen W.S.; Huang G.; Kang Z.; Gu Y.; Fan J.; Shou D. Development of wearable air-conditioned mask for personal thermal management. *Building and Environment*. Volume 205, November 2021, 108236.
- [50] Hong S.; Gu Y.; Seo J.K.; Wang J.; Liu P.; Meng Y.S.; Xu S.; Chen R.K. Wearable thermoelectrics for personalized thermoregulation. *Science Advances*. Volume 5, Issue 5, 17 May 2019.
- [51] Zhang Y.; Gao J.; Zhu S.; Li J.; Lai H.; Peng Y.; Miao, L. Wearable Thermoelectric Cooler Based on a Two-Layer Hydrogel/Nickel Foam Heatsink with Two-Axis Flexibility. *ACS Applied Materials & Interfaces*. Volume 14, Issue 13, March 2022.
- [52] Zhang, T.; Li K.; Zhang J.; Chen M.; Wang, Z.; Ma S.; Zhang N.; Wei L. High-performance, flexible, and ultralong crystalline thermoelectric fibers. *Nano Energy*. Volume 41, November 2017, Pages 35-42.
- [53] Zheng Y.; Han X.; Yang J.; Jing Y.; Chen X.; Li Q.; Zhang T.; Li G.; Zhu H.; Zhao H.; et al. Durable, stretchable and washable inorganic-based woven thermoelectric textiles for power generation and solid-state cooling. *Energy & Environmental Sciences*. Volume 15, Issue 6, March 2022.
- [54] K. Singha, S. Maity, P. Pandit, Md. Ibrahim, H. Mondal. 1 – Introduction to protective textiles. *Protective Textiles from Natural Resources*. The Textile Institute Book Series, 2022, pages 3-38.
- [55] C. R. L. da Silva, P. Landim, J. E. Guarneti. An introduction about the usability of protective clothing: a historical analysis. *International Conference on Applied Human Factors and Ergonomics*, Volume 5, July 2014.
- [56] P. Gibson, H. Schreuder-Gibson, D. Rivin. Transport properties of porous membranes based on electrospun nanofibers, *Colloids Surf. A Physicochem. Eng. Asp.* 187–188 (2001) 469–481
- [57] S. Lee, S.K. Obendorf. Transport properties of layered fabric systems based on electrospun nanofibers. *Fibers and Polymers*, Volume 8, (2007) 501–506.
- [58] W. Zhou, N. Reddy, Y. Yang. Overview of protective clothing. *Textiles for Protection*. Woodhead Publishing Series in Textiles. 2005, Pages 3-30.
- [59] T. LaTourrette, D. J. Peterson, JT Bartis, B. A. Jackson, A. Houser. Protecting emergency responders, volume 2: community views of safety and health risks and personal protection needs.
- [60] Eric VAN WELY. Current global standards for chemical protective clothing: how to choose the right protection for the right job? *Industrial Health*. Volume 55(6), 2017.
- [61] J. L. Hick MD, D. Hanfling MD, J. L. Burstein MD, J. Markham MD, A. G. Macintyre MD, J. A. Barbera MD. Protective equipment for health care facility decontamination personnel: Regulations, risks, and recommendations. *Annals of Emergency Medicine*. Volume 42, Issue 3, September 2003, Pages 370-380
- [62] S. Bhattacharjee, R. Joshi, A. A. Chughtai, C. R. Macintyre. Graphene Modified Multifunctional Personal Protective Clothing. *Advanced Materials Interfaces*. Volume 6(21), August 2019.
- [63] K. S. Novoselov, V. I. Fal'ko, L. Colombo, P. R. Gellert, M. G. Schwab & K. Kim. A roadmap for graphene. *Nature*, **volume 490**, pages192–200, (2012).

- [64] Hongkun He, Chao Gao. General Approach to Individually Dispersed, Highly Soluble, and Conductive Graphene Nanosheets Functionalized by Nitrene Chemistry. *Chem. Mater.* 2010, Volume 22(17), 5054–5064.
- [65] C. Lawrance. New materials and new applications. 6<sup>th</sup> Thermic Presentation, Textile Centre of Excellence, Huddersfield, UK, 31<sup>st</sup> January 2018. [https://www.interregeurope.eu/fileadmin/user\\_upload/tx\\_tevprojects/library/file\\_1517393608.pdf](https://www.interregeurope.eu/fileadmin/user_upload/tx_tevprojects/library/file_1517393608.pdf)
- [66] ANSI/ASHRAE. Thermal environmental conditions for human occupancy. American Society of Heating, Refrigerating and Air-Conditioning Engineers, (2010) ANSI/ASHRAE 55-2010, Atlanta.
- [67] R. de Dear, G. S. Brager, D. Cooper. Developing an adaptive model of thermal comfort and preference - Final Report on RP-884. *ASHRAE Transactions* 104(1), January 1997.
- [68] G. R. Newsham. Clothing as a thermal comfort moderator and the effect on energy consumption. *Energy and Buildings*, volume 26(3), 1997, pages 283-291.
- [69] P.O. Fanger. Thermal comfort. Analysis and application in environmental engineering. Danish Technical Press, Copenhagen, 1970, pp. 244.
- [70] S. Schiavon, K. Ho Lee. Predictive clothing insulation model based on outdoor air and indoor operative temperatures. Proceedings of 7th Windsor Conference: The changing context of comfort in an unpredictable world Cumberland Lodge, Windsor, UK, 12-15 April 2012.
- [71] ISO 7933:2004 (2004). Ergonomics of the Thermal Environment – Analytical determination and interpretation of heat stress using calculation of the predicted heat strain. The International Organization for Standardisation: Geneva, Switzerland.
- [72] ISO 7730:2005 (2005). Ergonomics of the Thermal Environment – Analytical determination and interpretation of thermal comfort using calculation of the PMV and PPD indices and local thermal comfort criteria. The International Organization for Standardisation: Geneva, Switzerland.
- [73] ISO 11079:2007 (2007). Ergonomics of the Thermal Environment – Analytical determination and interpretation of cold stress using required clothing insulation (IREQ) and local cooling effects. The International Organization for Standardisation: Geneva, Switzerland.
- [74] ASTM F1291-16 (2016). Standard Test Method for Measuring the Thermal Insulation of Clothing Using a Heated Manikin. American Society of Testing and Materials International (ASTM), Philadelphia.
- [75] ISO 15831:2004. Clothing - Physiological effects - Measurement of thermal insulation by means of a thermal manikin. The International Organization for Standardisation: Geneva, Switzerland.
- [76] [H. Anttonen](#), [J. Niskanen](#), [H. Meinander](#), [V. Bartels](#), [K. Kuklane](#), [R. E. Reinertsen](#), [S. Varietas](#), [K. Sołtyński](#). Thermal manikin measurements--exact or not? *International Journal of Occupational Safety and Ergonomics (JOSE)*, 2004; 10(3): pp. 291-300.
- [77] E. A. McCullough, B. W. Jones, J. Huck. A comprehensive data base for estimating clothing insulation. *ASHRAE Transaction*, volume 91, pp. 29-47.
- [78] [S. Veselá](#), [A. Psikuta](#) & [Arjan J. H. Frijns](#). Local clothing thermal properties of typical office ensembles under realistic static and dynamic conditions. *International Journal of Biometeorology*. October 2018, volume 62, pages 2215-2229.
- [79] Miloš Fojtlín, Agnes Psikuta, Jan Fišer, Róbert Toma, Simon Annaheim, Miroslav Jícha. Local clothing properties for thermo-physiological modelling: Comparison of methods and body positions. *Building and Environment*. Volume 155, 15 May 2019, Pages 376-388.



- [80] Naoshi Kakitsuba. Investigation into Clothing Area Factors for Tight and Loose Fitting Clothing in Three Different Body Position. *Journal of the Human-Environment System*. Volume 7(2): pages 75-81.
- [81] Psikuta A., Mert E., Annaheim S. & Rossi RM. 3D body scanning technology and applications in protective clothing. In G. Song & F. Wang (Eds.), *Firefighters' clothing and equipment: performance, protection, and comfort* (pp. 269-286). CRC Press.
- [82] ISO 9920:2007. Ergonomics of the thermal environment. Estimation of thermal insulation and water vapour resistance of a clothing ensemble. International Standards Organisation, Geneva.
- [83] Kalev Kuklane, Róbert Toma. Common clothing area factor estimation equations are inaccurate for highly insulating ( $I_{cl} > 2$  clo) and non-western loose-fitting clothing ensembles. *Journal of Industrial Health*. Volume 59(2), December 2020.
- [84] H. Hymczak, A. Gołąb, K. Mendrala, D. Plicner, T. Darocha, P. Podsiadło, D. Hudziak, R. Gocoł, and S. Kosiński. Core Temperature Measurement—Principles of Correct Measurement, Problems, and Complications. *International Journal of Environmental Research and Public Health*. 2021 Oct; volume 18(20): 10606.
- [85] Eva V. Osilla; Jennifer L. Marsidi; Karlie R. Shumway; Sandeep Sharma. *Physiology, Temperature Regulation*. StatPearls Publishing; [Internet]. Jan 2023.
- [86] I. Tabarean, B. Morrison, M. C. Marcondes, T. Bartfai, and B. Conti. Hypothalamic and dietary control of temperature-mediated longevity. *Ageing Res Rev*. 2010 Jan; 9(1): 41.
- [87] B. Lell, C. H. Brandts, W. Graninger, P. G. Kremser. The circadian rhythm of body temperature is preserved during malarial fever. *Wien Klin Wochenschr*. 2000 Dec 7; Volume 112(23):1014-5.
- [88] USARIEM. Scenario - Human Thermoregulatory Response Model. Research Institute of Environmental Medicine. <https://usariem.health.mil/index.cfm/research/products/scenario>
- [89] Lucy Dorman and George Havenith. *The Effects of Protective Clothing and its Properties on Energy Consumption during Different Activities*. Doctoral dissertation, Loughborough University, Environmental Ergonomics Research Centre.
- [90] Praveen Kumar. Role of CFD in evaluating occupant thermal comfort | simulation Hub Blog. <https://www.simulationhub.com/blog/role-of-cfd-in-evaluating-occupant-thermal-comfort>
- [91] I. Holmér. Protective clothing and heat stress. *Ergonomics*. Jan 1995; volume 38(1): pp. 166-82. doi: 10.1080/00140139508925093.
- [92] T. Erlandson, K. Cena, R. De Dear, G. Havenith. Environmental and human factors influencing thermal comfort of office occupants in hot—humid and hot—arid climates. *Ergonomics*. Volume 46, Issue 6, March 2014, Pages 616-628.
- [93] J.D. Anderson, J. Wendt. *Computational fluid dynamics*. New York, NY: McGraw-Hill (1995).
- [94] A Howard H. Hu. *Computational Fluid Dynamics*. Fluid Mechanics (Fifth Edition), 2012, Pages 421-472.
- [95] M. M. Bhatti, M. Marin, A. Zeeshan, Sara I. Abdelsalam. Editorial: Recent Trends in Computational Fluid Dynamics. *Front. Phys.*, volume 8, October 2020.
- [96] B. Andersson, R. Andersson, L. Håkansson, M. Mortensen, R. Sudiyo, B. V. Wachem. *Computational fluid dynamics for engineers*. Cambridge, England: Cambridge University Press (2011).

- [97] J. H. Ferziger, M. Perić. Computational methods for fluid dynamics. Berlin: Springer (2002).
- [98] Simscale/SimWiki. What is CFD | Computational Fluid Dynamics? <https://www.simscale.com/docs/simwiki/cfd-computational-fluid-dynamics/what-is-cfd-computational-fluid-dynamics/>
- [99] Marco Cannone. Harmonic Analysis Tools for Solving the Incompressible Navier–Stokes Equations. Handbook of Mathematical Fluid Dynamics. Volume 3, 2005, Pages 161-244.
- [100] White Frank. Viscous Fluid Flow. 3rd edition. McGraw-Hill Mechanical Engineering. ISBN-10: 0072402318.
- [101] N. Ashgriz, J. Mostaghimi. An Introduction to Computational Fluid Dynamics. Chapter 20 in Fluid Flow Handbook. <https://mussl.mie.utoronto.ca/wp-content/uploads/cfd20.pdf>
- [102] Bastian E. Rapp. Computational fluid dynamics. Microfluidics (Second edition). Modeling, Mechanics and Mathematics. Micro and Nano Technologies, 2023, Pages 653-666.
- [103] R. Eymard, T. Gallouët, R. Herbin. Finite volume methods. Handbook of Numerical Analysis. Volume 7, 2000, Pages 713-1018.
- [104] R. Horst, P.M. Pardalos and N.V. Thoai. Introduction to Global Optimization, Second Edition. Kluwer Academic Publishers, 2000.
- [105] R. Horst, H. Tuy. Global Optimization: Deterministic Approaches. Springer Science & Business Media, May 15, 1996 - Business & Economics - 730 pages.
- [106] Wikipedia. Global Optimization. [https://en.wikipedia.org/wiki/Global\\_optimization#:~:text=Global%20optimization%20is%20a%20branch.functions%20on%20a%20given%20set.](https://en.wikipedia.org/wiki/Global_optimization#:~:text=Global%20optimization%20is%20a%20branch.functions%20on%20a%20given%20set.)
- [107] J. Auziņš and A. Januševskis. Robust Multicriterion Optimization of Composite Material Elements. Scientific Laboratory for Machine and Mechanism Dynamics, Riga Technical University.
- [108] Kearfott, R. Baker. "A review of techniques in the verified solution of constrained global optimization problems." Applications of Interval Computations (1996): 23-59.
- [109] Wikipedia. Maximum and minimum. [https://en.wikipedia.org/wiki/Maximum\\_and\\_minimum](https://en.wikipedia.org/wiki/Maximum_and_minimum)
- [110] James C. Spall. Introduction to Stochastic Search and Optimization. Wiley, (2003). ISBN 978-0-471-33052-3.
- [111] D. Aleksendrić, P. Carlone. Soft computing techniques. Soft Computing in the Design and Manufacturing of Composite Materials. Applications to Brake Friction and Thermoset Matrix Composites, 2015, Pages 39-60.
- [112] A.M. Johansen. Monte Carlo Methods. International Encyclopedia of Education. (Third Edition), 2010, Pages 296-303
- [113] Sacks J., Welch W.J., Mitchell T.J., Wynn H.P. Design and analysis of computer experiments. Statistical Science, 4(4), November 1989, pp. 409-423.
- [114] Jones D.R., Schonlau M., Welch W.J. Efficient global optimization of expensive black-box functions. Journal of Global Optimization, 13(4), 1998, pp. 455-492.
- [115] Jones D.R. A taxonomy of global optimization methods based on response surfaces. Journal of Global Optimization, 21, 2001, pp. 345-383.
- [116] Sasena M.J. Flexibility and Efficiency Enhancements for Constrained Global Design Optimization with Kriging Approximations. PhD thesis, 2002.
- [117] Janusevskis J., Riche R.L. Simultaneous kriging-based sampling for optimization and uncertainty propagation. Technical report, Equipe: Calcul de Risque, Optimisation et Calage

- par Utilisation de Simulateurs - CROCUS-ENSMSE - UR LSTI - Ecole Nationale Supérieure des Mines de Saint-Etienne, July 2010. Deliverable no. 2.2.2-A of the ANR/OMD2 project. [online][11.03.2023] Available at: <http://hal.archives-ouvertes.fr/hal-00506957>.
- [118] Carl E. Rasmussen and Christopher K. I. Williams. Gaussian Processes for Machine Learning (Adaptive Computation and Machine Learning). The MIT Press, December 2005.
- [119] Auzins J., Janushevskis A. KEDRO User's Manual. 2023. 50 p. [online][11.03.2023] Available at: <http://www.mmd.rtu.lv/ProgramsA.htm>
- [120] D. Obradovic, L. N. Mishra and V. N. Mishra. Interpolation and Approximation of Functions. Journal of pure and applied mathematics. 27 March 2021, DOI: 10.37532/2752-8081.21.5.24.
- [121] Words and Buttons Online. Polynomial approximation and interpolation. <https://wordsandbuttons.online/polynomial-approximation-and-interpolation.html>
- [122] Yin-Wen Chang, Cho-Jui Hsieh, Kai-Wei Chang, Michael Ringgaard, Chih-Jen Lin. "Training and testing low-degree polynomial data mappings via linear SVM". Journal of Machine Learning Research. (2010), 11: 1471–1490.
- [123] Stackoverflow.com. Curve fitting with both interpolation and approximation. <https://stackoverflow.com/questions/75302758/curve-fitting-with-both-interpolation-and-approximation>
- [124] A G. H. Golub, C. F. Van Loan. Matrix Computations, fourth edition. Johns Hopkins University Press, February 2013.
- [125] Rajesh Kumar, R.K. Aggarwal, J.D. Sharma and Sunil Pathania. Predicting Energy Requirement for Cooling the Building Using Artificial Neural Network. Journal of Technology Innovations in Renewable Energy, 2012, 1, 113-121.
- [126] McMorris T., Swain J., Smith M., Corbett J., Delves S., Sale C., Harris R., and Otter J. 2006. Heat stress, plasma concentrations of adrenaline, noradrenaline, 5-hydroxytryptamine and cortisol, mood state and cognitive performance. International Journal of Psychophysiology. 61(2), pp. 204–215.
- [127] Nilsson H.O. Comfort Climate Evaluation with Thermal Manikin Methods and Computer Simulation Models. National Institute for Working Life & authors 2004. S-11391, Stockholm. ISBN 91-7045-703-4, ISBN 91-7283-693-8, ISSN 0346-7821.
- [128] Udayraj P.T., Apurba D., Ramasamy A. Heat and mass transfer through thermal protective clothing – A review. International Journal of Thermal Sciences. Volume 106, August 2016, pp. 32-56.
- [129] Zhao M., Gao C., Wang F., Kuklane K., Holmer I. A study on Local Cooling of Garments with Ventilation Fans and Openings Placed at Different Torso Sites. International Journal of Industrial Ergonomics, January 2013.
- [130] Kerstin Giering, Ingolf Lamprecht, Olaf Minet. Specific heat capacities of human and animal tissues. Proceedings of SPIE – The International Society for Optical Engineering, January 1996, 2624:188-197.
- [131] John P. Rugh, Desikan Bharathan. Predicting Human Thermal Comfort in Automobiles. Presented at the Vehicle Thermal Management Systems Conference and Exhibition, May 2005, Toronto, Canada.
- [132] Saxena A., Sahay B. Computer Aided Engineering Design, Springer, 2005, 394 p.
- [133] Janushevskis A., Auzins J., Janushevskis J., Viba J. Optimization of Subsonic Aerodynamic Shape by Using Metamodeling Approach. Proc. 5th Int. DAAAM Conference "Industrial

- Engineering – Adding Innovation Capacity of Labour Force and Entrepreneurs”. Editor R.Kyttner. ISBN 9985-894-92-8. Tallinn University of Technology. 2006, pp. 41-46.
- [134] Janushevskis A., Melnikovs A., Janusevskis J. Shape Optimization of a Lightweight Tetrapod Element Using CAD/CAE Tools and Metamodels. Proceedings IRF 2013. Editors: J.F.Silva Gomes, Shaker A. Meguid. ISBN: 978-972-8826-28-4. Fourth International Conference on Integrity, Reliability & Failure. Funchal, Portugal, 2013, 11 p.
- [135] Janushevskis, A., Vejanand S. R., Gulevskis, A. Analysis of Different Shape Ventilation Elements for Protective Clothing. WSEAS Transactions on Fluid Mechanics, Vol.17, ISSN: 1790-5087, 2022. pp. 140-146.
- [136] Sajjad, U.; Hamid, K.; Tauseef ur, R.; Sultan, M.; Abbas, N.; Ali, H.M.; Imran, M.; Muneeshwaran, M.; Chang, J.-Y.; Wang, C.-C. Personal thermal management—A review on strategies, progress, and prospects. *International Communications in Heat and Mass Transfer*, 2022, 130, 105739.
- [137] Ebi, K.L.; Capon, A.; Berry, P.; Broderick, C.; de Dear, R.; Havenith, G.; Honda, Y.; Kovats, R.S.; Ma, W.; Malik, A.; et al. Hot weather and heat extremes: Health risks. *The Lancet*, 2021, 398, 698–708.
- [138] Janushevskis, A., Vejanand S. R., Gulevskis, A. Shape optimization of ventilation elements for protective clothing by using metamodeling approach. Conference proceeding, Engineering for Rural Development, Jelgava, 24.-26.05.2023. pp. 164-172. DOI: 10.22616/ERDev.2023.22.TF032.
- [139] L.F. Richardson. The approximate arithmetical solution by finite differences of physical problems involving differential equations, with an application to the stresses in a masonry dam. *Philosophical Transactions of the Royal Society of London, Series A*, 210 (1910), pp. 307-357.
- [140] R. Courant, K. Friedrichs, H. Lewy. Die partiellen differenzengleichungen der mathematischen Physik. *Mathematische Annalen (Historical Archive)*, 100 (1928), pp. 32-74.
- [141] J.S. Shang. Three decades of accomplishments in computational fluid dynamics. *Progress in Aerospace Sciences*, 40 (2004), pp. 173-197.
- [142] B. Xia, D.-W. Sun. Applications of computational fluid dynamics (CFD) in the food industry: a review. *Computers and Electronics in Agriculture*, 34 (2002), pp. 5-24.
- [143] A.G. Davenport. How can we simplify and generalize wind loads? *Journal of Wind Engineering and Industrial Aerodynamics*. Volumes 54–55, February 1995, pp. 657-669.
- [144] M. Pedroso, I. Flores-Colen, J.D. Silvestre, M.G. Gomes, L. Silva, P. Sequeira, J. de Brito. Characterisation of a multilayer external wall thermal insulation system. Application in a Mediterranean climate. *Journal of Building Engineering*. Volume 30, July 2020, 101265.
- [145] H. Gol-Zaroudi, A.M. Aly. Open-jet boundary-layer processes for aerodynamic testing of low-rise buildings. *Wind and Structures*, Vol. 25, No. 3(2017), pp. 233-259 DOI: <https://doi.org/10.12989/was.2017.25.3.233>
- [146] J R. Feng, F. Liu, Q. Cai, G. Yang, J. Leng. Field measurements of wind pressure on an open roof during Typhoons HaiKui and SuLi. *Wind and Structures*, Vol. 26, No. 1 (2018), pp. 11-24 DOI: <https://doi.org/10.12989/was.2018.26.1.011>
- [147] M.F. Khaled, A.M. Aly, A. Elshaer. Computational efficiency of CFD modeling for building engineering: An empty domain study. *Journal of Building Engineering*. Volume 42, October 2021, 102792.
- [148] Wang Y, Cao Z. Industrial building environment: old problem and new challenge. *Indoor Built Environ* 2017, 26: 1035–1039.

- [149] Xu C, Liu L. Personalized ventilation: one possible solution for airborne infection control in highly occupied space? *Indoor Built Environ* 2018; 27: 873–876.
- [150] Y. Epstein, Y. Shapiro, S. Brill. Comparison between different auxiliary cooling devices in a severe hot/dry climate. *Ergonomics*, Volume 29, 1986 - Issue 1. Published on July 2010, pages 41-48.
- [151] W. Pasut, H. Zhang, E. Arens, Y. Zhai. Energy-efficient comfort with a heated/cooled chair: Results from human subject tests. *Building and Environment*, Volume 84, January 2015, Pages 10-21.
- [152] G. Lopez, T. Tokuda, N. Isoyama, H. Hosaka, K. Itao. Development of a wrist-band type device for low-energy consumption and personalized thermal comfort, 2016 11th Fr. 9th Eur. Congr. Mechatronics, MECATRONICS 2016/17th Int. Conf. Res. Educ. Mechatronics, REM. 2016. (2016). 209–212.
- [153] Y. He, N. Li, M. He, D.e. He. Using radiant cooling desk for maintaining comfort in hot environment. *Energy and Buildings*, Volume 145, 15 June 2017, Pages 144-154.
- [154] L. Huang, Q. Ouyang, Y. Zhu, L. Jiang. A study about the demand for air movement in warm environment. *Building and Environment*, Volume 61, March 2013, Pages 27-33.
- [155] Udayraj, F. Wang, W. Song, Y. Ke, P. Xu, C.S.W. Chow, N. Noor. Performance enhancement of hybrid personal cooling clothing in a hot environment: PCM cooling energy management with additional insulation. *Ergonomics*, Volume 62, 2019 - Issue 7, Pages 928-939.
- [156] F. Mneimneh, N. Ghaddar, K. Ghali, M. Itani. The effectiveness of evaporative cooling vest with ventilation fans on the thermal state of persons with paraplegia during exercise. *Building and Environment*, Volume 206, December 2021, 108356.
- [157] P. Xu, Z. Kang, F. Wang, Udayraj. A Numerical Analysis of the Cooling Performance of a Hybrid Personal Cooling System (HPCS): Effects of Ambient Temperature and Relative Humidity. *International Journal of Environmental Research and Public Health* 2020, 17(14), 4995; <https://doi.org/10.3390/ijerph17144995>
- [158] F. Wang, Y. Ke, Udayraj, B. Yang, P. Xu, N. Noor. Effect of cooling strategies on overall performance of a hybrid personal cooling system incorporated with phase change materials (PCMs) and electric fans. *Journal of Thermal Biology*, Volume 92, August 2020, 102655.
- [159] S.M. Watkins. *Clothing: The portable environment*. Iowa State University Press, 2nd edition, 1995; NII Book ID: [BB00640058](https://nii.org/nii/BB00640058).



**Sanjay Rajni Vejanand** was born in 1991 in Vadala, Porbandar district (Gujarat), India. He received a Bachelor's degree in Mechanical Engineering (2015) from Gujarat Technological University in Ahmedabad, India and a Master's degree in Engineering Science in Mechanics and Mechanical Engineering (2019) from Riga Technical University (RTU), Latvia. From September 2015 to June 2017, he worked as a mechanical design engineer at The CAD World in Rajkot, India. From December 2019 to February 2020, he worked as a mechanical engineer intern at Morfomichaniki, Frenaros (Cyprus). Since 2020, he has been working as a research assistant at Riga Technical University. His research interests revolve around topics such as CFD, CAD, fluid mechanics, finite element modelling, finite element analysis, metamodeling and optimization.